ETS·LINDGREN
An ESCO Technologies Company

SUMMA
FOUNDATION

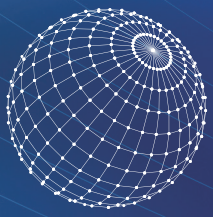

GlobalEM 2024

Abstract Book

Global Electromagnetics Conference

AT&T Conference Center • Austin, Texas USA

July 14 through 19, 2024

On the Response of Electrical Cables Excited by the Swiss Impulse Radiating Antenna

D. V. Giri
Dept. of ECE, University of New Mexico
Pro-Tech, 45 Cliff Road, Wellesley, MA 02481 USA.
Giri@DVGiri.com www.dvgiri.com

F. M. Tesche
EM Consultant
Avon, CT 06001, USA
Fred@Tesche.com

C. Romero
armasuisse Science and Technology
Thun, Switzerland
carlos.romero@ar.admin.ch

Abstract—*This paper describes an investigation of the responses of a two-conductor transmission line illuminated by the Swiss impulse radiating antenna (SWIRA). A description of the radiated fields from this antenna is first provided, and then the responses of various transmission lines to this excitation are illustrated. For simplicity, the line responses are represented by the open circuit voltage Voc that is induced at one of the ends of the line, with the opposite end of the line matched with the characteristic impedance of the transmission line. While these calculations are performed for the specific case of the line having a wire separation of d = 1 cm and wire radii a = 1 mm, simple expressions have been provided for transforming the calculated results to those appropriate for lines with other dimensions. Moreover, simple expressions are given for obtaining the short-circuit current at the load.*

Keywords- Coupling, IRA Fields, Transmission Lines, Cables

I. INTRODUCTION

Swiss impulse-radiating antenna (SWIRA) is a useful tool for testing electrical systems in electromagnetic (EM) environments. A computational model for determining the radiated EM fields from this antenna is available and the behavior of the E-field at various locations in front of the antenna has been determined. In this paper, the SWIRA model is used to determine a range of responses for 2-conductor electrical transmission lines that are illuminated by the antenna when it is operated in transient mode.

II. EXCITATION AND COUPLING TO LINE

Figure 1 illustrates the SWIRA geometry. This antenna consists of a parabolic dish reflector of diameter D = 1.8 m with a focal length F = 0.482 m.

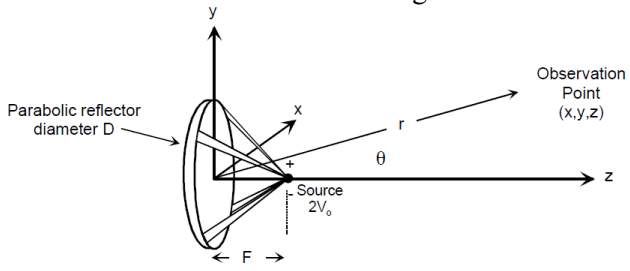

Figure 1. Geometry of the SWIRA and a distant field observation point.

The antenna is fed by a four-arm transmission line structure with a voltage source located at the focal point. With a pulsed voltage source $Vo(t)$, the antenna radiates a fast impulse-like waveform along the boresight (z) direction. This antenna has many well-established applications.

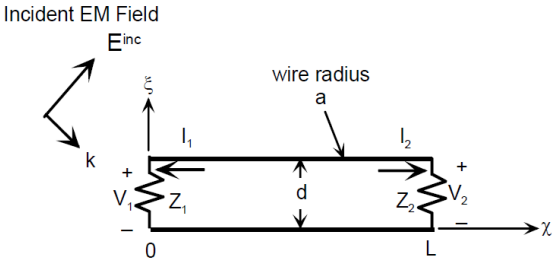

Figure 2. Illustration of a 2-wire transmission line excited by an incident EM field from SWIRA.

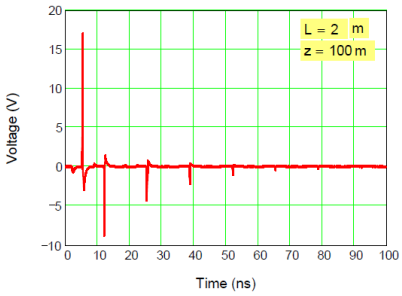

Figure 3. Plot of the open circuit voltage V_{oc} at load for a 2-meter transmission line located at 100 meters from the SWIRA.

III. SUMMARY

While there can be large variations in the line responses as the line moves about in the illuminated region in front of the SWIRA, an attempt has been to calculate and quantify the worst-case responses of the line. This is accomplished by considering either end-on or broadside excitation of the line while it is in the boresight direction of the antenna, where the E-field strength is the greatest.

We will present many cases and parametric variation of the coupling of the SWIRA fields to transmission lines.

The Most Ambitious Radio Astronomy Endeavor of the 21st Century?

EMC in a Large-scale Project
Plenary Paper

Howard C. Reader
MESA Solutions, 5 Thierry Street, Stellenbosch, 7600, South Africa
Emeritus Professor, Dept. EE Engineering, Stellenbosch, South Africa.
howard@mesasolutions.co.za www.mesasolutions.co.za

***Abstract*— "Few projects come close to the scope and ambition of the Square Kilometre Array (SKA) as a scientific endeavor. How can we fill in the gaps in our understanding of the Universe by reading its history as written in the language of its most abundant constituent, Hydrogen?" [1]. Along with pulsars, our cosmic clocks, study of these two principal radio astronomy topics is severely constrained by the widespread electromagnetic (EM) activity of our modern living. An overview of the science and interference will be used to illustrate the significance and extent of EMC activities during system design, construction, and operation.**

Keywords-EMC, Radio Astronomy, Square Kilometre Array

I. INTRODUCTION

In pursuit of seeing back to the Cosmic Dawn and the formation of the very first stars, of witnessing the epoch of galaxy formation and of attempting to understand universal conditions 13.7 billion years after the Big Bang, an SKA-sized telescope is needed. These and other ambitious goals are outlined by Braun et al. [2]. Reference will be made to general high-level science objectives and then to large-scale Electromagnetic Compatibility (EMC) system elements which impact 1) Strong-field tests of gravity with pulsars and black holes and 2) Galaxy evolution probed by neutral hydrogen.

The original objectives published in [1] stated that the instrument would be at least 50 times more sensitive than existing radio astronomy systems. The mid-band telescopes are located in the Karoo of South Africa (RSA) and the low-band arrays in the Murchison Valley of Australia. Fig. 1 places the SKA in the context of other science aspirations, where the direct imaging of cosmic dawn structures and the first glimpses of the Dark Ages are highlighted. Fig. 2 zooms into the telescopes and arrays that are beginning to do science. Fig. 3 gives a sense of the project scale from the RSA Astronomy Advantage Area (AAA), which is nationally protected by permissible EM Interference (EMI) thresholds. EMI is addressed at every level of development and operation in both Australia and RSA. Foundational project academic EMC research activities in RSA can be found in [4].

II. INFRASTRUCTURAL EMC

A. Radio Quiet Power Provision: Consortia Involved

Development teams and international consortia have been involved in designing "the world's most radio-quiet power stations" [5]. "Reducing EMI to the level we need is such a specialist job … there's only a handful of people … that can do it. If we went to the market and asked for someone to build a radio-quiet power station, we wouldn't get any bids, or they would be far too expensive due to the perceived risk." The developments, installation implications and testing of power and photo-voltaic systems will be discussed.

B. EMI, Metrology, Interfaces and Apertures

Some intriguing elements in this field will be reported.

Figure 1. Science aspirations outlined at the first Mega-Science Exhibition in India, 2019 [3]. The SKA is highlighted with respect to the Cosmic Dawn.

Figure 2. Mid-band telescopes (South Africa); Low-band arrays (Australia).

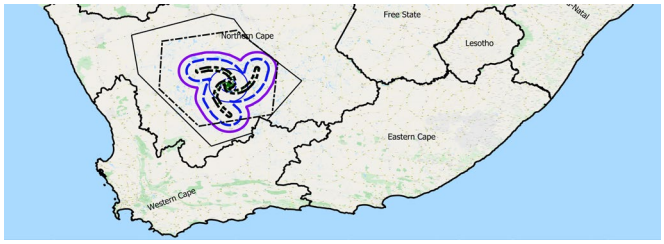

Figure 3. Nationally-protected regions suggesting the physical scales involved.

REFERENCES

[1] "History of the SKA Project", www.skao.int/en/about-us/91/history-ska-project; accessed January 2024.

[2] R. Braun, T.L. Bourke, J.A. Green, E.F. Keane and J. Wagg, "Advancing Astrophysics with the Square Kilometre Array", June 8-13, 2014, Giardini Naxos, Sicily, Italy; published 29 May 2015.

[3] T. Choudhury, "Vigyan Samagan (confluence of scientific ideas): The First Ever Mega Science Exhibition in India", SKAO Contact Issue 1: www.skao.int/en/news-events/contact-skao-magazine, pp.10-11.

[4] H.C. Reader, "Components of EMC Thinking Relevant to Radio Astronomy Sites", APEMC 2013, Melbourne, Australia, Session TC18-1, ISBN 978-1-9221-0702-2, May 2013, paper 145.

[5] M. Taylor, "World's most radio-quiet power station to be built for SKA-Mid", SKAO Contact Issue 12: www.skao.int/en/news-events/contact-skao-magazine,pp.24-25.

Transmission-line Transformers Having Irrational Effective Turns Ratios

James McLean
TDK Corp.
Cedar Park, Texas, USA
jim.mclean@tdk.com

Transmission-Line Transformers (TLTs) and baluns exploit leakage inductance and inter-winding capacitance to provide broadband frequency response and high-fidelity time-domain pulse reproduction. However, TLTs are limited to rational effective turns ratios (voltage or current ratios) [1], [2]. This arises from the series/shunt interconnection of the constituent "basic building blocks" which in turn are multiconductor transmission lines with integral common-mode chokes [1]. When a precise, irrational effective turns ratio is mandated, a conventional TLT may not be practicable. In principle, a sufficiently high-order TLT (TLT order is rigorously defined in ref. [2]) can come arbitrarily close to providing any turns ratio [2]–[5]. However, if the order of the TLT is high, parasitic behavior and losses arising from the large number of interconnections degrade the performance. Therefore, it is desirable to be able to provide an arbitrary effective turns ratio with a relatively low-order TLT. It has been shown in the literature that such irrational effective turns ratios may be obtained by "tapping" one or more of the multi-filar windings of a TLT [1], [6]. This naturally slightly degrades the TLT operation and hence the frequency- and time-domain responses. Although the approach is provided in the literature, no detailed analysis is given. Here we analyze such a "tapped" transmission line transformer in the time and frequency domains for the purpose of providing input/output matching to a large TEM transmission line for vehicular EMC testing. As an example, consider a design requirement calling for an impedance ratio of 1:2.5 transforming 50 Ω to 125 Ω. This requires a voltage ratio of $1:\sqrt{2.5}$ which is an irrational number. Therefore, the ratio cannot be exactly obtained with a TLT. Nevertheless, the ratio can be closely approximated by a sufficiently high-order TLT. For example, the rational voltage ratio of $7:11$ is within 1% tolerance of $1:\sqrt{2.5}$ and gives an impedance ratio of 2.4694. However, an 11-winding TLT is extraordinarily complex and parasitic effects are an issue. There are two candidate TLTs with relatively low order from which the ratio may be obtained by "tapping". It is possible to obtain an impedance ratio of 2.25 (voltage ratio of 1:3/2) transforming 50 Ω to 112.5 Ω. This can be implemented with a bootstrap/Ruthroff approach. It is also possible to obtain a ratio of 2.778 (voltage ratio of 1:5/3) transforming 50 Ω to 138.89 Ω. The SWR in both cases is approximately 1.11:1 which, of course, is quite good from the standpoint of power transfer. However, it is not always acceptable when longitudinal field uniformity in the TEM device is considered. Tapping either design should reduce this SWR to a lower value, although with some reduction in bandwidth. The tapped 50 Ω: 138.9 Ω bootstrap unun is shown in Fig. 1. At one, the other, or both of the two points marked "X" in the

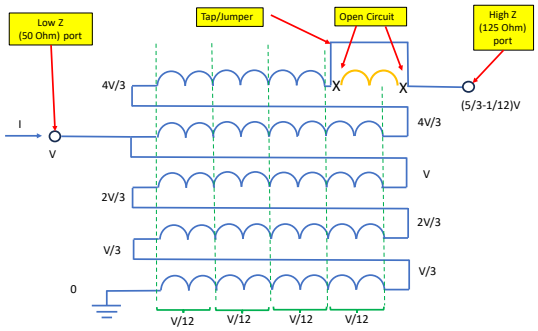

Fig. 1. Tapped quintafilar bootstrap unun. Without the tap, the unun transforms 50 Ω to 138.9 Ω. With the tap it transforms 50 Ω to 125 Ω.

fifth/top winding, the conductor must be open circuited. Thus, there are three possibilities. If the transformer operates as a conventional magnetically-coupled (exclusively) transformer, all three approaches give fairly similar performance. However, this is not true for the TLT. Moreover, the tapped 1:3/2 and the tapped 1:5/3 turns-ratio TLTs do not provide identical responses and thus there are six possibilities. This will be shown in detail. The tapped TLT is examined here using coupled transmission line analysis as well as full-wave FEM analysis. and one of the six approaches is shown to be clearly superior. Unun TLTs for use with a TEM transmission line intended for ISO-11451-2 and SAE J551/11 will be fabricated and characterized with the TEM structure.

References

[1] J. Sevick, Transmission Line Transformers, 4th, Ed. Noble, New York, 2001.
[2] E. Rotholz, "Transmission line transformers," *IEEE Trans. Microwave Theory Tech.*, vol. MTT-29, no. 4, pp. 327–331, Apr. 1981.
[3] P. Gomez-Jimenez, P. Otero and E. Marquez-Segura, "Analysis and Design Procedure of Transmission-Line Transformers," *IEEE Trans. Microwave Theory Tech.*, vol. 56, no. 1, pp. 163-171, Jan. 2008.
[4] London, S. E. and S. Y. Tomeshevich, "Line Transformers with Fractional Transformation Factor," Telecommunications and Radio Engineering, Vol 28/29, Apr 1974.
[5] London, S. E., "Broadband transmission line transformer," US Patent, 7839232B2, Nov. 23, 2010.
[6] F. J. van Dam , "A Stripline Antenna for Radiated Immunity Testing", Thesis, University of Twente, NL, 27 Oct., 2011

High Level Electromagnetic Susceptibility: A Practical Answer Using Machine Learning

M.A. Echeverri Bautista [(1)], A.P.M. Zwamborn [(2)]
(1) TNO, Electromagnetic Signatures & Propagation Dept.
(2) TNO, Electronic Warfare Dept.
The Hague, The Netherlands.
mario.echeverribautista@tno.nl

Abstract - This paper discusses an innovative way to look at the Electromagnetic susceptibility problem in complex systems. The approach is statistical in nature, and leverage on existing Machine Learning architectures to tackle a practical question: which system is potentially vulnerable to what waveform and to which extent. Furthermore, this work examines the figures of merit of using data-driven approaches to bridge the gap between physics-driven approaches and the complexity of real-life scenarios.

Keywords – Electromagnetic susceptibility, system, Machine Learning.

I. INTRODUCTION

Intentional Electromagnetic Interference (IEMI), has received a great deal of attention throughout the years, due to the consequences of successful EM attacks; a plethora of theory and techniques exists, to analyze and predict the response of systems and sub-systems, see [1] and references within for an excellent overview. In general, the analysis is performed using a mix of modeling techniques, including experiments. To this end, a well-accepted framework is Electromagnetic Topology (EMT) [2], introduced by Baum to approximate the EM behavior of a system. A probabilistic risk analysis for systems was discussed in [3]; moreover, the feasibility of such detailed methodology remains challenging in practical cases.

In this contribution we discuss the combination of the EMT philosophy together with a systematic characterization of waveforms as given in [4]. Moreover, Machine Learning (ML) architectures are leveraged in order to provide non-intuitive solutions the EM susceptibility problem.

II. HIGH LEVEL ELECTROMAGNETIC SUSCEPTIBILITY:

One of the main goals of EM susceptibility studies is to understand whether or not a system is vulnerable in an IEMI environment, e.g. what are the chances that the system will fail (functional damage or operational upset). The end goal is decomposed in a hierarchy, thus adding more specific requirements with each level's depth, as shown in Fig. 1:

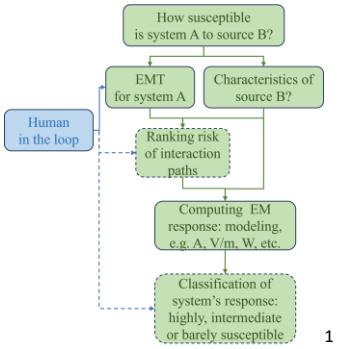

Figure 1. Decomposition of the high level question "How susceptible is system A to source B".

A possible (but fairly typical) workflow in order to determine the susceptibility of a system is shown in Fig. 1. The high level electromagnetic susceptibility (HLEMs) idea is then to merge systematic knowledge of waveforms (e.g. [4]) and systems (i.e. EMT [2]), existing modeling capabilities and a priori data of the system's response, in order to build an incremental ML system (thus improving as more data becomes available), that is able to produce a level of susceptibility (e.g. high, intermediate or low) given system's and source's features [5], as shown in Fig. 2:

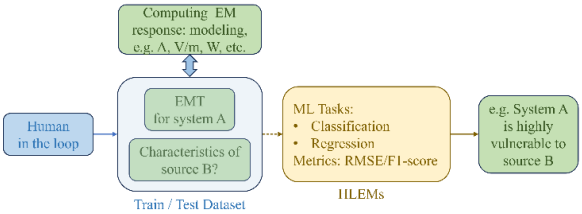

Figure 2. Schematic of the HLEMs framework.

REFERENCES

[1] N. Mora, "Contribution to the study of the vulnerability of critical systems to Intentional Electromagnetic Interference (IEMI)", Ph.D. dissertation, École Pol. Féd. De Lausanne, Lausanne, Switzerland, 2016.

[2] C. E. Baum, "Electromagnetic Topology: A Formal Approach to the Analysis and Design of Complex Electronic Systems," Interaction Note 0400, Sep 1980.

[3] E. Genender, H. Garbe, F. Sabath, "Probabilistic Risk Analysis Technique of Intentional Electromagnetic Interference at System Level", *IEEE Trans. On Electromagnetic Compatibility,* vol. 56, pp. 200-207, 2014.

[4] N. Mora, F. Vega, G. Lugrin, F. Rachidi, and M. Rubinstein, "Study and Classification of Potential IEMI Sources", System Design and Assessment Notes, vol. 41, 2014.

[5] C. M. Bishop, "Pattern Recognition and Machine Learning", New York: Springer, 2006.

This research is funded by TNO research program V2356.

Estimating Radiation from Pulsed Power Sources

R. Kooij[2], M.A. Echeverri Bautista[1], A.P.M. Zwamborn[2]
(1) TNO, Electromagnetic Signatures & Propagation Dept.
(2) TNO, Electronic Warfare Dept.
The Hague, The Netherlands.
roeland.kooij@tno.nl

Abstract – In this paper the radiated electric field by a spark gap switched dipole antenna is estimated. These back-of-the-envelope estimations are very useful for High Power Electromagnetic (HPEM) and Electromagnetic Pulsed power (EMP) measuring campaigns, where an initial assessment of the expected peak levels of radiated fields are required. The calculations are compared with full-wave simulations and different metrics for the evaluation of analytic approximations will be discussed.

Keywords – Estimation, High Power Electromagnetics (HPEM), Electromagnetic Pulse (EMP), spark gap, dipole antenna, measurement.

I. INTRODUCTION

With a growing demand for HPEM technology, such as for the use in Directed Energy Weapons (DEW), validation via measurements proceeds at a fast pace. Whether it is for studying the development of- or protection against HPEM/EMP sources, in all cases it is important to safely measure EM fields. HPEM/EMP can cause damage to electronic equipment, including measurement equipment such as oscilloscopes and spectrum analyzers. In this contribution, an estimation method is evaluated for radiated field strengths by a spark gap switched dipole antenna [1]. This type of radiator is simple in design and can easily be used to verify a measurement setup for HPEM/EMP measurements.

II. ANALYTICAL MODEL

This work estimates the radiated field by a spark gap switched dipole antenna, shown in Fig. 1. First the antenna input signal is estimated based on IEC 62000-4-2 stating the rise time of Electrostatic Discharge (ESD) to be 0.8 ns. The spark gap of the antenna is 2 mm. Using the breakdown voltage of air, the signal is estimated as a double exponential pulse with a rise time of 0.8 ns, fall time of 3 ns and peak voltage of 6 kV. Making use of Ohm's law, the radiated electric far-field of a half-wave wire dipole is given in (1).

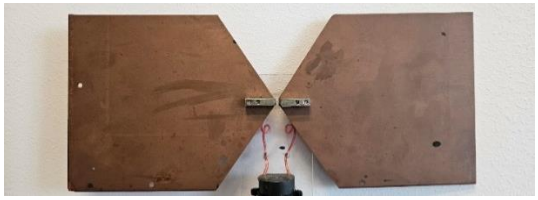

Figure 1. Spark gap switched wideband dipole antenna.[1]

$$|E_\theta| = \frac{60*I_0}{r}\frac{cos\left(\frac{\pi}{2}cos\theta\right)}{sin\theta} = \frac{60*V_0}{r*73.1}\frac{cos\left(\frac{\pi}{2}cos\theta\right)}{sin\theta} \quad (1)$$

Additionally, the radiated electric field is related to the input voltage as a constant by using the Figure of Merit, see (2).

$$FoM = \frac{E_p*r}{V_{in}} \quad (2)$$

At 2m distance this results in a peak electric field of 2.46 kV/m, hence the FoM = 0.82 which is comparable to other HPEM radiators listed in [2].

III. CST SIMULATION

The antenna in Fig. 1 was modelled in CST and simulated by applying the aforementioned double exponential pulse. An E-field probe at 2m distance broadside to the antenna calculated the field given in Fig. 2. The E-field peaks at 650 V/m, resulting in a FoM of 0.22, which is 26% or about -6 dB of the analytical value given previously.

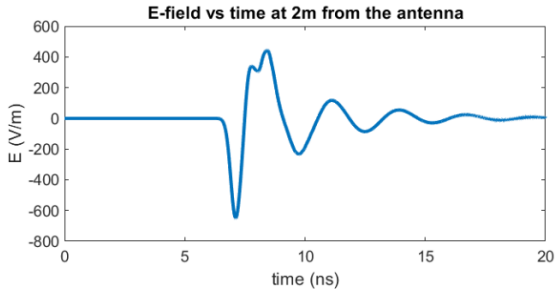

Figure 2. Simulated field at 2m distance from the antenna.

REFERENCES

[1] J. Ryu and J. Lee, "An Integrated Antenna-Source System of Very High Ultra Wide-Band Gain for Radiating High-Power Wide-Band Pulses," in IEEE Transactions on Plasma Science, vol. 40, no. 4, pp. 1019-1026, April 2012

[2] R. S. Doma and S. Azeemuddin, "Radiation of High-Power Fast Rise Time Pulses by Hydrogen Spark Gap Antenna at a High Repetition Rate," in IEEE Transactions on Plasma Science, vol. 49, no. 2, pp. 648-655, Feb. 2021

[1] Special thanks to G. de Vries BSc of the Dutch Authority for Digital Infrastructure for providing this antenna.

Relativistic Magnetron With TE11 Output Mode Using Upstream Cavity Walls

Frans Nyberg, Pablo Vallejos, Mattias Elfsberg,
Alan Aliyali, Tomas Hurtig
Weapons, Protection and Security
Swedish Defence Research Agency, FOI
Stockholm, Sweden
frans.nyberg.zou@foi.se

***Abstract*—**In the previous simulation studies [1], it is shown that the efficiency of the relativistic magnetron (RM) is higher when the radius of the input coaxial line that connects to the slow-wave structure is smaller. This study shows that it is due to the introduction of anode walls at the upstream boundary when using a smaller input coaxial line. To verify this effect, the RM is simulated with a larger input coaxial line and anode walls are added using a funnel-shaped structure at the junction between the coaxial line and slow-wave structure.

Keywords-high power microwaves; relativistic magnetron; diffraction output; TE11 mode; particle-in-cell

I. INTRODUCTION

The relativistic magnetron (RM) is a GW-class high power microwave source [2]. Using cold-cathode technology, emitted electrons interact with electromagnetic modes in a six-cavity slow-wave structure to generate microwaves. The microwaves propagate through the diffraction output in Fig. 1 (right). By having a diffraction output with two small and four large cavities, the π-mode is converted into a TE11-mode [1], [3]. In this study, particle-in-cell simulations are performed to study the junction between the coaxial line and slow-wave structure cavities. Upstream cavity walls are introduced using the funnel-shaped structure shown in Fig. 1 (left). The results are compared to a case where the funnel-shaped structure is tapered in alignment with the slow-wave structure cavities, thus removing the walls.

II. SIMULATION RESULTS

The simulated RM has axial magnetic field strengths of 0.26 T and 0.32 T, and voltages swept from 185 kV to 370 kV. Fig. 2 shows that when the walls are present, the efficiency is higher and can exceed 40% within certain voltage intervals. The peak output power at the highest efficiency when B = 0.32 T is 650 MW. The lower voltage limits are close to the Buneman-Hartree thresholds of 200 kV (at 0.26 T) and 254 kV (at 0.32 T) and the upper limits are well below the Hull cutoffs. The results show that when the funnel-shaped structure is applied, the efficiencies are similar to that of a small coaxial line in reference [1].

In conclusion, the main benefit of adding upstream cavity walls is maintaining a larger coaxial line (which has lower electric field strengths for a given voltage), while obtaining high efficiency.

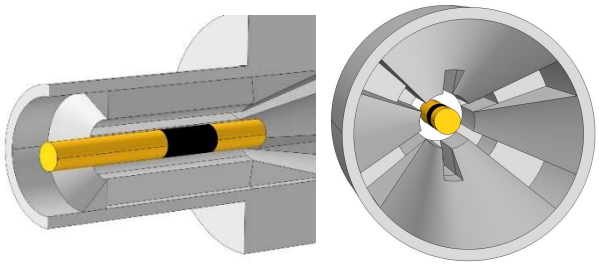

Figure 1. Relativistic magnetron model. The cathode is shown in yellow and the electron-emitting surface in black. (Left) Side view of the coaxial input line connecting to the slow-wave structure with a funnel-shaped structure placed in between. (Right) Upstream view of the diffraction output.

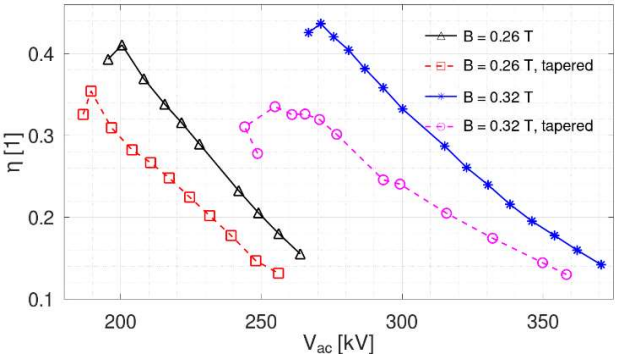

Figure 2. Efficiency η with respect to voltage V_{ac} for different magnetic field strengths. Solid lines correspond to the funnel-shaped structure, and dashed lines to a similar structure where the upstream cavity walls are removed.

REFERENCES

[1] F. Nyberg et al., "Development of a Relativistic Magnetron with TE11 Output Mode for High Power Microwave Applications," presented at the 2023 IEEE Pulsed Power Conf., San Antonio, TX, USA, Jun. 2023.

[2] M. I. Fuks and E. Schamiloglu, "70% Efficient Relativistic Magnetron With Axial Extraction of Radiation Through a Horn Antenna," IEEE Trans. Plasma Sci., vol. 38, no. 6, pp. 1302-1312, Jun. 2010.

[3] D. Sawert et al., "Modeling and optimization of a relativistic magnetron with transparent cathode and TE_{11} output mode," Int. J. Microw. Wireless Technol., Feb. 2024.

Direct Current Mode Stirred – A New Approach for the Correction Factor

Markus Rothenhaeusler
Airbus Defence and Space, Germany
EME Systems Engineering GE
85077 Manching, Germany
markus.rothenhaeusler@airbus.com

Martin Schwarz
Wehrtechnische Dienststelle für
Informationstechnologie und Elektronik
91171 Greding, Germany
martin2schwarz@bundeswehr.org

Alexander Schoisl
Airbus Defence and Space, Germany
Electronic Warfare
85077 Manching, Germany
alexander.schoisl@airbus.com

Abstract— The Direct Current Mode Stirred (DCMS) method is an innovative testing approach for replacing Radiated Susceptibility (RS) testing, that combines the benefits of Direct Current Injection (DCI), applied to test objects' surfaces, with those of a Reverberation Chamber (RC). The motivation behind this is to develop an efficient and cost-effective solution for high power electromagnetic RS tests. The proposed method has now already been applied to two different Equipment under Test (EUT) configurations with different lengths and diameters. The results show, that DCMS is highly efficient and generates comparable EMC effects. Additionally, a first attempt at formulating a Conversion Factor (CF) theorem, by the use of the antenna theory of equivalent surfaces, is presented. This promising CF shall convert the injected power in W of DCI into an equivalent external electrical field strength in V/m.

Keywords—DCI, Reverberation Chamber, DCMS, GENEC, GENEC XL, Conversion Factor

I. INTRODUCTION

The fundamentals of DCMS were already presented in [1]. Meanwhile DCMS has been tested with different EUTs, the GENEC (small generic missile) with a total length of 1.1 m and the GENEC XL (large generic missile) with a total length of 3.8 m. Results of DCMS with the GENEC have been published at EMC Europe 2023 in Krakow. The larger EUT, GENEC XL, has now also been integrated and tested with DCI, RC and a Semi Anechoic Chamber (SAC). The large amount of measurement data, gathered from both configurations, allowed for a deeper analysis and the introduction of a new Correction Factor (CF) theorem. This CF is not empirically based on measurement comparisons anymore, but on antenna theory of equivalent surfaces with injected power and includes mainly the geometrical dimensions of the EUT. This allows now, for the first time, to convert DCI susceptibility tests into RS tests by an equivalent antenna theory.

II. CORRECTION FACTOR

In [2] a CF was already introduced, but only calculated by comparison of the different measurement results. Nevertheless, the definition is still valid as:

$$k = \frac{E_{equ}}{\sqrt{P_{inj}}} \; in \; \frac{(V/m)}{\sqrt{W}} \tag{1}$$

In antenna theory the power density of an antenna radiation is defined by the equivalent surface A in m² and the injected Power P in W by the formula:

$$S = \frac{P}{A} = \frac{P_{inj}}{A_{EUT}} \tag{2}$$

The equivalent surface A can be interpreted for DCI as the surface A_{EUT}, which results in a power density S in W/m². Applying the general definition of power density and electrical field strength to (2) results in:

$$E_{equ} = \sqrt{S_{EUT} \cdot Z_0} = \sqrt{\frac{P_{inj}}{A_{EUT}} \cdot Z_0} \tag{3}$$

Now inserting (3) in (1) leads to the CF:

$$k = \sqrt{\frac{Z_0}{A_{EUT}}} \tag{4}$$

This CF is only dependent on the surface of the EUT, as the injected power is distributed over it. In future work the following restrictions have to be taken into account when applying (4) and corrections maybe necessary:

- During RC or SAC testing, when the EUT is in resonance, it may not have the same A_{EUT} as during DCI, due to different current nodes and bellies. A_{EUT} is therefore smaller for RC or SAC testing.
- The limited adaptation of the open coaxial return line to 50 Ω with minimum reflection levels S_{11} of 2-3 dB can cause standing waves which change A_{EUT}.
- The EUT in free space has different Eigenmodes than the EUT in the open coaxial return DCI system.

III. CONCLUSION

The CF from section II was applied to the measurement data from GENEC. The results appear promising and are briefly discussed below.

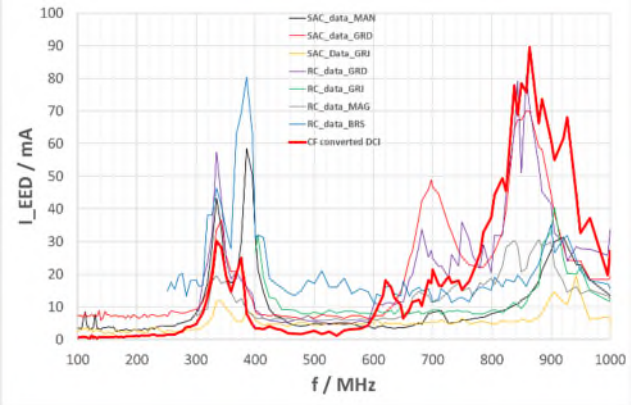

Figure 1. Correction Factor applied to GENEC result

Figure 1 shows the incoupling current into a wire loop of a sensor in the GENEC in mA versus frequency in MHz. They show a very good agreement of CF converted DCI and RC, SAC results, just at 700 MHz a peak is missing, but this was a ground reflection in the SAC and will be repeated. Also in the areas of 350 MHz the CF converted levels seem to be lower.

REFERENCES

[1] M. Rothenhaeusler, "Direct Current Mode Stirred – A new Susceptibility Test Method for EMC and HPEM", AMEREM 2018

[2] M. Rothenhaeusler, A. Ruhfass, T. Leibl: Broadband DCI as a multi usable EMC-test method, 2008 IEEE International Symposium on Electromagnetic Compatibility, Detroit, MI, 2008, pp. 1-5

Direct Current Mode Stirred - Simulation Results for an Open Coaxial Return Rig

Alexander Schoisl, Markus Rothenhäusler
Airbus Defence and Space, Germany
85077 Manching, Germany
alexander.schoisl@airbus.com

Martin Schwarz
WTD 81, EMV/EME (410)
91171 Greding
martin2schwarz@bundeswehr.org

Abstract— The Direct Current Mode Stirred (DCMS) test method is a combination of Direct Current Injection (DCI) with the resonant properties of a Reverberation Chamber (RC) to fulfill the high-level field requirements from 10 kHz - 18 GHz according to EMC standards. A series of measurements at various RC test sites is being undertaken to formulate a conversion theorem between injected power and equivalent external field strength, facilitating the establishment of DCMS as a standardized EMC test method in the future. This measurement campaign is supported by numerical simulations, which are the focus of this paper.

Keywords - Reverberation Chamber, DCMS, Numerical Simulation

I. INTRODUCTION

The computational electromagnetic (CEM) models used for this study were already introduced in [1] and [2], the measurement results are available from [3]. The core objective of this research is to compare the CEM simulation outcomes across the different operational modes, namely DCI, DCMS and RC operation, for a common cylindrical Equipment under Test (EUT), which is placed in an Open Coaxial Return Rig (OCRR). This comparison is achieved by analyzing the induced current into an electro-explosive device (EED), which serves as an indicator of potential interference effects on sensitive components. Furthermore, the evaluation extends to estimating the electric field strength within the EUT. These CEM simulations were conducted using three RC configurations, hereinafter named after the place where they are operated (Greding, Magdeburg, Linköping) and are compared to CEM simulations in free space.

II. SIMULATION RESULTS

Figure 1 depicts the simulation results for the maximum induced EED current for DCI, DCMS and RC operation. The current is normalized to $\sqrt{1\,\mathrm{W}}$ forward power, fed into the OCRR, for DCI/DCMS operation, whereas the RC result has been normalized to $\sqrt{4.2\,\mathrm{W}}$ forward power, injected into the chamber's field generating antenna, for direct comparison. This clearly emphasizes the promising efficiency of the DCI/DCMS method, compared to traditional RC operation. An excellent agreement of the

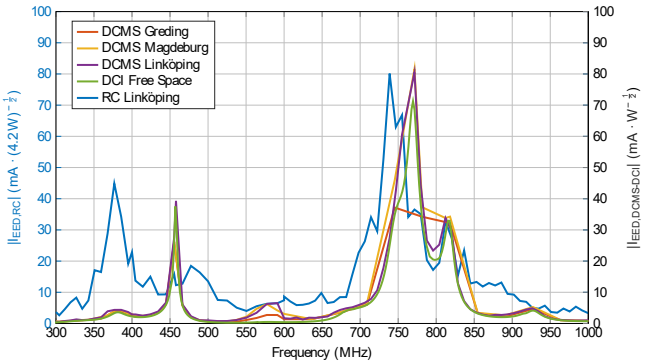

Figure 1. Comparison of max. induced EED current for different operation modes.

CEM simulation results between all DCMS, free space and DCI results can be observed. Since DCI and DCMS directly apply the interfering current directly onto the EUT, they require it to be placed in a return rig to match the generators wave impedance. During RC operation however, the OCRR is removed from the test setup. This change in boundary conditions is reflected in slightly shifted resonance frequencies, compared to DCI and DCMS excitation.

III. CONCLUSION

The findings from this study verified the CEM numerical models of different RC environments for the presented operation modes and serve as a baseline for CEM simulations with different EUTs in the future.

Appreciation goes to the German Customer WTD81 Greding GF410, who enabled this project as a Technology Demonstration.

REFERENCES

[1] A. Schoisl, M. Rothenhäusler, and M. Schwarz, "Computational Electromagnetics of Reverberation Chambers and an Open Coaxial Return Rig," in 2023 International Symposium on Electromagnetic Compatibility – EMC Europe, Sep. 2023, pp. 1–5.

[2] A. Schoisl, M. Rothenhäusler, and M. Schwarz, "Simulating an Open Coaxial Return Line in a Reverberation Chamber," in GlobalEM 2022 Abstract Book, Abu Dhabi, Nov. 2022, p. 33.

[3] M. Rothenhäusler et al., "Direct Current Mode Stirred – Susceptibility Testing Results of a small EUT and Comparison to RC and SAC Results," in 2023 International Symposium on Electromagnetic Compatibility – EMC Europe, Sep. 2023, pp. 1–6.

Simple Mathematical Models of Reflector IRAs with 2-Arm and 4-Arm Feeds

Everett G. Farr
Farr Fields, LC
Albuquerque, NM, USA
egfarr@gmail.com

***Abstract*—**While simple mathematical models are available for reflector Impulse Radiating Antennas (IRAs), they have not yet been cast into the form of the recently derived antenna equation. Doing so proves instructive, as it reveals properties that were previously obscured. We provide here simple mathematical models of 2-arm and 4-arm reflector IRAs, with feed arms positioned either vertically, or at ±45° to vertical. We cast these models into the form of the antenna equation, and we provide for each antenna its boresight impulse response, transfer function, and realized gain. To our surprise, the mid-band estimates for all these quantities are the same for both configurations. We provide an explanation for why that is a reasonable result. We also find that both 2-arm and 4-arm designs have an aperture efficiency of 30% for the typical values of input impedance of 400 Ω and 200 Ω, respectively.

Keywords-Impulse Radiating Antenna (IRA); antenna impulse response; antenna transfer function; realized gain.

I. INTRODUCTION

We provide here a simple estimate of fields and gain for a 2-arm IRA and a 4-arm IRA. In the case of a 4-arm feed, the feed arms are positioned orthogonally to each other at ±45° to vertical. The input impedance of the 2-arm IRA is nominally 400 Ω, and that of the 4-arm IRA is 200 Ω. Figure 1 shows the two configurations. We use these models to provide antenna impulse response, antenna transfer function, and realized gain. This paper is based on the results in [1]. We use [2] to calculate the antenna impulse response, antenna transfer function, and realized gain.

In practice, one generally uses a 4-arm configuration. However, it is useful to calculate both the 2-arm and 4-arm cases, as they provide a consistency check on the validity of both calculations.

II. DISCUSSION

At first, it seemed surprising that the 2-arm configuration provides roughly the same mid-band performance on boresight as the 4-arm configuration. Two questions immediately arise. 1) Is that a reasonable result? and 2) Why would one bother adding the second pair of arms if one gets the same result?

We start with the first question, concerning the reasonableness of the result. To demonstrate this, a bit of math is necessary, which will be provided in our presentation.

We next address the second question, the usefulness of the second pair of feed arms. We note three items. First, the impedance of sources tends to be lower than the impedance of antennas. Anything one can do to lower the antenna input impedance makes it easier to match the antenna impedance to the source impedance. Second, the radiated fields for a 2-arm configuration have a fan-shaped beam, wider in the H-plane and narrower in the E-plane. The beam shape for a 4-arm configuration is much closer to equal in the E- and H-planes. One normally prefers to have equal beamwidths in the E- and H-planes. Third, a common balun configuration is available at low power to match a 50-ohm feed to a 200-ohm antenna; no such balun is available for a 400-ohm antenna. For the above three reasons, 200-ohm antennas with four arms will continue to be popular.

III. CONCLUSION

We provide here simple calculations showing that the boresight performance of classical 2-arm and 4-arm reflector IRAs is approximately the same at mid-band and on boresight. An explanation for why that is reasonable is also provided. Both designs have an aperture efficiency of 30% for the typical values of input impedance of 400 Ω and 200 Ω, respectively.

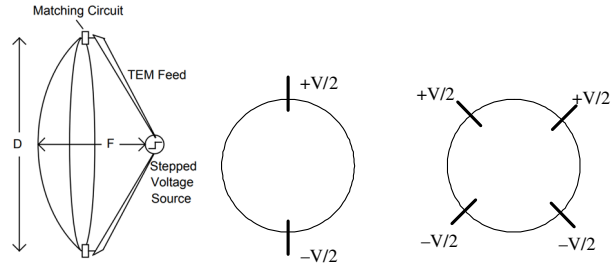

Figure 1. Sketch of a 2-arm IRA (left and center) and a 4-arm IRA (right).

REFERENCES

[1] E. G. Farr, "Simple Mathematical Models of Reflector IRAs with 2-Arm and 4-Arm Feeds," Sensor and Simulation Note 585, Summa Foundation, February 2023.

[2] Everett G. Farr, "Ten Fundamental Antenna-Theory Puzzles Solved by the Antenna Equation," *IEEE Antennas and Propagation Magazine*, February 2022, pp. 61-71.

Effect of Composite Absorbers Placed on Aperture Side within Enclosure on Shielding Effectiveness

Jong Hwa Kwon, Chang Hee Hyoung, Jung Hwan Hwang
Radio Research Division,
Electronics and Telecommunications Research Institute
Daejeon, KOREA, 34129
E-mail: hjkwon@etri.re.kr

Hyun Ho Park
School of Electrical and Electronic Engineering
The University of Suwon
Hwaseong, KOREA, 18323
E-mail: hhpark@suwon.ac.kr

Abstract — In this study, a lossy material such as a composite absorber is used to improve the shielding property of the metallic enclosure with an aperture. The composite absorber placed inside the enclosure serves to reduce the leakage field through an aperture and reduce standing waves inside the enclosure, thereby increasing the shielding effectiveness. The proposed method is verified by 3D numerical analysis.

Keywords - Shielding effectiveness, Metallic enclosure, Absorber, Aperture, Numerical Analysis

I. Introduction

Generally, metallic enclosures have been well known as a protection method used to electromagnetically shield and mechanically defend interior critical devices and components from external electromagnetic fields. However, practical considerations, such as air ventilation, power and signal cabling, and operator access, result in the presence of apertures or slots in the walls of the conductive enclosure. These apertures can compromise the shielding properties of the enclosure and negatively impact its ability to protect against external electromagnetic fields. To minimize this adverse effect, the design of shielding enclosures with apertures must consider the electromagnetic coupling mechanism through these apertures. [1]-[3]

The shielding performance of the conductive enclosures is determined by three elements as shown in Eq. (1). Shielding by reflection (R), absorption (A), and multiple reflections (B) is the effect of the material itself, and shielding by leakage and resonance is the effect of the structure. [1]-[3]

$$SE = (A+R+B)\text{-Leakage Effect-Standing-wave Effect} \quad (1)$$

This study proposes that a composite absorber be intentionally placed on an aperture side within enclosure to enhance its shielding property. The proposed structures for improving the SE of an enclosure with apertures is analyzed and verified by numerical analysis.

II. Propose Structure with Composite Absorber

A structure for analyzing the shielding properties of the enclosure with a composite absorber is shown in Fig. 1. The size of the shielding enclosure made of 3 mm thick PEC is 0.6 m × 0.5 m × 0.8 m. An aperture(100 mm × 10 mm) is placed vertically in the center of the enclosure's front panel. As an incident field for calculating the electric field within the enclosure with aperture, the plane wave is used with an electric field of horizontal polarization perpendicular to the aperture direction and traveling in the direction of the enclosure. The electric field was calculated in the frequency band of 1 MHz to 3 GHz at the center of the enclosure.

In this study, the 2 layer-typed absorber made with dielectric and magnetic absorbers is used. A dielectric absorber is the Eccosorb LS 26, and a magnetic one is FSA300 series, which is made by Laird[4] and provided the material data by CST Studio.[5]

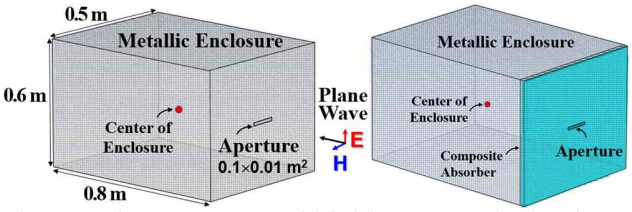

Fig. 1. Enclosure structure with/without magnetic absorber

III. Simulation Results

Fig. 2 shows the simulated results of SE according to the type of a composite absorber. Two different absorbers (LF26 + FSA300, FSA300 + LF26) with total 20 mm thickness were used. The effect of two absorbers on SE is similar, and SE is calculated to be more than 40 dB in the entire frequency band. The higher the absorption performance of the absorber, the higher the SE, and the higher the frequency, the higher the SE.

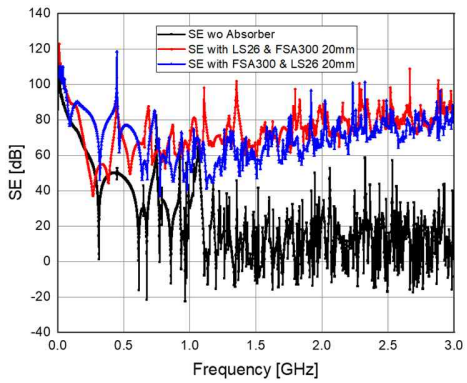

Fig. 2. Simulated Result of SE due to a composite absorber

IV. Conclusion

In this study, in order to improve the shielding property of metallic enclosures with apertures, the use of a composite absorber on the side with the aperture within an enclosure has been proposed and validated through numerical simulations.

Acknowledgment

This work was supported by IITP grant funded by the Korea government (MSIT) (No. 2020-0-00917)

Reference

[1] H. W. Ott, Electromagnetic Compatibility Engineering, 1st Ed., John Wiley & Sons, Inc, 2009
[2] C.R. Paul, Introduction to Electromagnetic Compatibility, 2nd Ed., John Wiley & Sons, Inc, 2006
[3] JH Kwon, CH Hyoung, JH Hwang, and HH Park, "Enhancement in Shielding Effectiveness by Electromagnetic Absorbers Applied to Aperture of Metallic Enclosure," The JKIEES, vol. 34, no. 5, pp. 409-414, May 2023.
[4] Laird, www.laird.com
[5] CST Studio, www.cst.com

Fusion of Parameterized and Physics-oriented Statistical Surrogate Models for EM Coupling on Wires in Complex Enclosures

Shen Lin, Zhen Peng
Electrical & Computer Engineering Department
University of Illinois Urbana-Champaign
Urbana, IL, USA
shenlin2, zvpeng@illinois.edu

Abstract — This paper presents a novel method in statistical electromagnetics for studying high-frequency coupling on wires installed in complex electronic enclosures. Our study involves the integration of two distinct types of statistical surrogate models: parameterized models, which are based on predefined parameter spaces for internal wire/cable components, and physics-oriented statistical models, which leverage statistical representations of cavity eigenfunctions and eigenvalues. The fusion of parameterized and physics-oriented statistical surrogate models results in a comprehensive and versatile statistical analysis framework, addressing the complex details and variability present in real-world electronic systems.

Keywords - Gaussian process, principal component analysis, statistical analysis, stochastic Green's function

I. INTRODUCTION

Recognized by many scientists and engineers in our research community, understanding the EM coupling to wires and cables in complex EM environments poses a challenging task. The problem often involves various aspects of uncertainties. In many instances, precise interior information (wire/cable location and routing, length and radius of the wire, load impedances at the termination, etc.) may be lacking. On the other hand, the high-frequency EM fields inside electronic enclosures are highly sensitive to the exact geometry of the enclosure, the location of internal sensors and electronics, and the operating frequency.

Our research objective is to develop a comprehensive stochastic modeling framework for the uncertainty quantification (UQ) of the field-to-wire coupling, considering both *component-level* and *environmental* uncertainties. Addressing this challenging high-dimensional UQ problem involves integrating two distinct yet complementary approaches for developing statistical surrogate models: parameterized models tailored to internal wire and cable components, and physics-oriented statistical models accounting for complex cavity environments. An overview of the proposed work and numerical ingredients is given in Fig. 1.

II. METHODOLOGY

In addressing cavity interior uncertainties, we utilize the stochastic Green's function [1] for modeling EM wave physics inside electronic enclosures without delving into complex details of the interior structures. The SGF acts as a physics-oriented, statistical surrogate model for the vector wave equation in large, complex enclosures, based on a statistical representation of the cavity eigenfunctions and eigenvalues through random wave model (RWM) and random matrix theory (RMT).

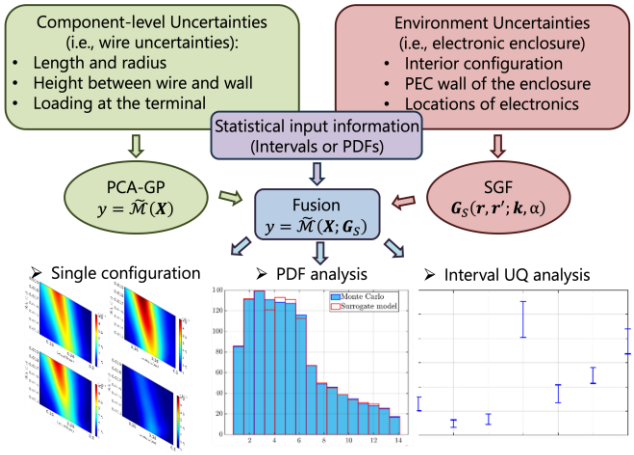

Figure 1. An overview of the proposed work.

The component-level uncertainties involve wire parameters such as length, radius, transmission line parameters, and load impedances at the terminals. While we may know the range of these parameters, their exact values remain unknown. A Gaussian process modeling method [2] is employed to predict these component-level uncertainties.

The fusion of parameterized and physics-oriented statistical surrogate models enables the prediction of EM coupling to ***stochastically*** defined conducting wires within a ***statistical*** cavity environment. To enhance computational efficiency, we propose the use of Principal Component Analysis (PCA) transformation to compress data from an ensemble of cavity configurations, allowing GP modeling of input-output relationships on reduced subsets of cavity environments. The proposed work has been validated numerically, including the commercial software and traditional Monte Carlo simulation.

REFERENCES

[1] S. Lin, S. Luo, S. Ma, J. Feng, Y. Shao, Z. B. Drikas, B. D. Addissie, S. M. Anlage, T. Antonsen, and Z. Peng, "Predicting statistical wave physics in complex enclosures: A stochastic dyadic green's function approach," IEEE Trans. Electromagnetic Compatibility, vol. 65, no. 2, pp. 436–453, 2023.

[2] P. Manfredi and R. Trinchero, "A data compression strategy for the efficient uncertainty quantification of time-domain circuit responses," IEEE Access, 8, 92019-92027, 2020.

Magnetron operating frequency change due to cathode expansion effect by the electron layer

Dong-Hyun Oh
Telecommunication Engineering Dept.
Jeju National University
Jeju City, Republic of Korea
odh054@gmail.com

Jung-Hoon Han
Dept. of Electr. Electron. Eng.
Korea Aerospace University
Goyangsi, Korea, Republic of
jh.han@kau.ac.kr

***Abstract*—When the magnetron operates, the cathode appears to expand due to the electron layer surrounding it. When the cathode expands, the cutoff frequency of the magnetron operating mode decreases. To demonstrate this, we conducted a simulation, where the cutoff frequency of the mode was around 2.526 GHz, and the operating frequency was 2.496GHz. The operating frequency of the mode cannot be lower than the cutoff frequency. This indicates that when the magnetron operates, the cathode radius expands, resulting in a decrease in the cutoff frequency. When the cathode radius is expanded from 1.0cm to 1.5cm, for the first time, the cutoff frequency becomes lower than the operating frequency. This indicates the minimum size at which the cathode radius is expanded.**

Keywords-magnetron; interaction region; admittance; electron charge density; cathode expansion.

I. INTRODUCTION

One of the high-power oscillators, the magnetron, consists of a cathode and an anode. Electrons in the magnetron undergo trajectory motion within the interaction region between the cathode and anode due to Lorentz force. These trajectories of electrons form an electron layer around the cathode, which electrically enlarges the cathode radius compared to its actual size. This paper investigates the effect of cathode radius expansion on magnetron performance and the minimum size at which the cathode can be expanded.

II. CHANGE IN CUTOFF FREQUENCY AS FUNCTION OF THE CATHODE RADIUS

A. Admittance of Cavity and Interaction Region

The cutoff frequency of the mode formed in the magnetron can be determined by the following equation [1].

$$Y_{cav}(f) = Y_{coax}(f). \quad (1)$$

Here, Y_{cav} means the admittance of cavity, and Y_{coax} means the admittance of interaction region formed in a specific mode. And the cutoff frequency is the point where the two-admittance values match. The cutoff frequency f_c is influenced by the radius of cathode, and as the cathode increases in size, f_c decreases. Fig 1. shows f_c as a function of cathode size, and r_c represents cathode radius.

B. Cathode expansion due to magnetron operating

When magnetron operates, the cathode radius appears to expand due to the electron layer around it. Fig. 2 shows the expansion effect of cathode radius. Left figure`s red line graph means magnetron`s operating frequency of 2.496GHz, and in the same mode, the f_c is 2.52585GHz. Since the operating frequency is lower than f_c, it can be inferred that the cathode has expanded. The right figure represents f_c of magnetron where r_c is expanded from 1.0cm to 1.5cm in the same mode. As the cathode has increased in size, f_c has decreased to 2.4924GHz. This value is smaller than the operating frequency of the magnetron, indicating the minimum size at which the cathode can be expanded.

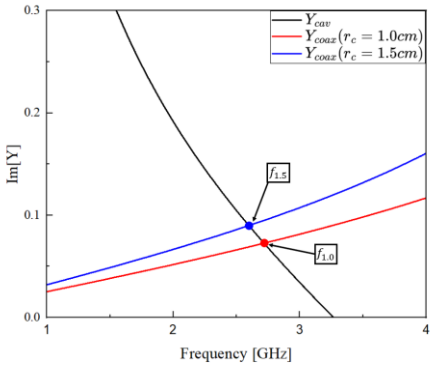

Figure 1. Change of cutoff frequency as cathode size.

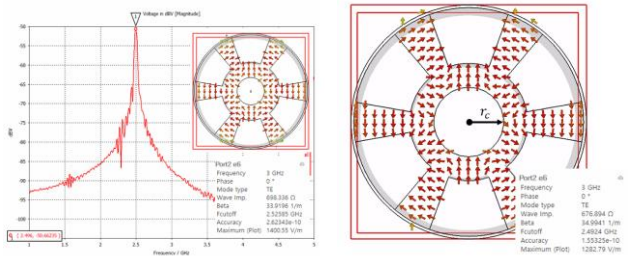

Figure 2. Expansion effect of cathode due to magnetron operating.

REFERENCES

[1] Vyas, Sandeep Kumar, Shivendra Maurya, and Vindhyavasini Prasad Singh. "Electromagnetic and particle-in-cell simulation studies of a high power strap and vane CW magnetron." *IEEE Transactions on plasma science* 42.10 (2014): 3373-3379.

Safety Advantages of Distributed Transmissions

B Petit, R Hoad, and P Sonigra
QinetiQ Ltd, Farnborough, Hampshire, GU14 0LX, UK
bjpetit@qinetiq.com

Abstract—Coherent, distributed High Power Radio Frequency (HP RF) transmissions are being developed and used for an increasing number of applications. This paper presents pros and cons of using coherent, distributed transmissions, focusing on safety related to electromagnetic fields (EMF). The types of HP RF hazard to consider are presented with reference to electric field limits. A comparison is drawn between monolithic systems and distributed systems providing the same power, highlighting the difference in coverage areas and field levels off target.

Keywords-High power RF, Coherent transmissions, EMF safety, distributed wireless power transfer, directed energy.

I. INTRODUCTION

High Power Radio Frequency (HP RF) transmissions are being developed and used for a number of applications, including; wireless power transfer, radio frequency directed energy (RF DE) systems, and satellite communications. As processing power and the availability of control systems increases over time, the option of using coherent, distributed transmissions has become more attractive. This paper presents pros and cons of using coherent distributed transmissions for HP RF applications, with a particular focus on safety related to electromagnetic fields (EMF).

II. EMF SAFETY

A. *EMF Hazards to Consider*

The primary EMF hazards to consider when assessing the safety of outdoor transmissions include:

- Humans
  - Control of Electromagnetic Fields at Work Regulations (UK legislation) [1]
  - International Commission for Non-Ionizing Radiation Protection (ICNIRP) Guidelines [2]
  - Directive 2013/35/EU [3]
- Safety Critical Electronics
  - Residential electronics and light industrial [4]
  - High Intensity Radiated Fields (HIRF) Environments [5]
- Flammable Atmospheres [6]
- Electro-explosive Devices (EEDs) [7]
- Interference to Radio Equipment (OfCom) [8]

B. *Safety Calculations*

The majority of standards present peak field limits, but safety aspects for humans are primarily concerned with average power. Consequently, if the signal being assessed is pulsed or heavily modulated, time averaging should be considered, as directed by the respective standard. This includes consideration of operational duty cycle, in addition to the signal or intra-burst duty cycle.

III. COMPARISON OF TRANSMISSIONS

A monolithic system risks transmissions straying into areas where EMF should be excluded, particularly if the system is isotropic or steerable over a range of angles. Distributed transmitters operating at lower power may be able to provide coverage over the required area whilst limiting fields away from exclusion zones (Figure 1).

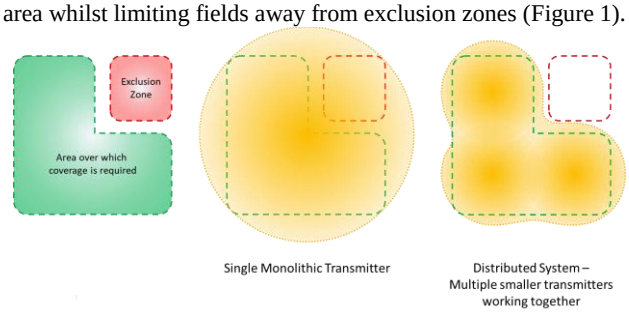

Figure 1. Power Coverage Control

The fields from monolithic systems may stray beyond the target in order to deliver enough power. A distributed system of lower power transmitters could deliver the same power to the target in a focused approach, meaning the EMF would dissipate at a faster rate beyond the target (Figure 2). The propagation of EMF relates directly to the assessments against the different RF hazards presented in Section IIA.

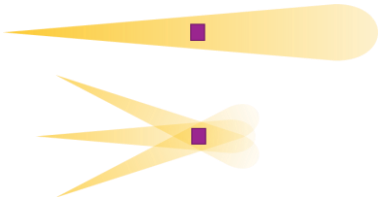

Figure 2. Power Dissipation Comparison

REFERENCES

[1] The Secretary of State, "The Control of Electromagnetic Fields at Work Regulations 2016," STATUTORY INSTRUMENTS, 1st July 2016. [Online]. Available: https://www.legislation.gov.uk/uksi/2016/588/made. [Accessed 14 July 2021].

[2] International Commission on Non-Ionizing Radiation Protection (ICNIRP), "ICNIRP Guidelines for Limititing Exposure to Electromagnetic Fields (100 kHz to 300 GHz)," Health Phys 118(5): 483-524; 2020, 2020.

[3] "DIRECTIVE 2013/35/EU OF THE EUROPEAN PARLIAMENT AND OF THE COUNCIL of 26 June 2013 on the minimum health and safety requirements regarding the exposure of workers to the risks arising from physical agents (electromagnetic fields)," *Official Journal of the European Union*, vol. L 179, no. 1, p. 1 to 21, 2013.

[4] British Standards Institution, "Electromagnetic compatibility (EMC) Part 6-1: Generic standards - Immunity standard for residential, commercial and light-industrial environments," British Standards Institution, 2019.

[5] Federal Aviation Administration, "High-Intensity Radiated Fields (HIRF) Protection for Aircraft Electrical and Electronic Systems," Department of Transportation, 2007.

[6] European Standards, "BS 6656:2002 Assessment of inadvertent ignition of flammable atmospheres by radio-frequency radiation. Guide," British Standards Institution, 2002.

[7] European Committee for Electrotechnical Standardization, "Assessment of inadvertent initiation of bridge wire electro-explosive devices by radio-frequency radiation – Guide," Cenelec, Brussels, Belgium, 2004.

[8] Ofcom, "Interference to radio equipment," Ofcom, 2024. [Online]. Available: https://www.ofcom.org.uk/spectrum/interference. [Accessed 29th February 2024].

A Technique for Coherent Distributed Wireless Power Transfer to a Non-Communicative Receiver

B Petit, R Hoad, and C Stokes
QinetiQ Ltd, Farnborough, Hampshire, GU14 0LX, UK
bjpetit@qinetiq.com

Abstract—Coherent, distributed wireless power transfer allows for energy to be delivered to a system in an efficient manner over a wide area. Most techniques rely upon either a steering signal (pilot beam) or feedback from the receiver. This paper presents a technique that has been developed for when the receiver is non-communicative, named Phase Alignment of Coded Echoes (PACE). The technique has been mathematically modelled and laboratory testing has been planned, which will use a bespoke test rig.

Keywords-component; Distributed Wireless Power Transfer, Coherent Combination, Non-communicative Receiver, Phase Alignment of Coded Echoes (PACE).

I. INTRODUCTION

A number of Distributed Wireless Power Transfer techniques have been demonstrated but usually rely upon either a steering signal (pilot beam) [1-4] or information feedback [5-9]. Other techniques, such as energy harvesting, do not create coherent combination of the distributed signals at the receiver [10-12]. This paper presents a technique for coherent, distributed wireless power transfer to a non-communicative receiver. The technique may be useful when the receiver does not have a transmission system, or does not have enough power to transmit.

II. PACE Technique Overview

Phase Alignment of Coded Echoes (PACE) aims to synchronize the signals from distributed power beacons in parallel at the point of the power receiver. This is achieved by each power beacon transmitting a carrier signal at the same frequency toward the power receiver. Each power beacon periodically modulates its signal using binary phase shift keying (BPSK) with a unique code, before resuming clear unmodulated transmission for maximum power transfer. The passive reflections from the power receiver are detected by each power beacon. Each power beacon picks out its own code from the reflected signals, along with that of the lead power beacon. The relative difference in time of arrival of the respective power beacons code with that of the lead beacon is then set as a phase offset for the respective power beacons. Subsequently, the modulated part of the signals from each power beacon should arrive at the same time at the receiver. If the phase of the carrier is tied to the modulation phase, this should synchronize the power beacons signals at the point of the power receiver.

III. VALIDATION

The technique has been validated through mathematical modelling using Matlab, see Figure 1. Region A shows the signals from the different power beacons arriving at the receiver. Region B is the period when the power beacons are adjusting the phases of their respective signals. Regions marked C illustrate coherent power transfer. Regions marked D illustrate repetitions of the modulated signals, retransmitted to maintain synchronization of the power beacons.

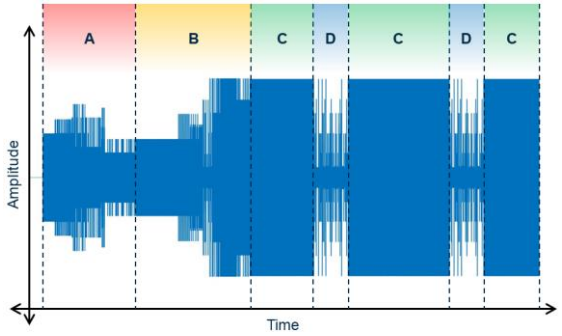

Figure 1. Mathematical Modelling of the PACE Technique

Figure 2 shows a test rig that has been developed for testing distributed wireless power transfer techniques using multiple power beacons. The rig makes use of multiple software defined radios, and uses a bespoke power receiver including rectenna circuits described in reference [13].

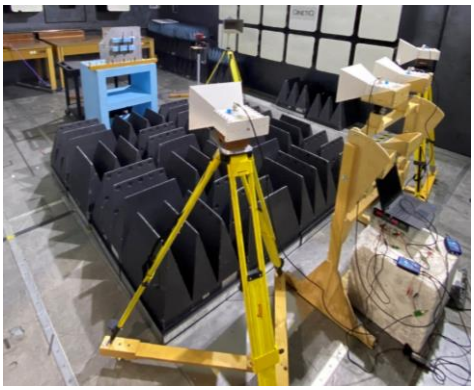

Figure 2. Laboratory Test Rig Setup

REFERENCES

[1] H. Ochiai, P. Mitran, H. V. Poor and T. Vahid, "Collaborative Beamforming for Distributed Wireless Ad Hoc Sensor Networks," IEEE TRANSACTIONS ON SIGNAL PROCESSING, vol. 53, no. 11, p. 4110 to 4124, 2005.

[2] Ossia, "Imagine a world where power is available everywhere," January 2018. [Online]. Available: https://cdn2.hubspot.net/hubfs/2870932/Ossia%20Overview%20Brochure.pdf. [Accessed 15th August 2019].

[3] J. He, X. Wang, L. Guo, S. Shen and M. Lu, "A Distributed Retro-Reflective Beamforming Scheme for Wireless Power Transmission," in IEEE AP-S, Vancouver, British Columbia, Canada, 2015.

[4] R. Mudumbai, G. Barriac and U. Madhow, "On the Feasibility of Distributed Beamforming in Wireless Networks," IEEE TRANSACTIONS ON WIRELESS COMMUNICATIONS, vol. 6, no. 5, p. 1754 to 1763, May 2007.

[5] R. Mudumbai, J. Hespanha, U. Madhow and G. Barriac, "Distributed Transmit Beamforming Using Feedback Control," IEEE TRANSACTIONS ON INFORMATION THEORY, vol. 56, no. 1, p. 411 to 426, 2010.

[6] Y. Fan, Y. Zhou, D. He and W. Xia, "Fast Transmit Beamforming With Distributed Antennas," IEEE ANTENNAS AND WIRELESS PROPAGATION LETTERS, vol. 16, p. 121 to 124, 2017.

[7] J. Xu and R. Zhang, "Energy Beamforming With One-Bit Feedback," IEEE Transactions on Signal Processing, vol. 62, no. 20, p. 5370 to 5381, 2014.

[8] K. W. Choi, L. Ginting, P. A. Rosyady, A. A. Aziz and D. I. Kim, "Wireless-Powered Sensor Networks: How to Realize," IEEE TRANSACTIONS ON WIRELESS COMMUNICATIONS, vol. 16, no. 1, p. 221 to 234, 2017.

[9] K. W. Choi, L. Ginting, D. Setiawan, A. A. Aziz and D. I. Kim, "Coverage Probability of Distributed Wireless Power Transfer System," in IEEE ICUFN, Milan, Italy, 2017.

[10] D. Mishra, S. De, S. Jana, S. Basagni, K. Chowdhury and W. Heinzelman, "Smart RF Energy Harvesting Communications: Challenges and Opportunities," IEEE Communications Magazine - ENERGY HARVESTING COMMUNICATIONS, p. 70 to 78, 2015.

[11] R. Vyas, B. Cook, Y. Kawahara and M. Tentzeris, "A Self-sustaining, Autonomous, Wireless-Sensor Beacon Powered from Long-Range, Ambient, RF Energy," IEEE, Georgia Institute of Technology, Atlanta, Georgia, USA, 2013.

[12] Powercast, "PowerSpot Images," Powercast, 2019. [Online]. Available: https://www.powercastco.com/products/powerspot/. [Accessed 14th November 2019].

[13] H. J. Long, F. Cheng, S. Yu, C. Gu and K. Huang, “High-efficiency broadband rectifier with compact size for wireless power transfer,” Microw Opt Technol Lett., vol. 2022, no. 64, pp. 2007-2013, 2022.

Refining Stochastic Green's Function with Short-Orbit Contributions

Sangrui Luo, Zhen Peng
Department of Electrical and Computer Engineering
University of Illinois Urbana-Champaign
Urbana, Illinois, USA
e-mail: sangrui2, zvpeng@illinois.edu

Abstract—This paper introduces a novel physics-oriented predictive model that combines stochastic and deterministic elements to analyze the electromagnetic (EM) coupling to complex cavities via openings. The key ingredient is an augmented stochastic Green's function (SGF) method, which elegantly incorporates short-orbit contributions into the cavity eigenfunction approximation. This enhancement notably improves the accuracy of statistical predictions for wideband EM coupling analysis.

Keywords: Chaos, electromagnetic coupling, Green's function, ray sensing, statistical analysis

I. METHODOLOGY

There has been a strong interest in the study of high-frequency wave physics in confined EM environments. Given the sensitivity of wave solutions to cavity details, it is crucial to develop statistical models accounting for the variations in field responses. Among related works in the literature, a stochastic Green's function (SGF) approach was introduced in [1] as an effective statistical solution to the wave equation in large, complex enclosures. Consider the 2nd order vector wave equation in a metallic cavity of volume V and cavity quality factor Q, the electric dyadic SGF is constructed from the eigenfunction expansion:

$$\overline{\overline{\mathbf{G}}}_{\mathrm{S}}(\mathbf{r},\mathbf{r}';k)=\sum_{m}\frac{\boldsymbol{\psi}_m(\mathbf{r})\otimes\boldsymbol{\psi}_m(\mathbf{r}')}{\left(k^2-k_m^2-j\frac{k^2}{Q}\right)} \tag{1}$$

where $\otimes$ indicates an outer product between two vectors. The $\boldsymbol{\psi}_m$ and k_m are cavity eigenfunctions and eigenvalues, derived from Berry's random wave model (RWM), considering orientations of polarization, and Wigner's random matrix theory (RMT), respectively.

It is noted that in the derivation of the SGF method, cavity eigenfunctions are locally modeled as an isotropic, random superposition of plane waves. The details of the geometry that affect the system-specific behavior (e.g. short-orbits) are dropped from the description. In this paper, we introduce a novel ray-sensing process to refine the RWM approximation of cavity eigenfunction. For illustration, we consider a scenario where a pair of source point r' and receiving point r, are located near the cavity wall with surface normal $\hat{n}$. To incorporate the direct bounce orbit contribution, the eigenfunction is adjusted as:

$$\boldsymbol{\psi}_m(\mathbf{r})=\widetilde{\boldsymbol{\psi}}_m(\mathbf{r})-\widetilde{\boldsymbol{\psi}}_m(\mathbf{r}_{\mathrm{i}})+2\hat{n}\hat{n}\cdot\widetilde{\boldsymbol{\psi}}_m(\mathbf{r}_{\mathrm{i}}) \tag{2}$$

where $\mathbf{r}_{\mathrm{i}}$ denotes the image position of $\mathbf{r}$ and $\widetilde{\boldsymbol{\psi}}_m$ is the normalized isotropic RWM without cavity boundary. A similar modification is derived for the eigenfunction $\boldsymbol{\psi}_m(\mathbf{r}')$. We can then show the mean value of the eigenfunction outer product in (1) as:

$$\langle\boldsymbol{\psi}_m(\mathbf{r})\otimes\boldsymbol{\psi}_m(\mathbf{r}')\rangle=-\frac{2\pi}{k_m V}\mathrm{Im}[\overline{\overline{\mathbf{G}}}_0(\mathbf{r},\mathbf{r}';k_m)-\overline{\overline{\mathbf{G}}}_0(\mathbf{r}_{\mathrm{i}},\mathbf{r}';k_m)+2\hat{n}\hat{n}\cdot\overline{\overline{\mathbf{G}}}_0(\mathbf{r}_{\mathrm{i}},\mathbf{r}';k_m)] \tag{3}$$

It is easy to prove that the expression inside the brackets essentially resembles the half-space Green's function, as in a two-ray ground-reflection model. The corresponding augmented SGF not only integrates the direct bounce orbit but also enforces the PEC boundary condition. The above procedure can be generalized to a finite number of orbits and complex cavity boundaries through a systematic ray-sensing process. We remark that our work naturally incorporates the cavity shape into the refinement of the cavity eigenfunction, in contrast to adding a deterministic ray tracing result to the statistical model in the literature.

II. NUMERICAL EXPERIMENT

The geometry of the test enclosure is given in Fig. 1. The mode stirrer is rotated through 12 positions over 360° in the full-wave simulation. The incident wave vector is (0, 0, −1), and the E-field is along the x direction. The *spatial-averaged* electric field intensity, |**E**c|, is calculated for each stirrer state from 0.5 to 2 GHz. The statistical prediction using the proposed work is also provided in Fig. 1. It's worth noting that the predictive model only uses the apertures and cavity boundary information, whereas the details of the mode stirrer are not required. As seen in the comparison, the predictive results accurately capture the frequency-dependent variation in the E-field amplitude.

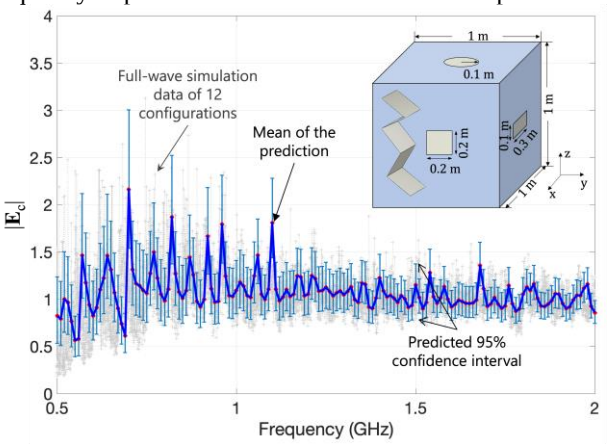

Figure 1. Statistical prediction of cavity spatial-averaged E-field

REFERENCES

[1] S. Lin, et al., "Predicting statistical wave physics in complex enclosures: A stochastic dyadic Green's function approach," *IEEE Trans. Electromagn. Compat.*, vol. 65, no. 2, pp. 436–453, 2023.

Electromagnetic Wave Propagation through Cavity Backed Pinholes

Dr.ir. Tom van Nunen
Electronic Warfare department
TNO
The Hague, The Netherlands
tom.vannunen@tno.nl

Abstract— Protection against electromagnetic weapons, such as HPM, requires a thorough analysis of the electromagnetic properties of the outer hull of the system. Apertures should be handled with care, and are to be kept small to prevent unwanted waves from penetrating the hull. However, this is not sufficient. Even when an aperture is electrically very small ($\ell << \lambda$), significant propagation is still possible when the volume behind the pinhole acts as an electromagnetic cavity resonator. Improvements of up to $(\lambda/\ell)^6$ compared to the non-resonant case can be achieved. This can have adverse consequences on the shielding effectiveness of the hull, and thus on the operation of the system. We present a model to predict the propagation through a resonator coupled pinhole.

Keywords- pinhole; shielding effectiveness; cavity resonator; aperture

I. INTRODUCTION

In the design of hulls of platforms like vehicles and ships, electromagnetic (EM) shielding is an important aspect. This protects the systems inside from possible hostile EM radiation outside, for example caused by a high power microwave (HPM) weapon. It might be assumed that small apertures, such as pinholes, are considered safe, as they are usually ill transmitters. However, when the aperture is connected to a resonator, the transmission can increase significantly at certain frequencies [1].

II. SIMULATION RESULTS

Simulations were performed on a 100×100 (h×Ø) mm cylindrical PEC cavity resonator, with a Ø 2 mm aperture, of which the natural TE_{111} resonance frequency f_{res} is 2.30952 GHz. The incident plane wave is 1 V/m, at a slight angle to ensure all modes are energized.

Fig. 1 shows the E-field inside the cavity at f_{res}, Fig. 2 shows them 10 MHz (0.431 %) off resonance. The field strength in the center of the cavity is given in Table 1. It can be seen that, at f_{res}, the field is significant. Furthermore, at an off-resonance frequency, the pinhole transmits hardly any energy, as expected. Just a few MHz off-resonance is sufficient to influence the transmission with tens of dBs. This effect might be detrimental to the system performance, and can be easily overlooked in both the design and testing phases.

TABLE I. FIELD STRENGTH IN CENTER OF CAVITY RESONATOR AT VARIOUS FREQUENCIES

Frequency	Max E-field	Δ f		Δ field
2.30952 GHz	-18.1 dBV/m	-	-	-
2.31102 GHz	-33.7 dBV/m	500 kHz	0.022 %	15.6 dB
2.31052 GHz	-39.1 dBV/m	1 MHz	0.043 %	21.0 dB
2.31252 GHz	-48.3 dBV/m	3 MHz	0.130 %	30.2 dB
2.31952 GHz	-58.5 dBV/m	10 MHz	0.431 %	40.4 dB
2.33952 GHz	-67.9 dBV/m	30 MHz	1.282 %	49.8 dB

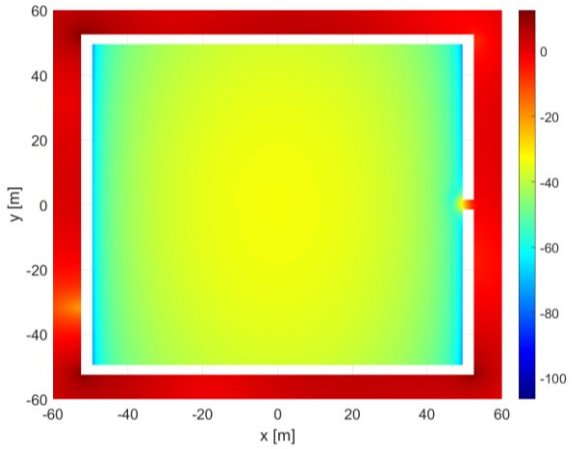

Figure 1. Simulated E-field inside the cylindrical cavity resonator at 2.30952 GHz, the TE_{111} mode.

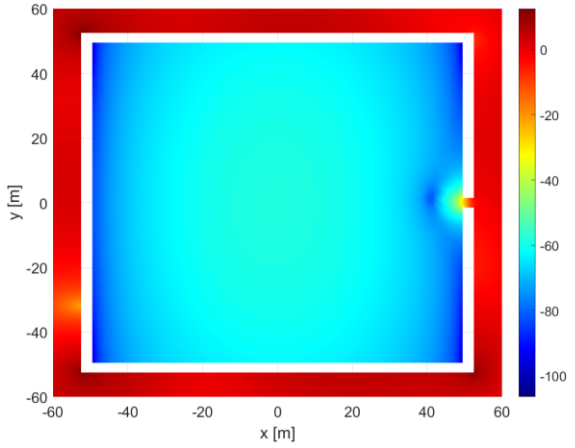

Figure 2. Simulated E-field inside the cylindrical cavity resonator at 2.31952 GHz, 10 MHz off resonance.

REFERENCES

[1] R. Merlin, "Pinholes Meet Fabry-Pérot: Perfect and Imperfect Transmission of Waves through Small Apertures," Phys. Rev. X, vol. 2, pp. 031015-1–031015-7, 5 September 2012.

Design of a HEMP Protection Power Filter To Meet MIL-STD-188-125-1A

Sergio N. Longoria
Technical Product Line Manager, RF Filters
ETS-Lindgren Inc., Cedar Park, Texas, USA
Sergio.longoria@ets-lindgren.com

Abstract—This paper discusses the criteria associated with the design of a power filter that can meet the new requirements of the revised standard MIL-STD-188-125-1A. The details of the new revised standard are ITAR controlled. However, this paper discusses what changes are needed on power filters in order to meet the new standard. We begin with the typical design considerations such as ratings, insertion loss and level of performance needed. The input circuitry of a HEMP power filter is of special consideration as this is what is called an ESA/Filter combination. We begin by discussing the type of filters and ESA circuit design considerations, selection of components, testing for E1, E2, and discuss further design considerations to meet the new standard.

I. THE HEMP FILTER AND ITS DESIGN

A. *The HEMP Power Filter*

In addition to a good protective shield, all conductors coming into the building should contain a combination Filter/ESA (Electronic Surge Arrestor). The ESA of choice is typically an MOV (Metal Oxide Varistor) because of its good combination of reaction time when mounted effectively, and energy handling characteristics. Power filters are composed of *LCR* elements, and at least in the USA, most filters for this application are Symmetric rather than Asymmetric. This is because a Symmetric filter can remove both CM (Common Mode) and DM (Differential Mode) noise. A typical filter will have an internal inductive input and an externally located ESA (Fig. 1)

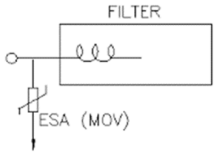

Fig. 1. Typical ESA/Filter combination.

That is because the ESA is meant to be replaced when needed. In this sense, the Filter/ESA can protect in only one direction. Thus, in addition to a good protective shield, all conductors coming into the building should contain a combination Filter/ESA (Electronic Surge Arrestor).

This makes the Filer/ESA suitable for use in mitigating both the E1 and E2 pulse effects. Because this electromagnetic event is a pulse, when reaching a conductor it will induce a fast rising current of up to 2500 Amperes as per MIL-STD-188-125. A fast-rising current generates a continued spectrum of frequencies ranging from a few kilohertz up to a few hundred Megahertz depending on the pulse's rate of rise (Fig.2). Because the MOV is a semiconductor that shunts current to ground, it is also necessary to address the pulse components in the frequency domain by means of a filter that will attenuate frequency components in a specified range. Any power filter design, in addition to providing the HEMP protection required, should also prove to be electrically safe. For this reason, HEMP filters undergo an assortment of tests such as hi-pot, insulation resistance, temperature rise, short circuit current, etc. Because the E2 pulse has a longer duration, the ESA must be selected to withstand the higher levels of energy present in an E2 pulse.

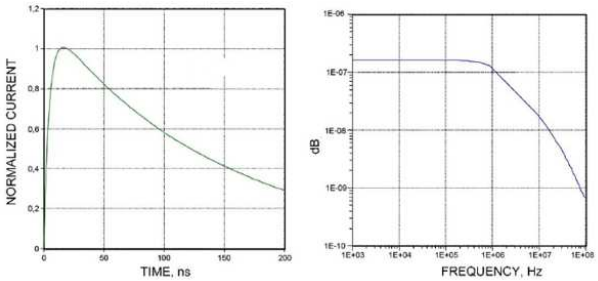

Fig. 2. E1 HEMP characteristics in the time and frequency domain.

B. *The HEMP Filter Design*

The typical power filter has a 2 or 3 Pi *LCR* circuit depending upon the type of filter required. In some cases, the filter is required to only perform to 80dB per MIL-STD-188-125-1. However, many applications require TEMPEST protection in addition to HEMP. These filters will require more components.

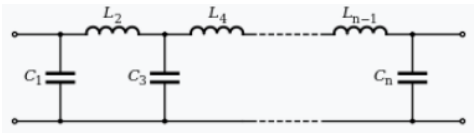

Fig. 3. *LCR* Filter component arrangement.

The selection of components is somewhat of a balancing act. The values of capacitance *C* must be kept from draining too much reactive current to ground. As the filter amperage rating increases, inductor values of *L* must decrease. This is to reduce power losses and avoid saturating the inductors—including the input inductor. A saturated inductor offers no performance advantages in terms of pulse and noise attenuation. The size and current rating of the inductors also dictate how big the enclosure housing needs to be to dissipate heat. Filter heat dissipation is typically achieved without the aid of external cooling measures.

C. *Meeting the New MIL-STD-188-125-1A*

In a nutshell, meeting the new standard with a TEMPEST filter means more inductance. Since lower current rated filters do have more inductance, it is possible that they may pass the new standard. But higher current filters with lower inductance will not. There are two approaches to meeting this problem. Either a complete re-design of the filter with higher inductance values, or a coil is added on the front end of existing designs.

Design of a 10 kbps and 128 kbps Data Filter with HEMP Protection

Sergio N. Longoria
Technical Product Line Manager, RF Filters
ETS-Lindgren Inc., Cedar Park, Texas, USA
Sergio.longoria@ets-lindgren.com

Abstract—This paper discusses the design criteria associated with the design of passive data filters with protection against a HEMP event. As is well known, in today's intercommunicated world, much of the electronic communications and controls take place over data wires. These wires can carry data in a myriad of formats and speeds. In this paper we specifically look at a 10kbps and 128kbps filter design with the express purpose of determining the protection performance of both against well-known standards such as MIL-STD-188-125-1. We begin by discussing the nature of the data, the passband needed and the pulse that the data wires need to be protected against. The paper will discuss the circuit design, selection of components, testing for E1, E2, and test results.

I. THE DATA FILTER AND ITS DESIGN

A. *The Data Signal*

A data signal typically is a square wave. Fourier transformation shows multiple sinewaves (Fig.1). Any complex wave can be broken down into sine waves that when added together give the original complex wave.

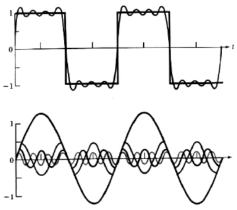

Fig. 1. Complex waves can be broken down into sine waves.

Thus, a data filter must be able to pass all the composite sine waves to reproduce at the other end the same square wave without loss of fidelity to the signal, or loss of information as it passes through the filter. When data is seen in the frequency domain, a fundamental (speed of transmission) and harmonics are seen (Fig.2.)

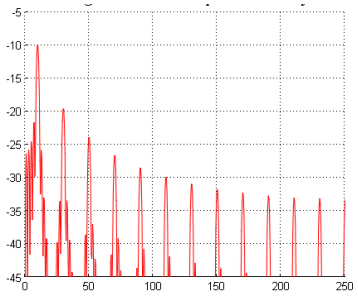

Fig. 2. Frequency domain view of a complex waveform.

A passive filter would allow multiple harmonics of the fundamental to pass through. It is considered enough to allow up to the 3rd harmonic of the fundamental for data fidelity; however, more is desirable.

B. *The HEMP Waveform*

The HEMP waveform or pulse shape is given in various well-known standards. This is essentially a double exponential pulse with an established rise time (Fig.3a.)

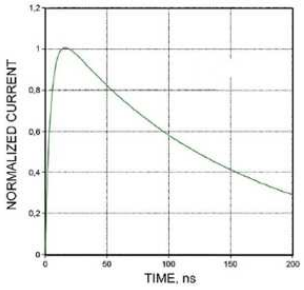

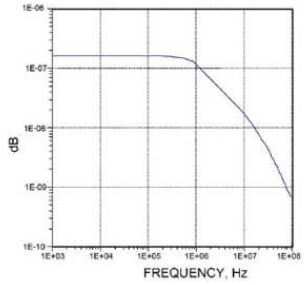

Fig. 3a. E1 HEMP waveform Fig. 3b. E1 HEMP frequency components

The composition of a signal like this shows that the pulse's rise time contributes to a continuous frequency component (Fig.3b). It is accepted that the typical HEMP waveform would generate continuous frequency components from a few kHz to about 300 MHz.

C. *Data Filter Design*

The typical filter may be designed as a Chebyshev or Butterworth filter with a flat passband (Fig.4).

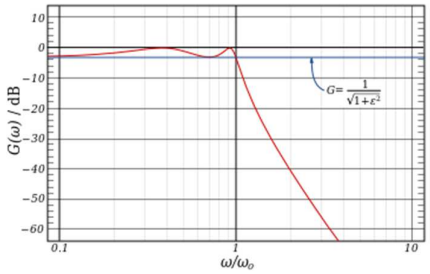

Fig. 4. Typical Chebyshev response

The selection of components is well known by using tables that can be scaled to accommodate the circuit impedances and number of elements according to the attenuation desired (Fig.5). Circuit impedance must be matched to minimize reflections and loss of signal. The filter should also have an inductive input impedance to work together with an ESA (Electronic Surge Arrestor) such as an MOV (Metal Oxide Varistor) or GDT (Gas Discharge Tube) selected to also absorb the energy of an E2 pulse.

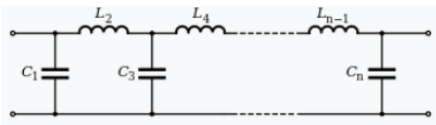

Fig. 5. *LCR* Filter component arrangement.

D. *Data Filter Testing*

In addition to the factory testing of a data filter, such as insertion loss and others, any initial design is subjected to E1 and E2 testing. This confirms if the design provides adequate protection by measuring the energy passing to the load. Most of the energy of a HEMP event will be in-band for a data filter. Thus, a 128kbps data filter with a wide passband up to 1 MHz will have trouble mitigating the pulse. The wider passband would typically result in greater power residuals (or transients) appearing in the data line which could still damage the system the filter intended to protect.

Collective Cherenkov Radiation Associated with Electron Beams and Amplification

Edl Schamiloglu
Department of Electrical and Computer Engineering
University of New Mexico
Albuquerque, NM 87131-0001, USA
edls@unm.edu

Alexander Figotin
Department of Mathematics,
University of California
Irvine, California 92697, USA
afigotin@uci.edu

Abstract—We have developed a convincing argument that the collective Cherenkov effect in traveling wave tubes (TWTs) is, in fact, a convective instability, that is, amplification. We also recover Pierce's theory as a high-frequency limit of our generalized Lagrangian theory. Finally, we derive for the first-time expressions identifying low- and high-frequency cutoffs for amplification in TWTs. This research is a promising path for developing very large bandwidth amplifiers.

Keywords – Cherenkov radiation, TWTs, high power microwaves.

I. INTRODUCTION

The collective Cherenkov effect is one of the fundamental mechanisms for stimulated emission of radiation from electron beams propagating in media with slow waves [1–3] such as in a traveling wave tube (TWT) [4]. It is well known that the mechanism of signal amplification in TWTs is based on the Cherenkov radiation effect occurring in dielectric media. Though some features of Cherenkov radiation depend on details of the dielectric environment, there is one feature that stands out as universal. This universal feature is manifested as a higher speed of the electron flow compared to the characteristic velocity in the dielectric medium.

II. CHERENKOV RADIATION

We have developed a convincing argument that the collective Cherenkov effect in TWTs is, in fact, a convective instability, that is, amplification. This argument is based on a first principles Lagrangian field theory, the details of which can be found in [5]. We study then fundamental limitations on the frequency dependence of the amplification in traveling wave tubes (TWTs). We find that there are low- and high- frequency cutoffs for the amplification. These frequency cutoffs depend on the two significant TWT parameters: (i) the ratio $\chi = \frac{\omega}{\dot{v}}$ of the phase velocity of the relevant mode of the slow wave structure (SWS) ω to the velocity of the electron flow $\dot{v}$; (ii) a single parameter γ that integrates into it as factors the intensity of the electron flow and the strength of its interaction with SWS. It turns out that $\gamma = 2\chi C_P^3$ where C_P is the Pierce gain parameter. We obtain explicit formulas describing the frequency cutoffs and their dependence on γ and χ. We also find that the amplification can occur when $\chi > 1$ and the TWT operational frequencies in this case are significantly higher compared to the conventional choice $\chi < 1$.

III. NEXT STEPS

We are extending this work into a very interesting direction. We are finding that the commonly imposed requirement of needing a "slow wave structure" demanding that the phase velocity of the "cold" waveguide be below the stationary velocity of the electron beam is not necessary for amplification. In fact, the amplification occurs regardless of whether the waveguide is a SWS. The case when the waveguide is not a SWS, in fact, leads to amplification at higher frequencies.

Work supported by AFOSR MURI Grant FA9550-20-1-0409.

REFERENCES

[1] M.V. Kuzelev and A.A. Rukhadze, "Stimulated radiation from high-current relativistic electron beams," Sov. Phys. Usp. 30, 507–524 (1987).
[2] M.V. Kuzelev and A.A. Rukhadze, "Mechanisms of spontaneous and stimulated emission of relativistic electron beams," in Problems of Theoretical Physics and Astrophysics (70th Anniversary of V.L. Ginzburg) (Nauka, Moscow, 1989), pp. 70–92.
[3] M.V. Kuzelev and A.A. Rukhadze, "Spontaneous and stimulated emission induced by an electron, electron bunch, and electron beam in a plasma," Phys. Usp. 51, 989–1018 (2008).
[4] J.R. Pierce, *Traveling-Wave Tubes* (D. van Nostrand, New York, 1950).
[5] E. Schamiloglu and A. Figotin, "The field theory of collective Cherenkov radiation associated with electron beams," Phys. Plasmas, vol. 31, 023101 (2024).
[6] E. Schamiloglu and A. Figotin, "Amplification limitations for traveling wave tubes" (in preparation, 2024).

Protection of High Voltage Power Grids from the High Altitude Electromagnetic Pulse (HEMP)

Dr. William A. Radasky
Metatech Corporation
Goleta, California, USA
wradasky@aol.com

Dr. Edward B. Savage
Metatech Corporation
Goleta, California, USA
savagee@cox.net

Abstract—This paper will review the increase in understanding of the high-altitude electromagnetic pulse (HEMP). There is new information being considered for both the E1 and E3 HEMP waveforms that will impact the protection of the critical infrastructures.

Keywords-High altitude electromagnetic pulse (HEMP), Early-time HEMP (E1), Late-Time HEMP (E3), International Electrotechnical Commission (IEC), HEMP Protection.

I. INTRODUCTION

In 1962 both the United States and the Soviet Union tested nuclear weapons in space to evaluate their impacts on radio communications and the effectiveness of using a nuclear detonation in space to intercept an incoming nuclear warhead, respectively. At that time both countries noted that commercial systems on the earth's surface under the bursts were affected in unexpected ways, and studies of the high-altitude electromagnetic pulse (HEMP) began.

II. RESULTS FROM THE U.S. EMP COMMISSION

After many years of research and due to the work of the US Congressional EMP Commission [1], more public discussion of the HEMP threat has occurred, and in 2019 a Presidential Executive Order [2] was published to ensure that the U.S. Government took steps to help commercial companies to protect the critical infrastructures from HEMP. These efforts have resulted in the publication of valuable technical reports and guidance for those responsible for protecting the critical infrastructures from loss of operation and damage. In 2021 the U.S. Department of Energy published a series of HEMP waveforms [3] to be used by the power industry and other critical infrastructures to evaluate their susceptibility to the HEMP. It is noted that the U.S. DOE has recommended the use of the IEC 61000-2-9 early- and intermediate-time waveforms and recommended an improved waveform for the late-time HEMP. The U.S. EMP Commission also recommended a new waveform for the late-time HEMP to be used to evaluate the vulnerability of the U.S. power grids [4]. These waveforms will be described so the reader can understand the complexities of the HEMP radiated environments.

III. TECHNICAL APPROACH

This paper will review the published studies dealing with the computation of the high-power electromagnetic fields generated by such bursts, their coupling to cables both inside and outside of buildings, the impacts on different types of electronics, the development of protection methods using techniques originally developed to achieve electromagnetic compatibility (EMC) for commercial products (e.g. IEC EMC standards), the development of specialized test methods to evaluate the protection methods and the development of international standards to document the best ways to protect and test equipment and facilities. With regard to the effects and protection methods, this paper will emphasize the high-voltage power grids throughout the world, although some effects can occur on medium voltage distribution grids.

This paper will review the work in the field from 1962 until today, with emphasis on the protection for:

- High voltage power system protection relays
- Other substation control electronics
- High-voltage transformers
- Medium-voltage line insulators

REFERENCES

[1] "Report of the Commission to Assess the Threat to the United States from Electromagnetic Pulse (EMP) Attack: Critical National Infrastructures," April 2008, http://www.empcommission.org/docs/A2473-EMP_Commission-7MB.pdf

[2] U.S. White House, Executive Order 13865 on Coordinating National Resilience to Electromagnetic Pulses, March 26, 2019; https://www.govinfo.gov/content/pkg/FR-2019-03-29/pdf/2019-06325.pdf

[3] Secretary of Energy Dan Brouillette to National Security Council Records, January 11, 2021, U.S. Department of Energy, "Physical Characteristics of HEMP Waveform Benchmarks for Use in Assessing Susceptibilities of the Power Grid, Electrical Infrastructures, and Other Critical Infrastructure to HEMP Insults," https://www.energy.gov/ceser/downloads/hemp-memo

[4] Recommended E3 HEMP Heave Electric Field Waveforms for the Critical Infrastructures, U.S. EMP Commission, July 2017, http://www.firstempcommission.org/uploads/1/1/9/5/119571849/recommended_e3_waveform_for_critical_infrastructures_-_final_april2018.pdf

Update of the IEC HEMP Environment Standard

Dr. William A. Radasky
Metatech Corporation
Goleta, California, USA
wradasky@aol.com

Dr. Edward B. Savage
Metatech Corporation
Goleta, California, USA
savagee@cox.net

Abstract—This paper describes the updates that are underway in the IEC to improve the HEMP Environment Standard, IEC 61000-2-9. The original document was published in 1996, but improvements in understanding have occurred in the early 2000s due to the work undertaken by the U.S. EMP Commission. The major updates are described in summarized form.

Keywords-High altitude electromagnetic pulse (HEMP), Early-time HEMP (E1), Late-time HEMP (E3), International Electrotechnical Commission (IEC), HEMP radiated fields

I. INTRODUCTION

The original edition of IEC 61000-2-9 (1996) [1] "Description of HEMP environment – Radiated disturbance," covered all three HEMP regimes, including the early-time, intermediate-time and late-time environments, with worst-case analytic waveforms provided to support protection efforts and testing. Since that time more information has become available mainly through the U.S. EMP Commission. This paper will review the improvements that are currently underway, with a possible publication date of December 2024. Due to the lack of space, each of the improvements will be listed, but the presentation will provide details.

II. E1 HEMP Variability

The first edition of IEC 61000-2-9 provided a single analytic worst-case E1 HEMP waveform. The second edition will provide additional waveforms that vary according to location on the earth, and in addition will show how a worst-case waveform can be constructed.

III. DEVELOPMENT OF A QEXP WAVEFORM

The first edition of IEC 61000-2-9 used the double exponential waveshape to describe the worst-case E1 HEMP waveform. As is well known, the analytic waveform is easy to use, but due to a discontinuous time derivative at $t = 0$, the waveform contains too much frequency amplitude above 200 MHz. While this point has been understood by most users of the standard, there have been cases where the waveform has been applied incorrectly. The real waveshape should be a quotient of exponentials, which has an exponential rise time and an exponential decay. A recommendation is provided as an option for those who need to deal with the higher frequency content.

III. FAR FIELD REGION FOR E1 HEMP

From time to time, there has been criticism or a lack of understanding concerning why the E1 HEMP waveform incident at the earth's surface does not have a zero area, as do other radiated fields. While the frequency content is strongest between 1 MHz and 200 MHz and the lower edge of the HEMP source region is at an altitude of 20 km, there is one aspect that is not completely understood. Edition 2 of IEC 61000-2-9 contains information to explain why the existing waveform does not cross over to reverse sign. The problem is that the rise of the HEMP pulse comes from the top of the source region (~50 km altitude) before the air conductivity becomes high enough to cause the E1 HEMP pulse to decay. In fact the line of sight through the source region is 30 km long straight down below the burst and several hundred kms toward the earth's tangent. Thus the size of the "antenna" is very large. The Fraunhofer formula shows that the HEMP waveform on the ground does not satisfy the far field condition.

IV. NEW E3 HEMP INFORMATION

The last item for discussion is additional information regarding the E3 HEMP waveform. In 2017 the U.S. EMP Commission published a new recommendation based on magnetometer measurements [2]. While previous published reports were based mainly on theoretical calculations, the addition of data resulted in the need to increase the E3 fields. In addition, it was decided that while the electric fields may be the easiest for analysts to apply in coupling studies, the actual "incident" environment is a magnetic field. The working group decided to present both the magnetic field analytically, with some consideration of the latitude of the observer, and also provided four electric field waveforms for different deep earth conductivities. These electric fields were also curve fit to provide an analytic version.

REFERENCES

[1] IEC 61000-2-9 Ed. 1.0 (1996-02-19): Electromagnetic compatibility (EMC) – Part 2: Environment – Section 9: Description of HEMP environment – Radiated disturbance. Basic EMC publication.

[2] "Recommended E3 HEMP Heave Electric Field Waveform for the Critical Infrastructures," U.S. EMP Congressional Commission, July 2017.

Summary of Recent HPEM Standards Activities of IEC SC 77C

E. Schamiloglu[1], B Petit[2], R Hoad[2], and W. Radasky[3]
1. University of New Mexico, Albuquerque, NM, 87131 USA
Email: edls@unm.edu
2. QinetiQ Ltd, Farnborough, Hampshire, GU14 0LX, UK
Email: bjpetit@qinetiq.com, rhoad@qinetiq.com
3. Metatech Corporation, 358 S. Fairview Ave., Suite E, Goleta, CA 93117 USA
Email: wradasky@aol.com

Abstract— Standardization in the field of High Power Electromagnetic (HPEM), environments, protection design and test methods is becoming increasingly important due to the increased risk to society from HPEM disruption. This paper will provide an overview of some recent developments in HPEM standards produced by the International Electrotechnical Commission (IEC) sub-committee (SC) 77C on High Altitude Electromagnetic Pulse (HEMP) and Intentional Electromagnetic Interference (IEMI) transient phenomena.

Keywords- Electromagnetic Compatibility (EMC), High Power Electromagnetics (HPEM), High altitude Electromagnetic Pulse (HEMP), Intentional Electromagnetic Interference (IEMI).

I. INTRODUCTION

Standards provide a useful resource for those wishing to provide consistent approaches and solutions to important problems. They are often produced by a committee of recognized experts within niche technical disciplines in response to real or perceived needs by society, government or industry [1]. The IEC-led standardization effort for the HPEM phenomena of HEMP and Intentional Electromagnetic Interference (IEMI) is on-going. This abstract highlights two recent IEC HPEM publications, 61000-5-6 and 61000-2-10. An update to other recent publications, 61000-4-23 and 61000-2-9 will be provided in the presentation.

II. IEC SC 77C STANDARDS

Within the civilian domain arguably the most active and prolific group is the International Electrotechnical Commission (IEC) Subcommittee 77C (IEC SC 77C) though it is noted that the IEEE, ITU–T and CIGRE Study Committee C4 have some activity in the field. IEC Technical Committee 77 (TC 77) is the "parent committee" of SC 77C, and is responsible for the majority of International Electromagnetic Compatibility (EMC) immunity standards. There are 22 published IEC SC 77C documents and these are summarized in Fig. 1. Those standards in black/bold text relate directly to HEMP whereas those in lighter blue text relate to IEMI.

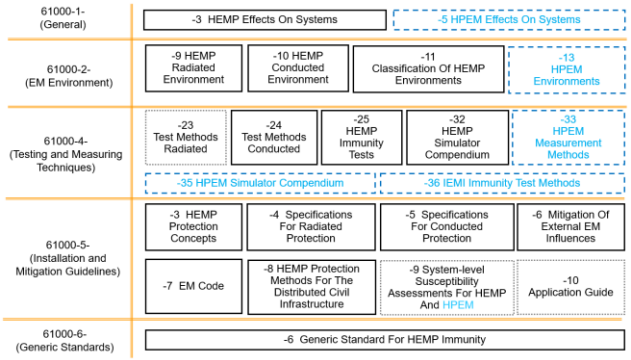

Figure 1. Documentation set produced by IEC SC 77C.

III. RECENT UPDATES

A. *IEC 61000-5-6 Ed 1.0 (Forecast for Publication: 03-2024)*

Users of SC 77C standards, which are primarily industry and infrastructure providers, are finding it increasingly challenging to implement "work-through" HPEM protection (e.g. [2]) due to the up-front costs and need for continuous maintenance and improvement. At the request of the users of IEC standards, we have introduced the concept of 'resilience' to HPEM disturbances as an informative Annex [3]. We are also updating the definition of IEMI and converting the document from a Specification to a full standard.

B. *IEC 61000-2-10 Ed. 2.0 (Published 11-2021)*

This standard is based on the radiated waveforms described in IEC 61000-2-9 [4]. 61000-2-10 describes the conducted environment induced on conductors from E1 HEMP for different positions and illumination cases. In particular it develops analytic conducted waveforms for power lines and other long lines, in the air or in the ground on a statistical basis. Recent work has updated the standard to include time waveform information for different types of simple antennas. In addition to identifying specific waveforms for particular cases, the work will describe more clearly the method to be used to determine the coupled voltages and currents for more complex antennas.

REFERENCES

[1] Giri D. V., Hoad R., and Sabath F., 'High-Power Electromagnetic Effects on Electronic Systems', Artech House, March 2020, ISBN: 978-1-63081-588-2.

[2] Mil-Std-188-125-1, "High-Altitude Electromagnetic Pulse (HEMP) Protection for Ground-Based C4I Facilities Performing Critical, Time-Urgent Missions," Part 1, Fixed Facilities, 2005.

[3] R. Hoad, B. Petit, 'A Resilience based Approach to HPEM Threat Mitigation', GlobalEM 2022, Abu Dhabi, UAE, November 2022

[4] IEC 61000-2-9 Ed. 1.0 (1996-02-19): Electromagnetic compatibility (EMC) – Part 2: Environment – Section 9: Description of HEMP environment – Radiated disturbance.

Long Range Wireless Power Transfer - An Application for High Power Electromagnetics

R Hoad[1], and B. Petit[1]
1. QinetiQ Ltd, Farnborough, Hampshire, GU14 0LX, UK
Email: rhoad@qinetiq.com; bjpetit@qinetiq.com,

Abstract— The concept of beaming electrical power, using the electromagnetic spectrum, from one distant location to another has been around since at least the late 1800's. The term Wireless Power Transfer (WPT) is now more commonly used to describe this concept and there is a growing interest in solving some of the technical challenges which need to be overcome to convert concepts into workable systems.

Keywords- Electromagnetic Compatibility (EMC), High Power Electromagnetics (HPEM), Wireless Power Transfer (WPT).

I. BACKGROUND

The notion of delivering electrical power to a distant location (>>100m) to remotely power a device, wirelessly has been of interest for well over a century. This concept is variously known as Wireless Power transfer (WPT), Power beaming or Free-Space Power Transmission.

The great inventor Nikolai Tesla was arguably the first pioneer to try to make it work but in the end calamities with his experimental setup at Wardenclyffe, Long Island, New York, USA lead to his ruin [1]. The notion gained interest again with the invention of Radar in the 1940's but it wasn't until the 1970's that a demonstration of long range (LR-WPT) using microwaves was achieved.

The 1975 demonstration by William C. Brown of Raytheon at the Jet Propulsion Lab (JPL) Goldstone facility in the US was motivated by a NASA led program to collect Solar Power in space and transmit the electrical energy generated back to the Earth [2]. Solar Power Satellite (SPS) or Space Based Solar Power (SBSP) remains a key application area and a motivation for LR-WPT. Indeed J. Mankins SPS-Alpha concept [3], motivated Prof. Kaya, together with Mankins to conduct a WPT experiment in 2008 over a distance of 150 km in Hawaii using a retro-directive phased array system.

Since 2008 a variety of attempts have been made to develop the components of a LR-WPT system and to demonstrate their effectiveness. An excellent summary of the history of LR-WPT by leading lights in the field can be found here [4] and [5].

Very recently researchers at Xidian University, China [6] have made a very impressive ground based demonstration of a space solar power satellite system including the LR-WPT element.

II. WPT SYSTEMS

A long range WPT system comprises of the components shown in Fig. 1.

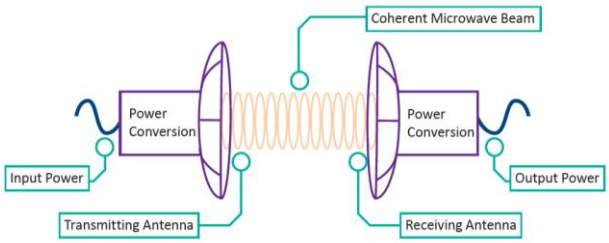

Figure 1. Components of a LR-WPT System

All components of the system require very high conversion (electrical to microwave to electrical) efficiency. This requires a high level of integration or close coupling between the power conversion and the antenna. Solid-State Amplifier technology integrated with a multiple element phased array antenna seem to be preferred for the transmitter element. For the receiving element the Rectifying antenna (Rectenna) is preferred. A rectenna integrates the receiving antenna with a rectifying diode(s) and a filter.

To date the Industrial Scientific and Medical (ISM) frequency bands, 2.4GHz and 5.8GHz have been favored primarily because technology is readily available in these bands and also because RF transmission in these bands is 'license-free'. However, other frequencies have and will continue to be explored.

II. SUMMARY

LR-WPT is of growing interest and is truly HPEM since KiloWatt to MegaWatt levels of microwave power must be transmitted to be useful. This paper will give an overview of the historical milestones, motivations, technologies, challenges and applications for LR-WPT.

REFERENCES

[1] N., Tesla, "The transmission of electric energy without wires, The thirteenth Anniversary Number of the Electrical World and Engineer", March 5, 1904.

[2] W. C. Brown, "The History of Power Transmission by Radio Waves", IEEE Trans. MTT, Vol. 32, No. 9, pp.1230-1242, 1984.

[3] J. Mankins, 'The case for Space Solar Power', Virginia Edition Publishing; First Edition (5 Jan. 2014)

[4] N. Shinohara, 'History and Innovation of Wireless Power Transfer via Microwaves', MTT-S IEEE Microwave theory and technology society, January 2021, IEEE Journal of Microwaves 1(1):218-228

[5] C. T. Rodenbeck, P. Jaffe, B H. Strassner, P. E. Hausgen, J. O. McSpadden, H. Kazem, N. Shinohara, B.B. Tierney, C. B. DePuma, and A. P. Self, 'Microwave and Millimeter wave power beaming', IEEE Journal of Microwaves, Vol 1, NO. 1, January 2021

[6] B. Duan, Y. Zhang, G. Chen et al., On the Innovation, Design, Construction, and Experiments of OMEGA-Based SSPS Prototype: The Sun Chasing Project, Engineering', https://doi.org/10.1016/j.eng.2023.11.007

Experiments with 6-Cavity S-Band (A6) Relativistic Magnetron

Andrey D. Andreev
Department of Electrical and Computer Engineering
University of New Mexico
MSC01 1100
Albuquerque, NM 87131-0001, USA
aandreev@unm.edu

Edl Schamiloglu
Department of Electrical and Computer Engineering
University of New Mexico
MSC01 1100
Albuquerque, NM 87131-0001, USA
edls@unm.edu

Abstract—The first "classic" A6 relativistic or high-voltage magnetron was built and tested ~50 years ago. It is one of the first operational hundred-megawatt-class HPM Sources. Today, the A6 RM is continuously studied both experimentally and computationally by many groups and laboratories around the globe. The University of New Mexico (UNM) has developed an A6 RM that may operate in two basic configurations of output power extraction: (i) radial output with microwave power extraction from one of six resonant cavities into a rectangular horn antenna, and (ii) axial output microwave power extraction from all six resonant cavities smoothly tapered in axial direction into a conical horn antenna. In both configurations, the A6 RM is driven by PULSERAD-110A electron beam accelerator that provides 100's of kV of accelerating voltage and several kA of electron-beam current during 10s ns of output pulsed power.

Keywords—relativistic magnetron; experimental measurements; calibration of measurement sensors

I. INTRODUCTION

UNM has initiated an experimental campaign to study A6 RM operation [1,2] during which the laboratory measurements of its output operational parameters are performed by scanning the diode voltage applied between the cathode and the anode of the magnetron, V_d, at known B_z, and obtaining the experimentally measured dependence of output microwave power P_1 on V_d, or $P_1(V_d)_{\text{exp}}$. After that, the collected earlier results of 3D PIC numerical simulations of output operational parameters of the A6 RM, $P_1(V_d)_{\text{num}}$ will be compared with experimentally measured $P_1(V_d)_{\text{exp}}$ for calibration of certain input operational parameters of the A6 RM. For instance, calibration of a voltage divider monitoring V_d will be performed.

II. EXPERIMENTS

Practical calibration of the diode voltage, V_d, driving the A6 RM with radial output may be relatively easily performed in the laboratory because its configuration with radial output of microwave power from one of resonators of the anode block allows to measure the averaged magnitude and time dynamics of the output microwave power P_1 directly using a waveguide coupler (Figure 1 (a)) placed in between the output/coupling iris of the resonator and a radiating antenna (Figure 1 (b)). After the experimentally performed scan of uncalibrated diode voltage, V_d, at a known B_z, the dependence $P_1(V_d)_{\text{exp}}$ of (i) measured output microwave power with calibrated crystal detector, P_1 (Figure 1 (c)), against (ii) measured diode voltage with uncalibrated voltage divider, V_d (Figure 1 (c)), will be constructed. And finally, the experimentally measured, but uncalibrated $P_1(V_d)_{\text{exp}}$ dependence will be compared with obtained in computer 3D PIC simulations $P_1(V_d)_{\text{num}}$ dependence and calibration of the voltage divider will be performed by comparing the two.

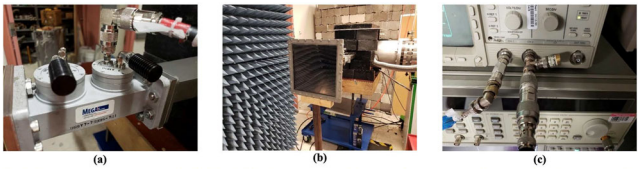

Figure 1. Measurements of output power of the A6 RM in UNM: (a) waveguide coupler between radiating antenna and output/coupling iris of resonator, (b) radiating antenna, and c) voltage integrator connected to "ch1" of TDS350 oscilloscope to measure uncalibrated diode voltage, V_d, and crystal detector connected to "ch2" of TDS350 oscilloscope to measure calibrated output microwave power, P_1.

We will also present various A6 RM current measurements, such as a total discharge and a leakage or end-loss currents measured before and after the A6 RM diode, respectively.

REFERENCES

[1] A.D. Andreev et al., "Experimental Measurements of High-Power Microwave (HPM) output from Relativistic A6 Magnetron at the University of New Mexico (UNM): ~350 MW of High-Power Microwaves (HPM) at ~4.675 GHz (2π-mode) during ~25 ns for Directed Energy (DE) and non-DE applications," Measurement Notes, Note # 66, February 2023, http://ece-research.unm.edu/summa/notes/Measure/mn66.pdf.

[2] A.D. Andreev et al., "Experiments on A6 Relativistic Magnetron Fed by a Solid Cylindrical Cathode: ~350 MW of High-Power Microwaves at ~4.675 GHz (2π-mode) during ~25 ns for Directed Energy (DE) and Non-DE applications," 2023 IEEE Pulsed Power Conference (PPC), San Antonio, TX, USA, 2023, pp. 1-5.

Work supported by ONR Grant N00014-23-1-2072.

Simulations of 8-Cavity X-Band Relativistic Magnetron

Andrey D. Andreev
Department of Electrical and Computer Engineering
University of New Mexico
MSC01 1100
Albuquerque, NM 87131-0001, USA
aandreev@unm.edu

Edl Schamiloglu
Department of Electrical and Computer Engineering
University of New Mexico
MSC01 1100
Albuquerque, NM 87131-0001, USA
edls@unm.edu

***Abstract*—The overall research supporting this effort aligns with the direction of the HPM community and the DOD and focuses on X-band and higher frequency HPM sources. Here the specific focus of attention is on two promising source architectures, the relativistic magnetron and MILO that provide specific value to growing the high frequency vacuum tube landscape as most devices in the X- to Ka-band frequency ranges are linear beam devices. This present effort describes initial steps in computer simulations of 100's MW-class 8-cavity X-band magnetron, and outlines the next steps required to design and test actual relativistic magnetron in the laboratory.**

Keywords—relativistic magnetron; MDO; MILO; PIC simulations

I. INTRODUCTION

In experiments with an 8-cavity X-band relativistic magnetron with diffraction output (MDO) (Figure 1 (a)) performed in the late 70's in the former USSR [1,2], the output RF power >500 MW in the TE_{41} or π-mode at operating wavelength ~3.3 cm (9.09 GHz) was achieved at magnetic field 0.56 T, and applied voltage ~600 kV with FWHP microwave pulse duration ~15 ns and electronic efficiency 13-15% [1,2]. The experiments showed that the MDO, as compared to the relativistic magnetron with radial output, had an enhanced resistance to the RF power breakdown at the output window. The following simulations of the diffraction output antenna showed that certain antenna modifications may provide output RF power mode conversion from the magnetron operating π-mode into one of the desired lower-level modes of the output MDO antenna, such as the TE_{11}-mode with Gaussian output radiation pattern (Figure 1 (b)) [3,4].

II. SIMULATION RESULTS

UNM has initiated a computational campaign to study the 8-vane X-band MDO [1,2] (Figure 1 (a)) operating at lower applied voltages, 300-400 kV, aiming on re-engineering the original MDO design (Figure 1 (a)), building and testing it in laboratory using available UNM pulsed power sources. Computer simulations of the magnetron (Figure 1 (a)) are performed in the following steps: (i) "cold" simulations of its slow wave structure (SWS) to calculate operating frequencies of all possible modes of magnetron operation, plot its dispersion diagram (Figure 1 (c)), and to derive operational domain of the magnetron (Figure 1 (d)) for desired operation mode, which is the TE_{41}- or π-mode (Figure 1 (e)), (ii) "warm" computer simulations of 2D model of the magnetron to reveal range of input operational parameters of interest, certain applied voltages at given magnetic fields, within which magnetron may operate in the π-mode (Figure 1 (f)) with operating frequency and wavelength affected by the electron space charge (Figure 1 (g)), and (iii) warm" computer simulations of 3D model of the magnetron to calculate output rf power, operating frequency and electronic efficiency of the magnetron at its most optimal input operating parameters.

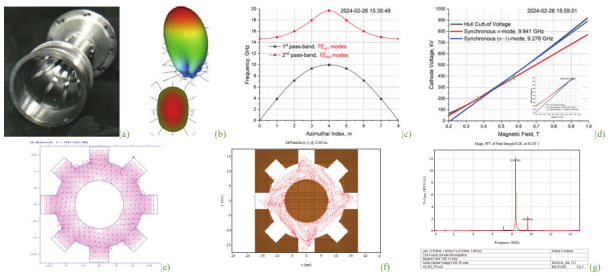

Figure 1. 8-cavity X-band relativistic MDO: (a) photograph showing the diffraction output, (b) output antenna pattern of TE_{11}-mode [4], (c) dispersion diagram, (d) operational domain, (e) electric field pattern of the π-mode in SWS, (f) π-mode oscillations, and (h) frequency of oscillations at 2.6 ns.

REFERENCES

[1] N.F. Kovalev et al., "Relativistic magnetron with diffraction coupling," Sov. Tech. Phys. Lett., vol. 3, no.10, p. 430, 1977.
[2] N.F. Kovalev et al., "High-power relativistic 3-cm magnetron," Sov. Tech. Phys. Lett., vol. 6, no.4, p. 197, 1977.
[3] A.D. Andreev et al., "Compact relativistic magnetron with output mode converter," 45th Annual Meeting of the Division of Plasma Physics of the American Physical Society, October 27-31, 2003, Albuquerque, New Mexico. Bulletin of the American Physical Society, October 2003, vol. 48, no. 7, p. 313.
[4] M.I. Fuks et al., "Mode conversion in a magnetron with axial extraction of radiation," IEEE Trans. Plasma Sci., vol. 34, p. 620, 2006.

Work supported by ONR Grant N00014-23-1-2072.

Controlling the Coupling of Plane Wave to Microstrip Mounted on the TEM/GTEM Wall in Radiated Immunity Testing

Adrian T. Sutinjo and Scott Haydon
ICRAR/Curtin
Curtin University
Bentley, Western Australia
adrian.sutinjo@curtin.edu.au

Abstract—Despite many published studies on coupling of plane wave to a microstrip line, an important special case of incident angle parallel to the ground plane has received considerably less attention. This special case is particularly vital to radiated immunity testing where the excitation voltage to the device under test (DUT) is delivered through a microstrip line on a printed circuit board (PCB) mounted on the Gigahertz/Transverse Electromagnetic (GTEM/TEM) cell wall. We point out that the published analytical coupling formula for this special case must be scaled by a factor of ½ since in the GTEM/TEM environment the incident electric field does not double as opposed to that assumed in the infinite ground plane for which the formula was derived. Next, we introduce a method to increase the coupling factor by approximately a factor of two or more by meandering the microstrip which recovers the coupled voltage to the value expected from the analytical formula.

Keywords-Electromagnetic compatibility; Immunity testing; Electromagnetic coupling; Electromagnetic radiative interference; Electromagnetic measurements.

I. INTRODUCTION

An example of the plane wave incidence on the microstrip line under consideration is illustrated in Fig. 1. The key properties are propagation direction parallel to the ground plane of the microstrip and the incident electric vector which is normal to the ground plane. This incident angle is particularly applicable to radiated immunity testing as per IEC 62132-2 [1] in a GTEM or TEM with the DUT mounted on cell wall as shown. In this case, the incident electric field is dictated by the voltage on the septum divided by the distance to the GTEM wall. Therefore, the total incident electric field does not undergo doubling due to addition of incident and reflected wave as was assumed in the analytical derivation for an infinite ground plane [2]. In high-power radiated immunity testing, this means the voltage induced would be half of the expected value which is often not practicably recoverable because it suggests quadrupling

This research was supported by the Commonwealth of Australia as represented by the Defence Science and Technology Group of the Department of Defence, through the Next Generation Technologies Fund.

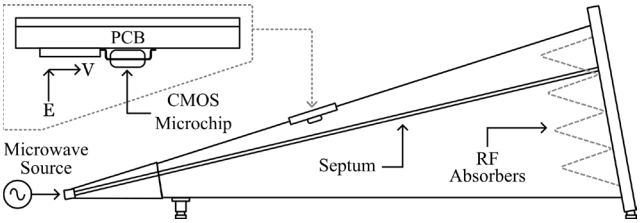

Figure 1. Plane wave excitation of a DUT connected to a microstrip line mounted on the top hatch of GTEM 5402-SAE.

the source power or doubling the thickness of the PCB.

II. METHOD AND RESULTS

A simple method to approximately double the plane wave to microstrip coupling is to meander the microstrip as shown in Fig. 2. The reason for this response can be understood by modelling each line segment as a 3-port S-parameter [3] which are then cascaded to form the meander. It can be shown that for a 3-line meander on FR-4 that the voltage at the backfire port due to 1 V/m incident E-field has a high pass response given by

$$|V| = 0.5h|-\sin(3.5kL)+2\sin(0.5kL)\,|, \qquad (1)$$

where h is thickness of the PCB and k is the freespace wavenumber. This shows that voltage of 1.5h is achievable as opposed to 0.5h for a single straight line.

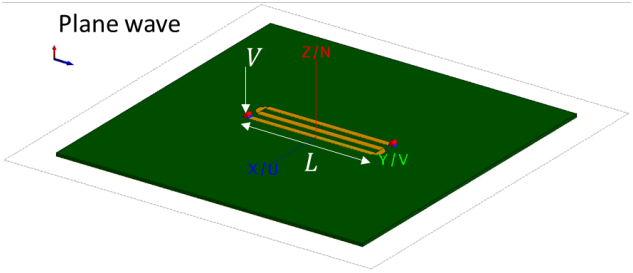

Figure 2. A meander line to increase voltage compared to a single straight line.

REFERENCES

[1] "Integrated Circuits-measurement of Electromagnetic Immunity Part 2: Measurement of Radiated Immunity, TEM Cell and Wideband TEM Cell Method," IEC 62132-2, 1st Ed., 2010.
[2] M. Leone and H. Singer, "On the coupling of an external electromagnetic field to a printed circuit board trace," IEEE Trans. Electromagn. Compat., vol. 41, no. 4, pp. 418–424, 1999.
[3] S. Xia, et. al., "A segmentation approach for predicting plane wave coupling to PCB structures," IEEE Trans. Electromagn. Compat., pp. 1–10, 2024.

Säntis Lightning Research Facility: Recent Developments and Findings

Farhad Rachidi
Electromagnetic Compatibility Laboratory
EPFL
Lausanne, Switzerland
Farhad.Rachidi@epfl.ch

Marcos Rubinstein
IICT
University of Applied Sciences and Arts Western
Switzerland, Yverdon-les-Bains, Switzerland
Marcos.Rubinstein@heig-vd.ch

Abstract— The Säntis Tower was instrumented in 2010 for lightning current measurements. The tower is consistently struck by lightning about 100 times a year. Since being put into operation, the measurement system has been continuously updated and significantly expanded. Currently, lightning parameters are collected at six different sites. This paper presents the latest development and a summary of recent findings.

Keywords- lightning; lightning current, lightning observations, lightning electromagnetic fields

I. INTRODUCTION

Our knowledge of lightning current parameters comes essentially from direct measurements obtained using instrumented towers and from artificially initiated lightning (e.g., [1]). From the 1950s through the 1970s, Prof. Karl Berger and his team recorded extensive experimental data atop two instrumented towers in Monte San Salvatore, near Lugano [2]. Their endeavor resulted in better knowledge of lightning and its processes, classification of different types of lightning, and a comprehensive characterization of lightning current parameters. Other telecommunications towers across the world have also been instrumented for lightning current measurements (the Peissenberg tower in Germany, the Gaisberg tower in Austria, the CN tower in Canada, the Eagle Nest tower in northern Spain, Morro do Cachimbo in Brazil, and the Tokyo Skytree tower).

II. SÄNTIS TOWER EXPERIMENTAL STATION

The Säntis lightning research experimental facility has been operational since 2010. The facility includes a 124-m tall tower (Säntis Tower) in Northeastern Switzerland, which is struck by lightning about 100 times a year. On the tower, Rogowski coils and B-dot sensors are installed at two different heights for lightning current and current derivative measurements. In addition, electric fields at different distances, X-rays, acoustic emissions, as well as high speed cameras are installed at various stations around the tower. Instruments, such as VHF interferometric sensors and Lightning Mapping Arrays (LMA) have also been used temporarily in the past. Details of the instrumentation can be found in [1].

III. SALIENT RESULTS

Since the instrumentation of the tower in 2010, more than a thousand lightning flashes have been successfully recorded. The obtained data have allowed to improve our understanding of lightning discharges and their various processes.

In this lecture, we will present a summary of the obtained results and findings and we will discuss the experimental campaign carried out in 2021 in the framework of the European Laser Lightning Rod project (LLR). This experiment provided evidence that the high-power laser can guide lightning discharges over several tens of meters [3]. In addition to the LLR project findings, observations of high-energetic radiation from upward lightning discharges will also be described.

ACKNOWLEDGMENTS - Funding provided by the European Union Horizon 2020 Research and innovation program FET-OPEN under the grant agreement no 737033-LLR and the Swiss National Science Foundation (grant 200020_204235).

REFERENCES

[1] V. A. Rakov *et al.*, "Lightning parameters for engineering applications, CIGRE Technical brochure 549," CIGRE, 2013.

[2] K. Berger, R. B. Anderson, and H. Kroninger, "Parameters of lightning flashes," *Electra. no.*, vol. 41, pp. 23–37, 1975.

[3] A. Houard *et al.*, "Laser-guided lightning," *Nat. Photon.*, vol. 17, no. 3, pp. 231–235, Mar. 2023, doi: 10.1038/s41566-022-01139-z.

Vector Transfer Functions for Extrapolating System Currents

Jonathan W. Morrow-Jones
Applied Research Associates, Inc.
Santa Barbara, California, USA
jmorrow-jones@ara.com

Heather Jiles, Michael Bak, and William Linzey
Defense Threat Reduction Agency
Ft. Belvoir, Virginia, USA

Abstract—Leveraging mixed polarizations of continuous wave and pulse antenna systems, this presentation demonstrates a method for testing and data processing that deconvolves the contributions from each polarization component to define vector transfer functions for currents.

Keywords-LLCW; CWI; Pulse Illumination; Transfer Functions; Extrapolation

I. INTRODUCTION

Standards for electromagnetic pulse (EMP) often rely on testing systems for coupling to electromagnetic waves. The data from these tests is processed to form transfer functions for extrapolating the coupling data to EMP environments [1]. A common method for measuring coupling is using continuous wave immersion / illumination (CWI), also called low-level continuous wave (LLCW). Another method is to use pulse illumination.

Although the standards identify broad rules for conducting this testing, there is still a great deal of latitude in the details of how the measurements are performed and how the data is processed for extrapolation. While measurement methods have been covered extensively [2], there is less information on nuances of various signal processing methods and how that can provide transfer functions that scale to different illumination methods.

II. BACKGROUND

Currents are induced on systems based on the electric field over the system. While this may seem obvious, it means that currents depend on the timing and distribution of the fields over the system. For the sake of testing, this subtlety is largely neglected. Instead, one measures a reference field, or a series of reference fields, at locations relative to the transmitting antenna that are representative of points on the system or facility that will be illuminated, but without the system or facility present. Transfer functions are formed by the ratio of measured currents or internal fields to the reference field for that location relative to the transmitting antenna,

$$\tilde{T}(f) = \tilde{I}_{meas}(f)/\tilde{E}_{ref}(f)\,, \tag{1}$$

where f is the frequency, and in this case $\tilde{E}_{ref}(f)$ is the reference electric field although it could also be a magnetic field, and here $\tilde{I}_{meas}(f)$ is the measured current but could also be an internal field. If measurements are made with a pulse system, the time-domain current and reference field and current are Fourier transformed into frequency domain,

$$\begin{aligned}\tilde{E}_{ref}(f) &= \int_{-\infty}^{+\infty} dt\ e^{-i2\pi ft}\, E_{ref}(t),\\ \tilde{I}_{meas}(f) &= \int_{-\infty}^{+\infty} dt\ e^{-i2\pi ft}\, I_{meas}(t).\end{aligned} \tag{2}$$

Using a single field to correlate with currents or internal fields is roughly equivalent to assuming the system is electrically small, meaning that the system is small relative to wavelengths. Since EMP standards generally consider frequencies between 100 kHz and 1 GHz, wavelengths vary between 0.3 m and 3 km. Given the limitations of illumination systems, the region being illuminated typically be less than 100 m corresponding to about 3 MHz. Many systems are significantly smaller. For instance, ground vehicles will range between about 4 m and 25 m in their longest dimension, which corresponds to frequencies between about 10 MHz and 75 MHz. Only portable electronics without long wires attached will be electrically small up to 1 GHz.

This does not mean the measured transfer functions are no longer valid at higher frequencies where the system is no longer electrically small, but it does potentially limit the range of validity of the transfer function to azimuths and elevations close to that of the test. As the system becomes electrically larger at higher frequencies, the sensitivity to azimuth and elevation will increase.

Extrapolating to threat assumes that the ratio response current or internal field to the stimulating field is the same as a function of frequency regardless of the stimulating field,

$$\tilde{I}_{threat}(f)/\tilde{E}_{threat}(f) = \tilde{I}_{meas}(f)/\tilde{E}_{ref}(f) = \tilde{T}(f), \tag{3}$$

or equivalently,

$$\tilde{I}_{threat}(f) = \tilde{T}(f)\,\tilde{E}_{threat}(f). \tag{4}$$

In time domain, this becomes,

$$I_{threat}(t) = \int_{-\infty}^{+\infty} df\ e^{i2\pi ft}\,\tilde{T}(f)\,\tilde{E}_{threat}(f)\,. \tag{5}$$

To apply (3), one must use the same type of field for both the reference and the threat. The measured reference field is multipath, including both line-of-sight and ground reflection, while the threat is typically defined as just the

line-of-sight field. In some cases, practitioners attempt to remove the ground reflection from the reference field, while other practitioners instead calculate the total threat field including both line-of-sight and ground-reflected fields.

III. STATEMENT OF THE PROBLEM

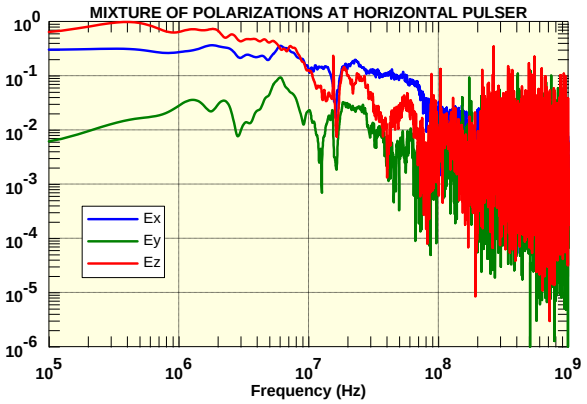

Figure 1.Example of polarization mix of the electric field at an off-center location at a horizontal pulser.

The main problem with the approach of (5) is that all antenna systems provide a mix of polarizations. Attributing all a response current or field to only one, intended polarization leads to errors that can be substantial. This mix of polarizations is well known for CWI systems, but it is even present in pulse illuminations. Figure 1 shows an example of the polarization components measured at an off-center location at horizontal pulser. The intended polarization is a horizontal field in the x-direction. However, between 6 MHz and 10 MHz, the horizontal x-direction and vertical z-direction are comparable, and below 6 MHz, the field is dominantly vertical. The behavior for many mobile CWI systems has similar behavior with similar crossover frequencies, Figure 2. The reason for this is that horizontal fields cancel out at low frequencies as the electric field is grounded out near a conducting surface. Attributing currents just to the horizontal x-polarization overemphasizes the actual contribution of the x-polarization. Extrapolations to threat environments tend to have artificial low-frequency oscillations that create unphysically large root actions for the resulting currents.

Another effect of using only one polarization to correlate with measured currents is that multipath fields have nulls where the reflected field destructively interferes with the line-of-sight field. In Figure 1, the vertical field shows a null at about 44 MHz, while the horizontal fields show a null at about 49 MHz. Currents generally do not show these nulls. The total field magnitude does not have deep nulls. Instead, there is generally always at least one component that becomes dominant in the regions where other components pass through nulls.

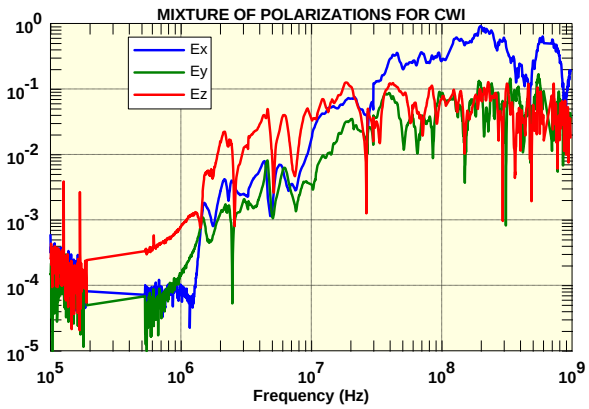

Figure 2. Example polarization mix using a mobile CWI system while illuminating in horizontal orientation.

Without accounting for the nulls, using the total reference field (line-of-sight plus ground reflected fields) in (1) leads to unphysical resonances in predicted currents unless the threat environment exactly emulates the nulls in the reference field. This limits the applicability of a transfer function to a particular angle of incidence. As noted, one approach is to remove the nulls by inferring the line-of-sight field from the total field. This approach has its own uncertainties as the ground reflected field is a function relative permittivity and the conductivity, both of which are functions of frequency. These are unknown, but the formulas for inferring the line-of-sight incident field [**Error! Bookmark not defined.**] assume approximately a perfect conductor. While this can remove the artificial resonances from the nulls, it does not address the bigger issue of the mixed polarizations driving currents.

IV. ALTERNATE APPROACH: VECTOR TRANSFER FUNCTIONS

A more correct approach is to recognize that measured responses of currents and internal fields are a function of the multiple polarizations adding together,

$$I_{threat}(t) = \int_{-\infty}^{+\infty} df\, e^{i2\pi ft}\, \tilde{\mathbf{T}}(f) \cdot \tilde{\mathbf{E}}_{threat}(f)\,, \qquad (6)$$

where

$$\tilde{\mathbf{T}}(f) = \tilde{T}_x(f)\hat{x} + \tilde{T}_y(f)\hat{y} + \tilde{T}_z(f)\hat{z}. \qquad (7)$$

Due to the mixed polarization of transmitting antennas, determining the components for the transfer functions, $\tilde{T}_x(f)$, $\tilde{T}_y(f)$, and $\tilde{T}_z(f)$, requires three or more independent illuminations. For CWI, common practice provides two of the requisite three by performing vertical and horizontal illumination. A third mix of polarizations can use an illumination from another azimuth or elevation. For pulse illumination, two system orientations in a horizontal simulator and one in the vertical simulator will capture three independent illuminations. If the three tests are designated as 1, 2, and 3, then the components, $\tilde{T}_x(f)$, $\tilde{T}_y(f)$, and $\tilde{T}_z(f)$, are found by solving the linear equations,

$$\begin{aligned}
\tilde{I}_{meas1}(f) &= \tilde{T}_x(f)\,\tilde{E}_{ref1,x}(f) + \tilde{T}_y(f)\,\tilde{E}_{ref1,y}(f) + \tilde{T}_z(f)\,\tilde{E}_{ref1,z}(f),\\
\tilde{I}_{meas2}(f) &= \tilde{T}_x(f)\,\tilde{E}_{ref2,x}(f) + \tilde{T}_y(f)\,\tilde{E}_{ref2,y}(f) + \tilde{T}_z(f)\,\tilde{E}_{ref2,z}(f), \quad (8)\\
\tilde{I}_{meas3}(f) &= \tilde{T}_x(f)\,\tilde{E}_{ref3,x}(f) + \tilde{T}_y(f)\,\tilde{E}_{ref3,y}(f) + \tilde{T}_z(f)\,\tilde{E}_{ref3,z}(f),
\end{aligned}$$

or

$$\begin{pmatrix} \tilde{I}_{meas1}(f) \\ \tilde{I}_{meas2}(f) \\ \tilde{I}_{meas3}(f) \end{pmatrix} = \begin{pmatrix} \tilde{E}_{ref1,x}(f) & \tilde{E}_{ref1,y}(f) & \tilde{E}_{ref1,z}(f) \\ \tilde{E}_{ref2,x}(f) & \tilde{E}_{ref2,y}(f) & \tilde{E}_{ref2,z}(f) \\ \tilde{E}_{ref3,x}(f) & \tilde{E}_{ref3,y}(f) & \tilde{E}_{ref3,z}(f) \end{pmatrix} \begin{pmatrix} \tilde{T}_x(f) \\ \tilde{T}_y(f) \\ \tilde{T}_z(f) \end{pmatrix}. \quad (9)$$

With linear independence between the different illuminations, the solution comes from inverting the matrix. If there are four or more independent data sets, the solution uses standard least-square methods where both sides are multiplied by the transpose of the matrix, then the transpose times the matrix is inverted.

V. CONTRIBUTION

The presentation will cover examples of using this methodology. It will show comparisons between CWI and pulse measurements using different antennas and angles of illumination. This will provide the most direct evidence that extrapolation methods can apply to realistic threat environments. This approach should provide transfer functions that can be applied for different illumination antennas or threat scenarios and different azimuths and elevation angles, especially in the electrically small limit.

VI. REFERENCES

[1]. Peng Chen, Hongmin Lu, WeiWu, Xin Nie and Fulin Wu, “Low Cost and Sustainable Test Methods to Study Vulnerabilities of Large-Scale Systems against EMP,” *Sustainability* **2023**, *15*, *320*, 25 December 2022.

[2]. William D. Prather, Jory Cafferky, Lenny Ortiz, and Jay Anderson, “CW Measurements of Electromagnetic Shields,” IEEE Trans. Electromagn. Comp., **55**, *3*, pp.500-507, June 2013.

SPARTAN™ Shield Monitoring System

David Robley, Jim Youngman, Blake Smith
Jaxon Engineering & Maintenance
Colorado Springs, CO 80919

***Abstract*—High Altitude Electromagnetic (EM) Pulse (HEMP) protective solutions are typically based on a topologically-complete EM barrier which provides a high level of shielding effectiveness (SE). As with other elements of this type of protective system, periodic SE testing of the barrier is necessary to ensure and verify required SE performance levels are maintained. However, frequent SE testing by HEMP maintenance technicians is generally neither feasible nor cost effective. To address this shortfall, Jaxon has developed the SPARTAN™, a permanently installed, automatic, cost-effective EM barrier shielding effectiveness monitoring system. SPARTAN™ can characterize the SE performance of EM barriers ranging in size from stand-alone small, shielded server cabinets to large-scale distributed HEMP-protected operations and data centers.**

I. Introduction

HEMP-hardened facilities must often meet stringent electromagnetic shielding effectiveness (SE) performance requirements to protect the equipment housed within. Periodic EM barrier maintenance and shielding effectiveness testing is essential to ensure the barrier continues to perform as designed and expected. However, frequent, comprehensive, and facility-wide SE testing to standards such as IEE 299 and MIL-STD-188-125-1 is often impractical due to cost, complexity, and operational impact considerations.

Many protected facilities rely solely upon maintenance of readily accessible and serviceable EM barrier points of entry (POEs). Periodic SE testing may be performed infrequently, if at all, allowing barrier degradations and compromised SE performance to go undetected for long periods of time, potentially putting protected mission critical equipment and systems at risk.

A permanently installed shield monitoring system mitigates this situation by enabling automatic SE testing of all or a portion of the entire EM barrier as often as desired. The results of this testing can identify areas of barrier EM leakage and provide a quantitative display of measured SE performance in comparison to established requirements.

The SPARTAN™ system employs a patented SE measurement methodology which delivers reliable results in the most difficult of ambient RF environments. As is often required in sensitive facilities and applications, the SPARTAN™ system is also fully TAA compliant.

II. SPARTAN™ System

A. Basic Info

Each measurement "sweep" made by the SPARTAN™ system consists of a collection of individual SE measurements made at up to 200 discrete frequency points logarithmically spaced over a range from 100 MHz (minimum) to 1 GHz (maximum). Maximum conducted output power is 1 W. Most system settings and parameters can be adjusted by the operator as necessary.

Fig. 1. SPARTAN™ RX rack with expansion and extention modules

At the heart of the SPARTAN™ system is an exhaustive set of automatic measurements to mitigate receiver jamming and compression, as well as an iterative sweep algorithm which maximize SE measurement range (MR). These features enable the SPARTAN™ system to make SE measurements while avoiding compression, jamming, and noise in the ambient RF environment.

B. Control User Interface

The SPARTAN™ shield monitoring system is controlled by an application with a user-friendly graphical user interface (GUI) running on a laptop computer. Through the GUI, the user can trigger an immediate SE test on any zone or initiate automatic testing of all zones, where a zone is a user-defined TX and RX antenna pair. Automatic testing operates continuously until stopped by the user. The system can also be configured to abort testing when an SE result indicates that field strength levels outside the facility generated by the transmit side of the SPARTAN™ system could exceed allowed values.

The SPARTAN™ GUI can be tailored for specific application needs. The system provides means to easily compare results from current and archived testing performed at any number of test zones. All ambient environmental and nominal SE measurement results are archived for review and analysis. Data file contents include both processed shielding effectiveness values and reference RF environmental noise levels which are saved in an ASCII formatted text file to simplify export to other applications.

C. System Modularity

The base SPARTAN™ system is comprised of two rack mounted subsystems: a three rack-unit (RU) transmitter unit which typically resides inside of the protected volume, and a two RU receiver typically residing outside. The base SPARTAN™ model offers six receive antenna ports and seven transmit antenna ports that can be configured to sufficiently cover the wall and ceiling shielded surfaces of a

facility with a protected floor area of up to approximately 1000 sqft.

SPARTAN™ transmit and receive modules communicate via ethernet over fiber optic cables, allowing for maximum flexibility of installation. The control computer may be collocated with either transmit or receive modules or be placed elsewhere as desired.

Transmit and receive expansion modules (each two RU) may be daisy-chained to either or both of the base transmit and receive modules, providing system scalability to ensure complete coverage for protected volumes of any size. Remote extension modules are also available for unique shielding topologies consisting of multiple stand-alone shielded volumes, even if separated by large distances. Combinations of transmit, receive, expansion and extension modules can be customized to suit any EM barrier topology and size, ranging from individual server racks to large, hardened facilities to multiple independent protected volumes.

D. Antennas

The SPARTAN™ system typically employs simple, magnetically mounted, passive monopole antennas for transmitting and receiving; typical antenna gain is 1.4 dB. A series of antennas are deployed on a grid pattern throughout larger facilities, allowing for complete coverage with sufficient sensitivity to detect small shield degradations and faults. The antenna grid placement also provides leak localization, allowing the user to quickly identify a region of the facility that may require further investigation or remediation.

The antennas are connected their corresponding transmit or receive modules via low-loss coaxial cable. Cable loss as a function of frequency is compensated in software. Cable runs of 300 feet or more can be accommodated by the system.

III. SPARTAN™ PERFORMANCE

The SPARTAN™ system is designed for maximum performance for those parameters that matter most when making SE measurements, while minimizing cost for all deployment scenarios.

A. Fault Detection

The SPARTAN™ system frequency coverage provides users regular monitoring across the region of the HEMP frequency spectrum where typical EM barrier degradations are typically most often detected. Common EM barrier degradations detected by the SPARTAN™ system include dirty RF shielded door contact surfaces, dirty RF door handle "through pints," corroded or damaged RF gaskets on shielded cabinets, cracked or missing welds, and untreated conductive shield penetrations. Early shielding fault detection reduces risk to mission critical equipment and systems, enabling a low-risk approach to facility HEMP hardening. In addition, MIL-STD-188-125-1A states that "a built-in shield monitoring capability should be considered for the entire shield for HM/HS (hardness maintenance/hardness surveillance purposes)."

B. SE Measurement Range and RX Noise mitigation

The maximum value of SE that can be measured by a given TX and RX antenna pair, as a function of frequency, is usually called the SE measurement range (MR). The SE MR of the SPARTAN™ system varies based on the ambient or environmental RF noise (i.e., not generated by a SPARTAN™ TX module) at the physical location where an RX antenna is located. In the absence of environmental ambient RF noise sampled by the RX antenna, the SE measurement range is identical to the system dynamic range.

The SPARTAN™ system employs a patented method of measurement and noise mitigation, ensuring the quality of the SE measurement and maximizing the SE MR in noisy ambient RF environments. Strategic measurement algorithms enable the SPARTAN™ system to "see through" noisy ambient RF spectra, often boosting SE MR by 20 dB or more at individual measurement frequencies where ambient noise would otherwise dominate the measurement. As a result, the SPARTAN™ system maintains ample sensitivity even in the noisiest RF ambient environments, typically providing an SE MR of 120 dB to 130 dB.

C. Automatic testing vs manual testing

The SPARTAN™ system is designed to run continuously, individually testing a given zone, or automatically testing at multiple zones. Users may start or stop automated testing at any time and manually operate the system. This allows the user or maintenance technician to take an SE measurement at an aperture POE protective device (PPD) such as an RF shielded door, service the door (perform hardness maintenance actions such as cleaning knife edges and fingerstock), and then re-trigger the system to verify the effectivity of the service action.

D. Data Analysis / Stoplight

Interpretation of SE measurement results by the untrained eye can be confusing. Environmental ambient RF noise may give the illusion of an actual EM barrier deficiency, potentially resulting in continued false alarms and unneeded maintenance actions. Care must be taken when reviewing shielding data to differentiate between a real problem and a false alarm due to ambient RF energy.

The SPARTAN™ system aids users in data analysis by interpreting test data and reporting results using a stoplight scheme. The system reads SE and environmental data, and searches within these results for signs of actual EM barrier degradation. The system differentiates between environmental noise and "real" shield leakage. Complete data sets may be viewed, and stoplight indicator displayed for quick reference using user preselected threshold parameters. A sample SPARTAN™ system SE measurement data plot is shown below.

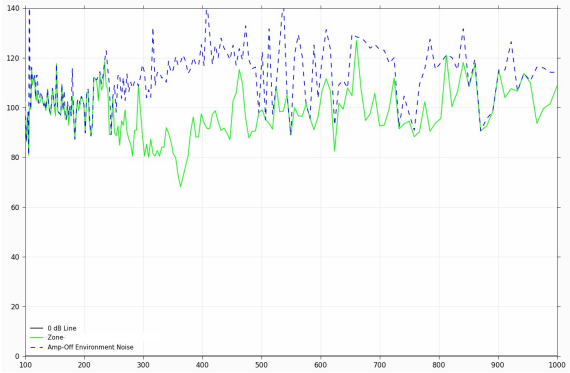

Fig. 2. Sample test data indicating a real shield deficiency

SAND2024-03615A

Development of Bayesian Component Failure Models in E1 HEMP Grid Analysis

Niladri Das, Ross Guttromson, & Tommie A. Catanach

Models are being developed to determine the wide-area effects on electric power systems from High-Altitude Electromagnetic Pulses (HEMP). While deterministic methods are primarily used in this analysis, evaluating E1 HEMP responses across large interconnections proves computationally challenging. Additionally, pulse testing components to determine their probability of failure presents difficulties and is financially expensive, resulting in limited data points. However, the use of a Bayesian prior from, obtained from a subject matter expert can supplement the test data in Bayesian inference, allowing for the development of a robust, cost-effective statistical component failure model These models can then be implemented with minimal computational burden in simulation environments, such as sampling of Cumulative Distribution Functions (CDFs).

Introduction: The methods presented in this paper will focus on the development of statistical component failure models for use in the HEMP Transmission Consequence Model (HTCM)[1], responding to a simulated E1 HEMP only. Although E3 HEMP is considered in the HTCM software, a different method is used and will not be discussed here. When a E1 HEMP occurs, it couples to conductors, resulting in a voltage and current pulse traveling toward each end. Normally, a component is attached to the end of the conductor and is insulted by the voltage and current pulse. A Component Failure Model is a statistical failure model that determines if the component fails as a result of a conducted insult. The model is uniquely parameterized for each type of component, and is constructed in the form of a CDF, conditional upon HEMP coupled voltage. Therefore, a failure event is determined by sampling the associated cumulative density function.

E1 Emp Component Testing: While a large number of laboratory tests for a component yield the most accurate results, the high cost of testing often limits tests to only one or a few articles, leading to low confidence. This work presents an improved method for converting test data into a statistical failure model using Bayesian inference.

Development Of Bayesian Statistical Failure Model Using Limited Test Data: A Bayesian approach to develop a statistical failure model can integrate related data sets including SME estimates, across a hierarchy of classes. The introduction of hierarchy into data sets establishes robustness to the problem where limited test data exists and provides a statistically rigorous way to make scientific inferences about the properties of a class of components (or across classes) by using test results from one or many `similar' components and/or an SME failure estimate.

Developing the Bayesian Model Prior: The Bayesian model prior is developed using the SME estimates. We use Bayesian optimization (BO) and Markov Chain Monte Carlo (MCMC) method to develop the prior.

Method Of Bayesian Failure Model Development: We use the prior, failure likelihood function and perform Bayesian inferencing using MCMC to develop the posterior of the hierarchical model parameters. We marginalize the posterior to obtain the statistical failure model in the form of a CDF.

Application Of the Bayesian Statistical Method: The consequences to the grid of many failures of the same component type across a wide area must be determined by modeling these failures in a large simulation such as the HTCM. Using the limited test data for a class of grid component, the objective is to generate a statistical failure model for that component class that can be used in a wide-area grid simulation.

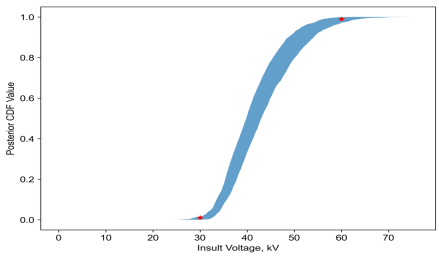

Figure: The posterior CDF is shown, incorporating test data, SME data (shown in red) and uncertainty of the SME estimate.

Conclusions: Due to computational challenges and limited test data for evaluating components exposed to E1 HEMP, Bayesian inferencing is a viable approach for developing statistical failure models. Our approach incorporates error due to the SME estimates, finite test measurements, Bayesian optimization error, and Bayesian inferencing error.

[1] C. Hansen, T. Catanach, A. Glover, J. Huerta, Z. Stuart, and R. Guttromson, Modeling Failure of Electrical Transformers due to Effects of a HEMP Event, Sandia National Laboratories, SAND2020-7406.
[2] D. E. Sanabria, T. Bowman, R. Guttromson, M. Halligan, K. Le and J. Lehr, “Early-Time (E1) High-Altitude Electromagnetic Pulse Effects on Trip Coils”, Sandia National Laboratories, SAND2020-12123 September, 2020

1. The HTCM is in its third year of development and is scheduled to be completed on October 1, 2024

Sandia National Laboratories is a multimission laboratory managed and operated by National Technology and Engineering Solutions of Sandia, LLC, a wholly owned subsidiary of Honeywell International Inc., for the U.S. Department of Energy’s National Nuclear Security Administration under contract DE-NA0003525.

High-Resolution Time Reversal Multiple Signal Classification for Enhanced Landmine Localization

Hamidreza Karami, Marcos Rubinstein
Institute for Information and Communication Technologies
University of Applied Sciences
Yverdon-les-Bains, Switzerland

Farhad Rachidi
Electromagnetic compatibility laboratory
Ecole Polytechnique Fédérale de Lausanne
Lausanne, Switzerland
farhad.rachi@epfl.ch

Carlos Romero, André Koch
Armasuisse Science and Technology
Thun, Switzerland
carlos.romero@ar.admin.ch,
andre.koch@dynamicphenomena.ch

***Abstract*—**In this paper, a high-resolution time-reversal MUltiple SIgnal Classification (MUSIC)-based method is proposed for detecting and localizing buried objects using either a B-scan or a C-scan. The proposed method offers the following advantages: i) it eliminates the need for the back-propagation step typically required in the conventional time reversal method, and ii) it enhances the resolution of object localization by leveraging null-space super-resolution methods. Experimental measurements demonstrate that the proposed method can be used in practical applications.

Keywords- Time reversal, ground penetrating radar (GPR), buried objects, landmine

I. INTRODUCTION

A report from 2023 [1] highlighted the reality of landmines and Explosive Remnants of War (ERW) incidents, documenting 4,700 casualties. Civilians accounted for 85% of these victims, with nearly half being children. This staggering toll has spurred the research community to prioritize the development of safe and reliable landmine clearance techniques.

Among the nondestructive methods for landmine detection, two electromagnetic techniques predominate: electromagnetic induction [2] and Ground Penetrating Radar (GPR) [3]. While metal detectors based on electromagnetic induction are a widely favored tool for landmine detection, their efficacy is often compromised by false alarms triggered by nearby metallic objects and their incapacity to detect non-metallic mines. GPR-based methods stand out for their ability to detect non-metallic mines. They are characterized by significant depth of penetration, higher resolution, and reduced sensitivity to soil conductivity.

II. APPLICATION OF TIME REVERSAL-BASED METHODS TO LANDMINE LOCALIZATION

A comparison between various Electromagnetic Time Reversal (EMTR)-based methods, namely Classical EMTR, Iterative EMTR, DORT, and TR-MUSIC, applied to landmine localization was carried out in [4]. These methods were implemented using different numerical techniques, such as the Method of Moments (MoM), Finite-Difference Time-Domain (FDTD), the Finite Element Method (FEM), and the Finite Integration Technique (FIT). The study and its findings showcased the exceptional performance of TR-MUSIC, highlighting its robustness against noise, diverse soil compositions, whether homogeneous or layered, with varying electrical properties. The study also demonstrated its effectiveness for a variety of targets in terms of number, size, shape, and placement through numerical simulations. Unlike other EMTR-based methods, TR-MUSIC stands out for its remarkably high resolution, achieving around $\lambda/10$ or better, even with a moderate number of sensors. This capability enables the detection of multiple closely-positioned targets and it holds promise to reduce the number of false positives [4].

III. METHOD DESCRIPTION

Conventional TR-based methods suffer from two main drawbacks, namely, (1) the requirement for an antenna array, and (2) decreased performance due to the mismatch between the forward and backward propagation media. To overcome these limitations, we propose a High-Resolution approach based on Time Reversal (HRTR).

The proposed method employs a single antenna for both transmitting and receiving signals. In the proposed method, the transfer function of the medium, including the effects of antenna parameters, soil, and buried objects, is first measured. Then, time reversal is applied numerically to construct the correlation matrix. In this step, the electromagnetic environment is considered as reciprocal. Within the HRTR method, the backpropagation step — requiring an exact model of the medium in the forward step — is eliminated.

Subsequently, the MUSIC algorithm, which is a null-space-based super-resolution technique, is applied to localize the buried objects. Numerous experimental studies have been conducted in this research, all of which validate the accuracy and resolution of the proposed method in comparison to conventional GPR methods.

REFERENCES

[1] "International Campaign to Ban Landmines, Landmine Monitor 2023."

[2] R. Smith, "Electromagnetic Induction Methods in Mining Geophysics from 2008 to 2012," vol. 35, pp. 123–156, 2012.

[3] D. J. Daniels, *Ground penetrating radar*, vol. 1. Iet, 2004.

[4] H. Karami, A. Koch, C. Romero, M. Rubinstein, and F. Rachidi, "Landmine detection using electromagnetic time reversal based methods," *Proceedings of Global EM 2022, Global Electromagnetics Conference*, 2022.

Immunity of LNAs to Bursts of RF Pulses

A. Anzellotti, R.P.C. Kooij, A.P.M. Zwamborn
TNO, Electronic Warfare Dept.
The Hague, The Netherlands.
andrea.anzellotti@tno.nl

Abstract— One of the effect-mechanisms of a radio-frequency (RF) directed energy weapon (RF-DEW) is to damage an electric circuit beyond repair. The pertaining question to be answered is to determine the estimated amount of radio frequency (RF) energy needed to disable a radio receiver by damaging its low noise amplifier (LNA). This study is part of a wider research program whose long-term goal is the quantification of the minimum amount of power that a RF-DEW needs to deliver to effectively operate as anti-drone system. Five different off-the-shelf LNAs, representative of the many LNA varieties currently available on the market, were chosen. Several samples of each LNA were stressed by means of bursts of RF pulses at increasingly larger power levels till failure occurred. Our experiments indicate that the amount of power needed to cause failure is 15 dB to 35 dB higher than the absolute maximum rating reported in the pertinent datasheet. In view of the results obtained so far, it seems that the minimum RF power to ensure permanent failure by means of pulses depends on the technological process and it is around +41 dBm for GaAs/InGaP and around +51 dBm for SiGe:C.

Keywords: Directed energy weapons, electrical overstress in LNAs, damage mechanisms.

I. INTRODUCTION

Directed energy weapons (DEW) are designed to permanently/temporarily disable electronic systems by focusing electromagnetic energy on the target. DEWs have been the object of military research for decades, but with the end of the cold war the interest in these systems dwindled. Recently the interest towards them is awoken; particularly in view of their potential anti-drone applications.
Insight in the minimum amount of energy needed to disable the target is paramount to design an effective DEW system. Unfortunately, this parameter depends on many variables (target typology, RF-sensitivities of on-board systems/subsystems/components etc.) and so a thorough investigation would require a huge number of experiments. However, drones rely on radio systems for essential functions such as communication, localization and navigation and radio systems are far more susceptible to RF signals than other systems, because their antennas greatly facilitate indoor coupling. Furthermore, radio systems contain a receiver, whose weakest component is the LNA. Hence, we can envision that estimating the LNA immunity to an incoming burst of RF energy is a viable way to estimate the immunity of the whole drone.

II. EXPERIMENTAL DESIGN

A. Component selection

Since the maximum amount of RF power a solid state circuit can tolerate was expected to depend on the technological fabrication process, we decided to run the tests on different LNA varieties, manufactured by different processes (i.e. SiGe-C, GaAs and InGaP). Furthermore, we anticipated a dependency on the bias level, we chose components meant for 3V, 3.3V, 5V and 12V operation. The list of component selected for the experiments is shown in Table 1. For each LNA, we bought several samples, trying to minimize the chance of getting components belonging to the same production batch by buying from different retailers.

Manufacturer	***Part number***	***Description***	***Technology***	***Bias condition***
Minicircuits	PMA2-33LN+	Monolithic 0.4-3GHz LNA	E-pHEMPT	56mA@3VDC
Minicircuits	GALI-52+	Monolithic DC-2GHz LNA	InGaP	50mA@12VDC
Analog Devices (Hittite)	HMC376LP3	0.7-1GHz LNA	GaAs pHEMPT	73mA@5VDC
NXP	BGU7224	2.4 GHz ISM LNA	SiGe:C	13mA@3.3VDC
Analog Devices (Maxim)	MAX2612	LNA 40MHz to 4 GHz	GaAs pHEMPT	69mA@5VDC

Table 1: LNAs selected for the stress tests.

B. (Stress) Test procedure

The test procedure consisted in (electrically) stressing the LNAs by means of a bursts of ten CW-1GHz pulses (1µs duration, 1% duty cycle) and repeating the test at increasingly larger power levels till failure occurred. After failure, the component was examined to assess the damage.

III. RESULTS

The results of the stress tests are shown in Table 2. In all but one case, the overstress caused total loss of gain, in one case it caused an oscillation.

Part number	***Technology***	***Supply***	***Abs.Max Rating***	***Minimum power to cause failure during burst test***	***Post-mortem inspection***
PMA233LN+	E-pHEMPT	3 V	+27 dBm	~41 dBm	No gain, no current drawn
GALI-52+	InGaP	12 V	+13 dBm	~40 dBm	No gain, extra current drawn
HMC376LP3	GaAs pHEMPT	5 V	+15 dBm	~43 dBm	First signs of damage, 44 dBm for hard failure (no current consumption).
BGU7224	SiGe:C	3.3 V	+10 dBm	51 dBm	Extra current; oscillation waiting samples to be tested
MAX2612	GaAs pHEMPT	5 V	+20 dBm	43 dBm	No gain, no current drawn

Table 2: Results of RF burst test.

However, the most relevant finding is that the amount of RF-power necessary to permanently damage the LNAs using bursts of short pulses exceeds the absolute maximum rating specified in the datasheet by 14 to 47 dB!
Furthermore, it seems that the minimum RF-power needed to ensure failure depends on the technological process and is around +41 dBm for InGaP/GaAs and +51 dBm for SiGe:C.

Towards Low-Cost Single-Port Imaging of Reflective Targets with a Resonant Metalens

Elias Le Boudec, Farhad Rachidi
Electromagnetic compatibility laboratory
Ecole polytechnique fédérale de Lausanne
Lausanne, Switzerland
elias.leboudec, farhad.rachidi@epfl.ch

Felix Vega
Directed Energy Research Center
Technology Innovation Institute
Abu Dhabi, United Arab Emirates
felix.vega@tii.ae

Hamidreza Karami, Marcos Rubinstein
Institute for Information and Communication Technologies
University of Applied Sciences and Arts Western Switzerland, Yverdon-les-Bains, Switzerland
hamidreza.karami, marcos.rubinstein@heig-vd.ch

***Abstract*—We use a resonant metalens to locate subwavelength reflectors on a plane at frequencies and bandwidths lower than traditional synthetic aperture radars, enabling low-cost or high-penetration imaging.**

high-resolution imaging; microwave metamaterials; synthetic aperture radar (key words)

I. INTRODUCTION

Imaging reflective targets is a topic of broad interest, including radar and ground-penetrating radar for landmine detection. Usually, imaging relies on generating a probe signal that is, first, broadband (i.e., a time-domain pulse) and, second, sufficiently high-frequency for the targets to be electrically large. These requirements lead to expensive signal sources at the expense of radiated power, which reduces the penetration depth.

The resonant metalens [1] is a metamaterial used in far-field imaging experiments to reconstruct subwavelength source spatial distribution. In the transverse plane, the lens features metallic rods whose length is resonant above the frequency of interest and whose density is deeply subwavelength. These characteristics allow the far-field radiation of subwavelength features. Note that conventional reflectometry cannot be applied because the resonant nature of the lens introduces spurious reflections.

In this paper, we investigate the use of a resonant metalens designed for operation below 2.7 GHz to localize reflective targets.

II. METHOD

We use a resonant metalens built from 22 stacked low-loss PTFE printed circuit boards spaced 3.8 mm apart. Each board features 40 vertical copper traces of length 65.2 mm distributed every 4 mm. The metalens is placed a few millimeters on top of a short dipole antenna mounted on a two-dimensional scanner. In a calibration stage, we sample the scattering parameter $S^c_{11}(f_i, x_j, y_k)$ with a vector network analyzer over a grid $(x_j, y_k) \in [0, 80\,\text{mm}] \times [0, 80\,\text{mm}]$ and in the frequency range $f_i \in [1.7\,\text{GHz}, 2\,\text{GHz}]$. We then place a reflector consisting of a copper-taped iron washer 22 mm above the metalens and measure the test scattering parameter $S^t_{11}(f_i, x_j, y_k)$. To localize the reflector, we compute the relative scattering parameter energy $\sum_i |S^t_{11}(f_i, x_j, y_k)/S^c_{11}(f_i, x_j, y_k)|^2$. We expect a local minimum (i.e., a better coupling) close to the reflector coordinates.

This work has been financially supported by the Technology Innovation Institute through agreement no. TII/DERC/2254/2021.

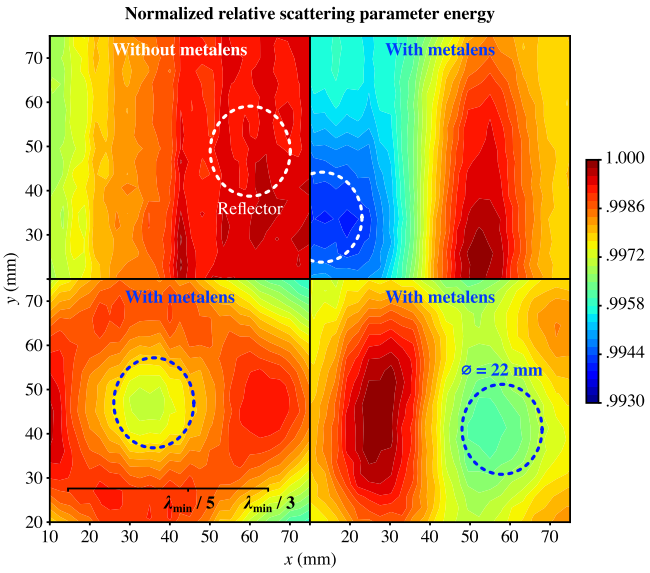

Figure 1. Localization of a reflector using the relative scattering parameter energy.

III. RESULTS AND CONCLUSIONS

Figure 1 presents the normalized relative scattering parameter energy. Without the metalens, the reflector is not visible, while it is when using the metalens, as seen from the different reflector positions. Indeed, the energy is locally minimized at the reflector positions.

The inset in the figure shows the electrical size with respect to the highest frequency. The metalens allows the localization of a subwavelength reflector. This opens the door to low-cost or high penetration-depth single-sensor imaging, such as synthetic aperture radar or ground-penetrating radar.

REFERENCES

[1] F. Lemoult, G. Lerosey, J. de Rosny, and M. Fink, "Resonant Metalenses for Breaking the Diffraction Barrier," *Physical Review Letters*, vol. 104, no. 20, p. 203901, May 2010.

Reliability Test for HEMP Protection Filters

TaeHeon Jang, Global-EMH Inc., Hwaseong-si, Gyeonggi-do, Korea, thjang1@naver.com

Abstract— HEMP protection filters are the primary method of protection against conducted HEMP disturbances. The IEC SC77C published the Amendment 1 to IEC 61000-4-24 Ed. 2.0 in August 2023. This completes the IEC 61000-4-24 performance test methods for HEMP protection filters for power lines and signal lines (in Chapter 5) and RF communication antenna ports (in Chapter 6). However, it is also practical to consider how to ensure that HEMP protection filters maintain their performance in the environments in which they are used and how to establish a replacement life cycle for maintenance. This paper presents the reliability test requirements for HEMP protection filters.

Keywords-Reliability test; HEMP, Filter; IEC 61000-4-24

I. INTRODUCTION

The typical method of protecting critical facilities from conducted HEMP disturbances is usually the installation of HEMP filters at electrical entry points. The basic performance requirement for HEMP filters is the Pulse Current Injection (PCI) test. However, it is also realistic to consider how these HEMP protection filters will perform in the environments they will encounter during operation and how a replacement life cycle for maintenance can be established. These requirements are sometimes expressed in terms of reliability testing. This paper introduces the Unified Facilities Guide Specification, UFGS-13 49 20 (October 2007) from the United States and the Korean reliability assessment specification RS-KTL-2012-0018 for HEMP protection filters.

II. HEMP PROTECTION FILTER RELIABILITY TEST ANALYSIS

A. UFGS 13 49 20, RFI/EMI Shielding

UFGS 13 49 20.00 10 pertains to RFI/EMI Shielding and is part of the Unified Facilities Guide Specifications (UFGS). This guide specification covers the requirements for electromagnetic shielded facilities, including the requirements of EM shielding enclosure, EM shielding doors, electromagnetic filters and electrical surge arresters (ESA). Requirements for electromagnetic filters and ESA include power ratings, voltage drop, insertion loss, operating temperature range, current overload capability, reactive shunt current, dielectric withstand voltage, insulation resistance, ESA extreme duty discharge current, and minimum operating life.

B. RS-KTL-2012-0018, Reliability Assessment Specification for HEMP Protection Filter

HEMP protection filters that can be applied to this specification are HEMP filters for power lines, audio/data, control/signal, and HEMP filters for 200 A or less. The reliability tests consist of quality tests and life cycle tests. The quality tests consist of performance tests and environmental tests. The performance tests consist of insertion loss test, PCI test, voltage drop test, and leakage current test. The environmental tests consist of low temperature tests, high temperature tests, thermal shock test, and overload test. The most unique feature of this standard is the life cycle test, which develops and specifies the test conditions and test methods for the high temperature life test and the PCI life test as TABLE I, II and III.

TABLE I. PERFORMANCE TEST CONDITIONS

Test items	Test conditions	Criteria
Insertion Loss	10 kHz to 10 MHz	≤ 20log(f)-60, in dB
	10 MHz to 1 GHz	≤ 80, in dB
PCI	Mil-Std-188-125-1	Mil-Std-188-125-1
Voltage Drop	50 % of rated load, or 100 A (the less)	If ≤ 50 A, ≤ 2 %
		If > 50 A, ≤ 3 %
Leakage Current	With rated voltages	Manufacturer Spec.

TABLE II. ENVIRONMENTAL TEST CONDITIONS

Test items	Test conditions
Low Temperature	Storage condition: -40 °C, 16 Hours Operating condition: -40 °C, 2 Hours
High Temperature	Storage condition: +85 °C, 16 Hours Operating condition: +50 °C, 2 Hours
Thermal Shock	-40 °C ~ 85 °C, rapid Repeat 5 cycles
Over Loads	140 % of the rated, 15 minutes

TABLE III. LIFE TEST CONDITIONS

Test items	Test conditions	
High Temperature Life Test	For three test samples operating, +85 °C ± 2 °C , 1 000 Hours	
PCI Life Test	Power Lines	40 × E1, 2 500 A
	Audio/Data	203 × E2, 250 A
	Control/signal	196 × E1 2 500 A

III. CONCLUSION

It is planned to revise IEC 61000-4-24 and IEC 61000-5-5 to include maintenance-related testing and reliability testing.

REFERENCES

[1] UFGS-13 49 20.00 10, October 2007 - RFI/EMI SHIELDING
[2] RS-KTL-2012-0018, Reliability assessment specification for HEMP Protection Filter, Korea Testing Laboratory
[3] Hyo-Sik Choi, Tae-Heon Jang and Won-Seo Cho, Study on Electrical Performance and Reliability Assessment of HEMP Protection Filters applied in Communication Facilities, 2017 APEMC, June 20-23, 2017, Seoul, Korea

High-Frequency Electromagnetic Field Coupling to Infinite Single and Double Helical Wires

Sergey V. Tkachenko, Felix Middelstaedt, Ralf Vick
Otto-von-Guericke University Magdeburg, Germany
e-mail: sergey.v.tkachenko@ieee.org

Carlos Alberto Romero, Farhad Rachidi
École Polytechnique Fédérale de Lausanne, Switzerland
e-mail :farhad.rachidi@epfl.ch

Abstract—The paper deals with the problem of high-frequency electromagnetic field coupling to infinite single and double helical wires (twisted wires). Rigorous solutions using the thin-wire approximation are provided. The solutions are obtained through Fourier transformation and the results are expressed in terms of a series of Bessel Functions, distinguishing common- and different-mode currents. Two classical cases of excitations, plane wave and lumped source, are further discussed.

Keywords- thin wires; helix wire; screw wires; Mixed Potential Integral Equations; Fourier transformation;

I. INTRODUCTION

The necessity to consider the coupling of high-frequency electromagnetic (EM) fields with helical wires and twisted wires arise in different problems of EMC (antenna design, using twisted wires to reduce EM coupling, etc.), metamaterials, nanomaterials, and biology (e.g., DNA double helix). The methods applied so far are either restricted to numerical methods, which do not allow gaining insight into the physics of the phenomenon, or are based on the transmission line theory, which breaks down at high frequencies, when the wavelength is about or smaller than the transverse dimensions of the helix.

In this paper, we present rigorous close-form solutions for the problem of electromagnetic field coupling to infinite single and double helical wires. The derivation is solely based on the thin-wire approximation.

II. RESULTS

We start with the Mixed Potential Integral Equations (MPIE) describing current and potential induced by an external EM field of arbitrary frequency on a thin wire of arbitrary form. The equations are then particularized to infinite single and double helical wires. Due to the helical symmetry of the wires, one can introduce one natural length for the case of a twisted helix pair, simplifying the corresponding MPIE. Moreover, this symmetry makes it possible to write separately MPIE equations for the common (CM) and differential (DM) modes, which in this case are decoupled.

Due to the helical symmetry of the wire's geometry, the kernels of the MPIE depend only on the differences of arguments (natural parameters), which make it possible to solve it by Fourier transformation for any arbitrary excitation. The corresponding solutions contain Fourier imagine of the kernels as infinite integrals, which are not convenient for further analysis. We expressed these integrals in terms of a series of Bessel functions.

This work was supported by the GermanResearch Foundation (DFG) under ProjectVi 2007/7-2.

The results are validated by comparison with numerical solutions. The limiting cases of a straight wire and the low-frequency transmission line approximation can be readily obtained from the derived general equations.

Using the derived equations, we investigated the excitation of an infinite helical wire considering two classical cases:(i) plane wave excitation, and (ii) lumped-source excitation. For a plane wave excitation, the inverse Fourier transformation can be performed analytically. In contrast to the case of a straight wire over a conducting plane, the result contains numerous forced waves that are significant across various frequency ranges. This phenomenon arises from the periodic nature of the system.

To calculate the spatial distribution of the current in the case of a lumped source excitation,we employed numerical inverse Fourier transformation. The investigation reveals that, similar to the case of straight wires, multiple current modes emerge near the source. The high-frequency modes decay with distance, leaving only the long-range mode, akin to the TEM mode of a lumped excitation of DM currents along a pair of parallel straight wires.However, this mode exhibits distinct characteristics compared to the TEM mode, particularly concerning the propagation constant. At low frequencies, when the wavelength is larger than the wire spacing, the complex wave number, which characterizes the propagation, has a very small imaginary part. As a result, the transmission line approximation remains valid. However, beyond a certain frequency the imaginary part of the wavenumber increases rapidly, leading to the emergence of additional high-frequency long-range modes. The zoning structure of current wave propagation (allowed and forbidden zone) is linked to the periodic nature of the investigated structure, and is similar to the findings in [1], where the SEM frequencies for finite helical wires exhibit extremely large imaginary part.

In future research, understanding the forced waves and propagation constant of the long-range mode could lay the ground work for developing asymptotic methods for analyzing DM propagation along finite twisted wires, similarly to the methodology applied previously for analyzing straight long wire above ground in [2].

REFERENCES

[1] S. V. Tkachenko, F. Middelstaedt and R. Vick, "The Method of Modal Parameters for the Wire Segments With Symmetrical Geometry and Singularity Expansion Method," in IEEE Lett.on EMC Practice and Appl., vol. 4, no. 1, pp. 2-6, March 2022.

[2] S. Tkatchenko, F. Rachidi and M. Ianoz, "High-frequency electromagnetic field coupling to long terminated lines," in IEEE Trans.on EMC, vol. 43, no. 2, pp. 117-129, May 2001.

Characterization of the Wave Propagation Generated by an Indoor EMP Simulator

Ali Yaqoob, David Martinez, Hamad Alyahyaee, Islem Yahi, Felix Vega, Chaouki Kasmi
Directed Energy Research Center
Technology Innovation Institute
Abu Dhabi, UAE
Ali.yaqoob@tii.ae

Abstract—This research investigates EM wave propagation within a removable EMP simulator housed in a Semi-Anechoic Chamber (SAC). By integrating findings from experimental setups and computer simulations, the study aims to understand the EM wave propagation within the modular system with its distinct architecture and dimensions. This contribution is pivotal for advancing electronic resilience against EMP threats and paves the way for innovative testing solutions in EMC evaluations.

Keywords- EMP; EM wave; CST; HEMP; Propagation

I. INTRODUCTION

High Altitude Nuclear Electromagnetic Pulse (HEMP) challenges modern electronic systems, primarily due to its ability to generate EM fields of immense strength and rapid rise times. The implications of such pulses on critical infrastructure and sensitive electronic equipment have driven extensive research into understanding HEMP effects. This paper introduces a novel exploration into the wave propagation phenomena within an Electromagnetic pulse (EMP) simulator inside a SAC (23 m x 18 m x 7 m). Despite the vast body of research on EMP and its effects, the propagation of electromagnetic waves under such conditions remains unexplored or confidential thus not published in the scientific community. Our study aims to bridge this gap by providing an analysis of wave behavior, leveraging both simulation models and measurement data to characterize the electromagnetic wave propagation within the SAC.

II. METHODOLOGY

Our study aimed to examine wave propagation of an EMP simulator inside a SAC, which complies with MIL-STD-461G and IEC61000-4-25. We used a 520 kV Marx generator with a 2 ns rise time. The setup consists of thirty lines connected to a resistor array, totaling 110 ohms, across the SAC. In the CST Microwave Studio simulation, we placed 401 E-field probes. In the measurement, one voltage and three D-dot probes were used simultaneously for each measurement scenario. The voltage probe and one D-dot probe were fixed in position for reference with 9.74 m between them. The D-dot reference probe's location is considered in the middle of the test volume based on previous work where the test volume was verified [1]. The data is discarded when the measurements at the reference probe do not satisfy the standard MIL-STD-461G in terms of rise time, field magnitude, and pulse duration [2]. In total, there were 54 experimental measurements for the voltage and reference probes.

III. RESULTS

To ensure the consistency of the system, the delta between the time at the peak of the voltage probe and the time at the peak of the reference probe was analyzed statistically. Figure 1. shows a consistency in the measurement. When we compare the mean of the 54 measurements to the simulated value (which is 33.83 ns) of the delta peak time, we get an error of less than 1%. Comparing the delta peak time of the measurement with the theoretical value (which is 32.499 ns) we see an error of around 4.2%. In theory it takes 89 ns for the reflection from the wall to reach the reference probe. In simulation it takes 91 ns for the reflection to reach. In measurement it is 85 ns.

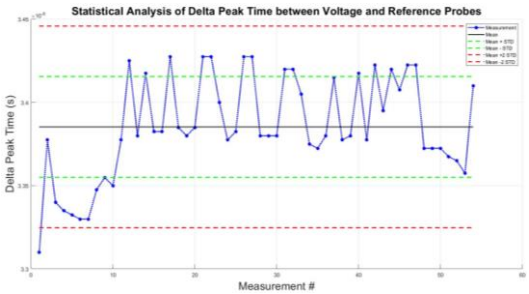

Figure 1. Statistical analysis (mean and standard deviation) of peak time difference between voltage probe and reference probe.

IV. CONCLUSION

Analyzing the results helps us understand the waveform better, including the effects of reflections on the waveform of the EMP simulator. Investigating the reflections further will allow a better understanding of the wave characteristics falling out of the standard and thus having a better definition of the test volume. As mentioned earlier, the results were consistent with low error between measurement and simulation.

REFERENCES

[1] D. Martinez et al., "Experimental and Numerical Validation of an indoor EMP Simulator," in proc. Joint Asia-Pacific EMC (APEMC) and Indian Conference on Electromagnetics (INCEMIC) 2023, Bengaluru, India, 22-25 May 2023.
[2] Department of Defense Interface Standard, "Requirements for the Control of Electromagnetic Interference Characteristics of Subsystems and Equipment," MIL-STD-461G, 2015.p

GLOBALEM 2024-Building Resilience of the Electrical Grid to EMP and GMD

Plamen Doynov, PhD
CTO, EMP Shield, Inc.
Burlington, KS 66839
pdoynov@empshield.com

Abstract—It is essential to build resilience of the electrical power grid and all interdependent critical infrastructure segments to natural and technology generated electro-magnetic interference (EMI). The sources of EMP are referenced, including the evolution of environment and test standards and their and use for development of protection and mitigation utilities. Established resilience definitions and processes are presented and their use as guiding principles for building resilience to critical infrastructure. *5R Resilience*™ is presented, based on Robust, Redundant, Resourceful, Response, and Recovery strategic principles for implementation. The design of EMP mitigation technology and devices is discussed for AC and DC power and communication networks.

Keywords: Resilience; electromagnetic pulse (EMP); high-altitude nuclear EMP, intentional EMI; directed energy weapons (DEW); electronic warfare (EW); Geo-magnetic disturbance (GMD); solar corona mass ejection (CME).

I. INTRODUCTION (HEADING 1)

The term electromagnetic pulse (EMP) is used to describe a transient burst of electromagnetic energy and the associated electromagnetic disturbances due to energy coupling to conductive surfaces and lines. It is a high-intensity electromagnetic field generated by technology-based or natural sources: a nuclear bomb detonation at high altitude, a directed energy system for high-power EM generation, other devices for IEMI, space weather as a result of solar coronal mass ejection (CME), gamma rays, and other cosmic phenomenon resulting in Geomagnetic disturbance (GMD) and large scale EMP effects. (Fig. 1).

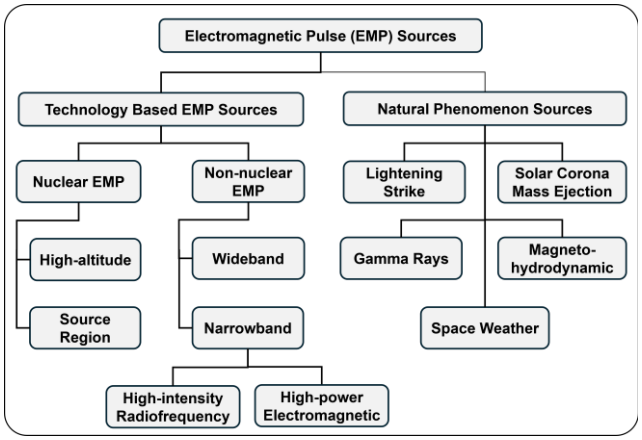

Figure 1. Electromagnetic Pulse Sources.

II. RADIATED AND CONDUCTED EMP

A. *High-altitude Nuclear EMP*

Unlike natural phenomenon, the HEMP comprises more complex time and frequency domain characteristics, and it is considered as a multi-pulse event, described in terms of sequence of three components, defined by the International Electrotechnical Commission (IEC) as E1, E2, and E3 phases (Fig. 2).

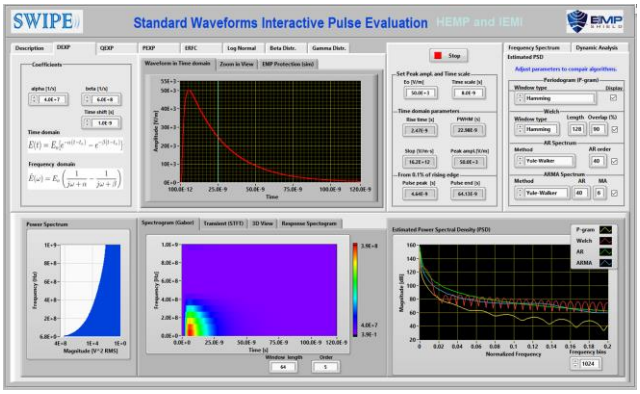

Figure 2. HEMP waveforms in time and frequency domain.

B. *Building Resilience of the Electrical Grid to EMP*

Table 1 illustrates the technical and socio-economic aspects of building electrical grid resilience to mitigate vulnerabilities to EMP with design and deployment of protection systems and post-event response and recovery processes [1, 2].

Table 1. The 5R of Resilience and their socio-economic impact.

The Five R of Resilience and Their Dimensional Impact — R5 Resilience™

R5 Impact	Technical	Organizational	Social	Economic
Robustness	Building codes and standards for construction of new and retrofitting existing structures	Emergency operations planning with contingency alternatives	Improved degree of community preparedness based on vulnerability assessments	Extent of regional economic stability and diversification
Redundancy	Capacity for technical substitutions and "work-arounds"	Alternative sites and channels for managing disaster event operations	Availability of backup options for lifeline support during disaster	Ability to regulate, substitute, and conserve resources
Resourcefulness	Availability of equipment and materials for restoration and repair	Capacity to improvise, innovate, and expand operations	Capacity to address continuity of operations and human needs	Industry and business ability to improvise and implement solutions
Response	Implementing active and passive protection	Deployment of System of systems rapid mitigation	Limiting interruption of normal operations	Minimizing impact on capacity and revenue
Recovery	System downtime and overall restoration time	Time between impact and early recuperation	Time to restore lifeline and community services	Time to regain capacity and lost revenue

REFERENCES

[1] Resilient Power Working Group, "Resilient Power Best Practices for Critical Facilities and Sites with Guidelines, Analysis, Background Materials, and References," Cybersecurity and Infrastructure Security Agency (CISA), DHS, 2022.

[2] Domestic Electromagnetic Spectrum Operations (DEMSO) Working Group, "Resiliency Guide," San Antonio Electromagnetic Defense (SA-EMD), 2022.

GLOBALEM 2024 - Protection of LV and MV Electrical Grids with Solid-State Transformers

Plamen Doynov, PhD
CTO, EMP Shield, Inc.
Burlington, KS 66839
pdoynov@empshield.com

Abstract— Solid-State Transformers (SSTs) are subject to intensive research and development. Based on current technological advancements, SSTs form a promising replacement of low frequency transformers (LFT) on medium and low-voltage AC or DC grids (MV/LV). SSTs offer a smaller form factor implementations and high efficiency with the integration of new functionalities and services. The interface between MV and LV grids imposes multiple electrical stresses, resulting to failures of the SSTs and, respectively, continuous efforts for optimization of existing topological configurations and development of new improved designs. This paper identifies the possible utilization of SSTs for building resilience of MV/LV grids to electromagnetic interference (EMI) using enhanced surge protection of SST modular circuits. Analyzes of currently used protection mechanisms of SSTs are discussed and proposed protection schemes are adapted to provide resilience against the effects of natural and technology-based electromagnetic pulse (EMP).

Keywords: Solid-state transformer (SST); electromagnetic pulse (EMP); high-altitude nuclear EMP, intentional EMI; Magnetohydrodynamic induced current (MIC); Medium and Low voltage grids; Smart grid; Electrical grid resilience.

I. INTRODUCTION

The technology progress, based on wide-bandgap semiconductor materials, has led to the development of high-power components and realization of Solid-State Transformers (SSTs), where the power conversion is realized with a medium or a high-frequency link, replacing the large, low frequency transformers (LFT). SSTs provide a promising solution to achieve voltage transformations in a compact and flexible manner [1]. Many SST topologies have been proposed since it was first patented in 1970. Nevertheless, all topologies can be grouped into four types, as shown in Figure 1.

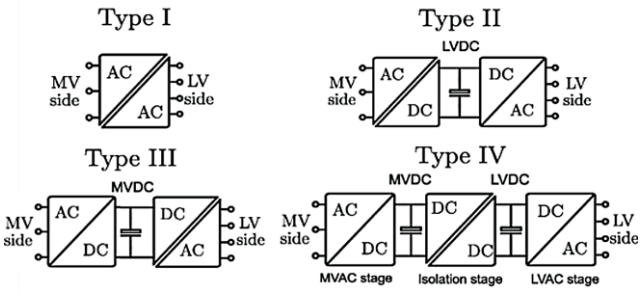

Figure 1. Solid-state transformer topologies.

The SSTs are also grouped in categories, based on common design approach and derived combinations: single cell, matrix type, isolated back or front end, and isolated modular multilevel converter. SSTs are aimed to interface the MV AC grid (6−36 kV) with LV AC or DC grids (50−400V). SSTs achieve a high efficiency conversion from AC to DC, while allowing power flow control, active filtering, reactive power compensation, direct connections of DC/DC converters using a more efficient and simpler network, increased power carrying capacity to admit more distributed energy resources (DERs), electric vehicles (EVs) charging stations, mix of the energy sources and storage system, etc. SSTs provide an optimal interface between DC and AC networks, becoming a key enabler to the introduction of DC and hybrid DC/AC grids with enhance monitoring, protection, control, and respectively better resilience and management.

II. SSTs SOLUTIONS FOR THE SMART GRID

A. Main Problems of Current Power Transformers

The low-frequency power transformers currently in use present problems to the new paradigms proposed by the smart grid (SG):

- they are large and inconvenient for high-density urban areas.
- they are not able to control the power flow.
- they have a limited voltage control in discrete steps and within a reduced voltage range.
- the primary and secondary sides share the same frequency, constraining the interconnection between two different grids.
- not modular, single large device and a single point of failure.

B. Advantages of SSTs

Waveform Quality - deviations and disturbances in one side are not transmitted into the other side.

Voltage and Frequency Regulation - energy balance between primary and secondary side.

Reactive Power Injection – controlled converters at each side, allow an independent control over the reactive power.

Power Flow Control - ability to work as a voltage or a current source.

Black-Start and Protection - an actuation time in the order of microseconds for time and thresholds programmed control according to the use-case requirements.

REFERENCES

[1] J. E. Huber and J. W. Kolar, "Applicability of Solid-State Transformers in Today's and Future Distribution Grids," IEEE Trans. Smart Grid, vol. 10, no. 1, pp. 317-326, 2019.

[2] Ferreira Costa, L.; De Carne, G.; Buticchi, G.; Liserre, M. The Smart Transformer: A solid-state transformer tailored to provide ancillary services to the distribution grid. IEEE Power Electron. Mag. 2017, 4, 56–67.

Experimentally Testing the Time Domain Random Coupling Model within a Complex Scattering System

Isabella Giovannelli, Steven M. Anlage
Maryland Quantum Materials Center
Department of Physics
University of Maryland
College Park, MD, United States
igiovann@umd.edu, anlage@umd.edu

Thomas M. Antonsen
Department of Electrical and Computer Engineering
University of Maryland
College Park, MD, United States
antonsen@umd.edu

Abstract— We extend the Random Coupling Model (RCM) from the frequency domain into the time-domain. The RCM makes predictions for the coupling of electromagnetic radiation into complex over-moded structures, and the statistics of induced voltages on loads inside that enclosure. This extension allows treatment of time-varying load impedances, short orbits, and nonlinear objects located inside the enclosure. We compare time-domain RCM predictions to the measured statistics of time-domain signals in scaled complex structures.

Keywords- induced-voltage statistics, random coupling model, microwave scattering.

I. INTRODUCTION

The goal of our work is to obtain a detailed statistical description of induced voltages and currents in susceptible objects located inside complex scattering environments, such as aircraft, ships, buildings, etc. The Random Coupling model (RCM) is a promising candidate for such a statistical description as it has been demonstrated to explain the statistical properties of electromagnetic radiation inside an individual over-moded complex enclosure [1] as well as a network of such enclosures [2]. The RCM considers electromagnetic waves that enter the enclosure through one or more ports and apertures. Statistical predictions are enabled by identifying three system-specific features: (1) the radiation impedances of the ports and apertures of the enclosure, (2) the dimensionless loss parameter ($\alpha = k^3V/(2\pi^2Q)$, where $k = \omega/c$, V is the volume of the enclosure, and Q is the quality factor of a typical mode in the system) that governs the statistical fluctuations of the system impedance matrix, and (3) prominent "short orbit" signals that travel directly (or with one bounce) from the input port to the output port.

RCM is a frequency dependent model and consequently any and all experiments have been done exclusively in the frequency domain. Recently, this work has been expanded to the time domain where an explicitly time-dependent version of the RCM, called TD-RCM, was produced [3]. The TD-RCM allows for more complex modeling of wave dynamics and permits extraction of new information that could not be previously obtained with the RCM. For example, the TD-RCM allows for early-time short-orbit signals to be considered and added to simulations. It also allows for the incorporation of time-varying port load impedances, which again the previous RCM could not do. Finally, the TD-RCM allows treatment of nonlinear objects inside the enclosure, such as microwave diodes, and this has been used to successfully model the behavior of a microwave-cavity-based reservoir computer, capable of processing complicated high-speed data streams [4].

Currently, we are testing the TD-RCM experimentally through microwave and mm-wave experiments on complex enclosures with movable perturbers. The results for the statistics of induced voltage in a port as a function of time after pulse excitation are examined and compared to the predictions of TD-RCM simulations. In this talk we plan to briefly review the RCM with a focus on the TD-RCM. We will also discuss our associated experiments in detail, including how the microwave experiment is set up and how we acquire our results. We will end by discussing future directions for this work and potential applications.

This work was supported by ONR under grant N000142312507, DARPA/WARDEN under grant HR00112120021, ONR/DURIP FY21 under grant N000142112924, and ONR/DURIP FY22 under grant N000142212263.

REFERENCES

[1] Gradoni, G, *et al*., "Predicting the statistics of wave transport through chaotic cavities by the Random Coupling Model: a review and recent progress," *Wave Motion* vol. 51, 606-621 2014, https://doi.org/10.1016/j.wavemoti.2014.02.003.
[2] Ma, Shukai, *et al*. "Wave scattering properties of multiple weakly coupled complex systems." *Physical Review E*, vol. 101, no. 2, 3 Feb. 2020, https://doi.org/10.1103/physreve.101.022201.
[3] Ma, Shukai, Thomas M. Antonsen, *et al*. "Time-domain generalization of the random-coupling model and experimental verification in a complex scattering system." *Physical Review Applied*, vol. 19, no. 6, 16 June 2023, https://doi.org/10.1103/physrevapplied.19.064052.
[4] Ma, Shukai, *et al*. "Short-wavelength Reverberant Wave Systems for Enhanced Reservoir Computing," *Physical Review Research* vol. 4, 023167, 2022, https://doi.org/10.1103/PhysRevResearch.4.023167.

FDTD Simulation of Voltages Induced on Secondary Circuits in a Substation Owing to Switching Surges

Akiyoshi Tatematsu, Kensuke Teramoto, and Daiki Tashiro
Electric Facility Technology Division
Central Research Institute of Electric Power Industry
Yokosuka, Kanagawa, Japan
akiyoshi@criepi.denken.or.jp

Abstract—Voltages are induced on a secondary circuit in a substation owing to the operation of disconnectors and circuit breakers in a substation in addition to lightning strikes. The induced voltages may cause faults and malfunctions of sensitive electronic devices. In this study, we simulate a test platform of primary and secondary circuits in a substation using an electromagnetic transient analysis code developed on the basis of the hybrid technique of the three-dimensional finite-difference time-domain method and transmission-line theory. Then, we calculate voltages induced on the control cable by switching transients in the primary circuit with a rise time of several nanoseconds, and compare the calculated results with measured waveforms for validation.

Keywords-FDTD method, substation, secondary circuits, switching transient

I. INTRODUCTION

When disconnectors and circuit breakers are operated, switching transients occur in the primary circuit of a substation. Then, voltages are induced on the secondary circuits in the substation owing to the effect of the ground potential rises of the grounding structure, electromagnetic coupling, and surge transition at instrument transformers, which may cause malfunctions and faults of electronic devices in the secondary circuits [1]. To protect electronic devices from electromagnetic disturbances, it is useful to simulate switching transient phenomena and design effective protection measures. In this study, using the hybrid technique of the finite-difference time-domain (FDTD) method and transmission-line (TL) theory, we calculated voltages induced on a control cable in a test platform of primary and secondary circuits in a substation by simulating steep-front switching transients in gas-insulated switchgear (GIS), and we compared the calculated results with measured waveforms for validation.

II. SIMULATED AND MEASURED RESULTS

Fig. 1 shows the test platform of primary and secondary circuits in a substation, which was mainly composed of a grounding grid, a GIS model comprising a gas-insulated bus model and voltage and current transformers (VT and CT), and a protection-relay unit. Here, the signal-output terminal of the VT was connected to the protection-relay unit via an unshielded control cable. We generated a steep-front switching transient with a rise time of 4.4 nanosecond in the primary circuit, which simulates switching transients caused by the occurrence of restrikes at a disconnector in a GIS, and then we measured voltages induced on the control cable at the protection-relay unit (point A in Fig. 1). In the simulations, we modeled the grounding grid, gas-insulated bus model, and circuit used for generating the steep-front switching transient by the three-dimensional FDTD method, whereas electromagnetic transient phenomena in the control cables were solved on the basis of the one-dimensional TL theory taking into account the effect of the surge transition from the primary circuit to the secondary one at the VT. As shown in Fig. 2, we confirmed that the calculated waveforms and frequency spectrum of the induced voltages agree well with the measured results.

REFERENCES

[1] CIGRE WG C4.208, "EMC within Power Plants and Substations," CIGRE Technical Brochure, no. 535, Apr. 2013.
[2] A. Ametani, H. Motoyama, K. Ohkawara, H. Yamakawa, and N. Suga, "Electromagnetic disturbances of control circuits in power stations and substations experienced in Japan," *IET, Generation, Transmission & Distribution*, vol. 3, no. 9, pp. 801-815, Sep. 2009.

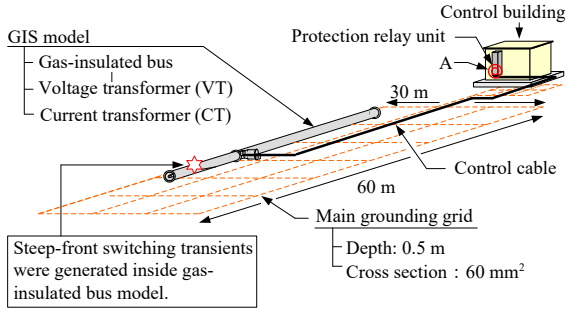

Fig. 1 Experimental setup of a test platform of primary and secondary circuits.

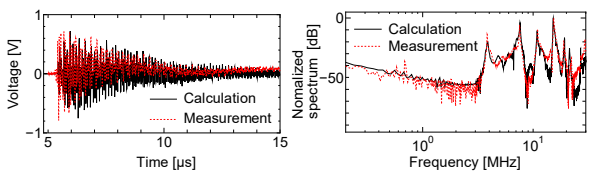

(a) Waveform (b) Normalized spectrum

Fig. 2 Simulated and measured results of induced voltage.

Modelling Method to Evaluate Residual Stresses at Power Lines HEMP Protective Devices Output

G. MEJECAZE, J.-P. ADAM
CEA, DAM, CEA-Gramat
F-46500 Gramat, France
guillaume.mejecaze@cea.fr

Abstract—This article presents the modelling method of a power lines HEMP protective device loaded by real impedances such as those of a flyback Switch-Mode Power Supply. This protective device is stricken by a high current/voltage conducted pulse, induced by the coupling of a High-altitude ElectroMagnetic Pulse (HEMP) on a global electric power distribution network. Some experiments have been performed on a power lines HEMP protective device to validate its model in LTspice simulation software.

Keywords-HEMP; power lines protective device; surge arrester; Monte-Carlo simulation; Pulsed Current Injection

I. INTRODUCTION

Several studies show that the conducted parasitic current/voltage, of hundreds of amperes and several kilovolts, induced by the coupling of a HEMP on a global electric distribution network, involves the destruction of the power supplies of equipment plugged to the grid [1]. To protect them, electrical systems have to be shielded in Faraday cages. To supply the cage, power lines HEMP protective devices are used. These devices are tested with specific conducted generators to measure the residual stresses at their outputs. They are often performed by loading the protective device with short-circuit or 50 Ω resistor: the residual stresses are perhaps not representative of the reality. Therefore, a modelling method is presented aiming to perform Monte-Carlo simulations of the global setup made by the injection source and a power lines HEMP protective device loaded by impedances of a flyback power supply. Different values ranges of load and protective device components are set to cover a large number of impedances and to get representative residual stresses.

II. SETUP MODELLING

A. Injection source

A specific Pulsed Current Injection (PCI) source is used to test HEMP protective devices. It generates a current pulse with a rise time < 20 ns, a half width time ~ 500 ns and 2 kA amplitude on short-circuit. This source has been modelled with its physical components.

B. Power lines HEMP protective device

A HEMP protective device permits to reduce the disturbance level under an admissible value mentioned in different standards such as MIL-STD-188-1-2.

This study has been carried out with the support of Direction Générale de l'Armement belonging to the French Ministry of the Armed Forces.

The protective device first stage is a surge arrester allowing to disperse high currents due to HEMP. The second stage is a low pass filter, which attenuates the residual stress caused by the first stage. All passive components of the protective device have been modelled from impedances and saturation currents (for inductors) measurements. An uniform distribution has been used to specify each component tolerances (20% for inductors, 30% for capacitors) according to manufacturer specifications. The surge arrester has been modelled with the Pouncey-Lehr model [2], which has been adapted from measurements of ignition voltages in function of the pulse slope $\frac{dV}{dt}$ at its terminals.

C. Flyback power supply impedances ranges

To define the impedances ranges for the modelling of flyback power supplies, impedances measurements have been performed in common and differential modes on 35 power supplies of various output powers (15 to 65 W) and output voltages (3,3 to 24 V). Two or three equivalent RLC circuits have been built in each mode to define high and low envelopes of the impedances, which include all the impedances measurements. The different values of RLC components have permitted to define the impedances ranges to use in simulation with uniform distributions. "Fig. 1" presents the global simulation.

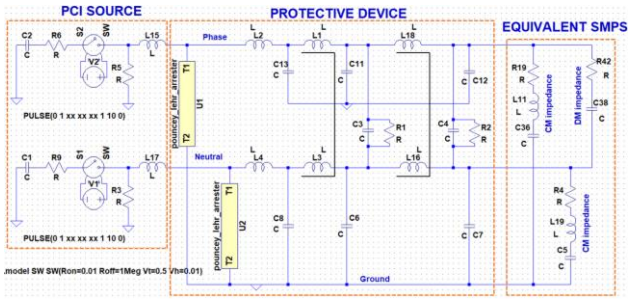

Figure 1. Global simulation of the setup.

III. CONCLUSIONS

This paper presents a modelling method of a power lines HEMP protective device loaded by flyback power supplies. All components, including the surge arrester, have been modelled to allow performing Monte-Carlo simulation thanks to uniform distribution on each component. Before using this simulation to evaluate the residual stresses at protective devices output, some models, such as the surge arrester one, must be improved and residual measurements have to be performed on the power supply when it is in operation.

REFERENCES

[1] G. Mejecaze, "Failure Scenario of Power Supply Due to Conducted Electric Pulse From E1 HEMP," IEEE Trans. On EMC, 2023

[2] J. C. Pouncey and J. M. Lehr, "A parametric SPICE model for the simulation of spark gap switches," Rev. Sci. Instrum., 2020

HEMP Resilience in the transition to the new electricity grid

Tobias Okech
Engineering
MPE Ltd
Hammond Rd, Liverpool, United Kingdom
tokech@mpe.co.uk

Abstract— The new electricity grid is a significant technical shift in how we generate and distribute electrical energy. The new grid describes the future of the modern electricity grid that is larger, increasingly smart, with less distinction between generators and consumers.

Fundamentally the shift is the integration of vast amounts of non-linear solid-state devices in both generation and distribution spread over a wider area. This change introduces different technical challenges concerning the grid's resilience to HEMP (High-altitude Electromagnetic Pulse).

Non-linear devices are pivotal in integrating non-synchronous generation into the grid. Their relative fragility however can make the systems that are built from them and which depend on their power vulnerable to disruption from HEMP without additional protections such as filters.

Electromagnetic pulses, whether from natural sources like solar flares or man-made sources like nuclear detonations, pose a significant threat to electrical and electronic systems. The old electricity grid, centralised and primarily electromechanical, exhibited a different set of vulnerabilities compared to the new electricity grid. The new electricity grid's reliance on solid-state devices, spread across a more extensive geographic area, presents HEMP vulnerabilities that differ in both size and shape.

This paper discusses some of the additional complexities and vulnerabilities associated with HEMP in the context of the new electricity grid. It underscores the imperative for continued development and implementation of HEMP protection measures for the electricity grid and end consumers.

The evolution from the old electricity grid to the new presents a complex challenge, requiring innovation. Addressing these challenges requires a concerted effort from engineers, policymakers, and the public to ensure that the grid's transition does not come at the expense of its HEMP resilience.

HEMP; infrastructure; filtering; renewables; transistors

I. INTRODUCTION

The new electricity grid, characterised by its heavy reliance on renewable energy sources and decentralisation, is already significantly in existence on a small-scale in regions leading in renewables and decarbonisation. This paper aims to prime the reader on the HEMP vulnerabilities of commonly used active devices, assess the broader system-level susceptibilities that incorporate these devices, and discuss the potential impacts on the electricity grid. By identifying these vulnerabilities, the paper aims to highlight the importance of developing and implementing effective mitigation measures to safeguard critical grid consumers against HEMP threats.

- A review of HEMP induced equipment failure.
- Review of the current direction of travel on Grid evolution and consumers.
- A discussion about the potential changes to vulnerability of this course.
- Possible mitigations.

Propagation of HEMP conducted disturbance inside a building electrical network

L. CUROS, I. LACHAUD
CEA, DAM, CEA-Gramat,
F-46500 Gramat, FRANCE
laurine.curos@cea.fr

Abstract—This paper presents an experimental investigation of disturbance propagation inside building electrical grid. A conducted current disturbance induced by the coupling of a E1 high-altitude electromagnetic pulse is studied. Elements influence of low voltage grid and propagation in electrical conductors is analyzed to correctly anticipate the amplitude of parasitic current at equipment input. Our setup is representative of a domestic installation.

Keywords-HEMP, electrical grid, disturbance propagation.

I. INTRODUCTION

Intentional Electromagnetic threats such as High Altitude ElectroMagnetic Pulse (HEMP) are able to generate electrical disturbances. In fact, HEMP couples efficiently on aerial lines of the electricity distribution network producing parasitic currents/voltages of several hundreds of amperes and kilovolts. This induced parasitic involves disturbances and even destruction of the different electronic devices plugged to the grid [1, 2]. In case of HEMP scenario, it is important to understand the impact of electrical grid of a building, industrial or domestic, on the current disturbance propagation to electrical devices input. This paper presents conducted experimentations on a developed model of house electrical grid.

II. EXPERIMENTAL CURRENT INJECTION

A Pulsed Current Injection source (PCI) is used to inject in common mode the resulting conducted current according to MIL-STD-188-125-1-2 (short pulse) at the input of low voltage grid model. This electrical grid model, presented in "Fig. 1", is representative of a low voltage distribution network of a house, composed by electricity meter, 500 mA circuit breaker and switchboard from which 4 lines go to power equipment (L0 to L4). Each line of 3 conductors (Phase, Neutral, Protective Conductor) presents different characteristics (flexible or rigid material, sheathed cable or individual conductors, length, section). To simulate equipment impedances connected at the end of each line, purely resistive impedances, representative of "small signal" power supply impedances, are plugged ("Fig. 1"). Current measurements during injection have shown the minor influence of own conductors characteristics (material, geometrics, and section). However, resulting current amplitude at equipment input depends on the conductor length, on the ground of the considered network, on the injected disturbance at the building electrical grid input and on the equipment impedance at the end of line.

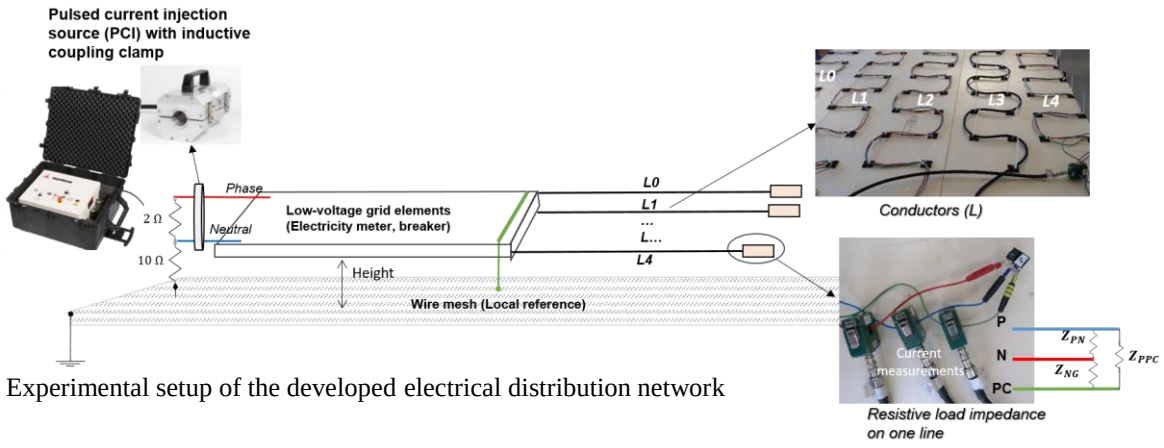

Figure 1. Experimental setup of the developed electrical distribution network

III. CONCLUSION

This paper contributes to understand the impact of the different elements constitutive of an electrical distribution network to correctly anticipate the conducted parasitic currents at the equipment input and so, be able to predict the electronic equipment failure level using simulation tools.

REFERENCES

[1] Radasky WA, Hoad R. "An overview of the impacts of three high power electromagnetic (HPEM) threats on Smart Grids," International Symp. Electro.Compatibility - EMC EUROPE, 2012. p. 1–6.
[2] Mejecaze G, Curos L, Dubois T, et al. "Failure Scenario of Power Supply Due to Conducted Electric Pulse From E1 HEMP".IEEE Trans. Electro.Compatibility. 2023;65(2):464–474.

This Study has been carried out with the support of Direction Générale de l'Armement (DGA) belonging to the French Ministry of armed Forces.

Adding EMP Hardening to EMC Filters

Bektas COLAK[1,2]
[1]*University of New Mexico, Albuquerque, NM USA*
bcolak@unm.edu
[2]*Gebze Technical University, Gebze, Kocaeli, Turkiye*
bcolak@gtu.edu.tr

Jane M. Lehr
[1]*University of New Mexico, Albuquerque, NM USA*
jmlehr@unm.edu

***Abstract*—**Electro Magnetic Pulse (EMP) protection circuits include the surge arrester spark gaps, delay inductors and nonlinear resistive elements such as Metal Oxide Varistors (MOV). MOVs are designed to absorb the energy content of lightning pulses which have a pulse risetime of a few microseconds. Thus, the fast risetime of the E1-type pulse of a few nanoseconds is unsuitable for MOVs. Serial inductive elements may be used to slow the E1 pulse shape to allow for the efficient use of MOVs in this application. Additionally, spark gap-type surge arresters may be used to limit the peak level of the pulses. EMC filters have limited geometrical constraints for their shielded cases. To fit these additional elements for EMP hardening in front of the EMC filter, an optimization on element values is required. In this work, a simulation-based design is developed in LT Spice and experimental data is obtained for comparison by a prototype E1 pulse generator developed in UNM's APERIODIC Lab.

***Keywords*—**EMP, Pulse Generator, MOV, Spark Gap, EMC Filter

I. INTRODUCTION

System level EMP hardening requires a combination of shielding, filtering, and grounding of the targeted infrastructure. To check the performance of each component, EMP generators are used per related standards. The conducted version of the EMP test protocol is specified by MIL STD 188-125-1 [1].

E1-type pulse shape has a risetime less than 20ns and a FWHM parameter between 500 and 550 ns. To absorb the energy content of this fast risetime and relatively long pulse duration pulse shape at the Point of Entry (POE) of the infrastructure, a special combination of protection elements is required. A well-known absorbing element is a voltage dependent, nonlinear resistive component known as a metal oxide varistor (MOV). MOVs are designed to absorb natural insults such as lightning strikes in microsecond region therefore not suitable for faster rise time E1 type EMP shape unless an inductive element is used before the MOV component to slow down the rising time. The effect of MOV in EMC filters against E1 Pulse is given in [2].

In this work, the effect of the inductive element added in front of the MOV is investigated for EMP hardening of EMC filters. Since the size of the outer metallic shield is fixed for high current EMC filters, the design of the inductor is critical. To alleviate this design obstacle, a surge arrester spark gap is added as a protection element to decrease the energy content of the E1 type pulse. The concept is investigated first in simulation using LT Spice using a validated spark gap model [3]. To compare the simulation results, a Marx generator with a peaking switch has been constructed to produce the conducted E1-like pulse shape. The simulated of Marx output is compared with the measured result with peaking circuit (Fig.1)

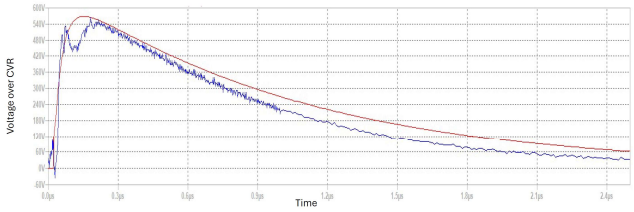

Fig.1. Results of simulation (red) and measurement (blue).

The effect of delaying inductive element is given in Fig.2. Performance of the EMP hardening circuit including MOV and delay inductor elements measured at the output of the filter over 2-ohm resistor to ground. The effect of a surge arrester spark gap element on the residue current level is shown. (Fig.3)

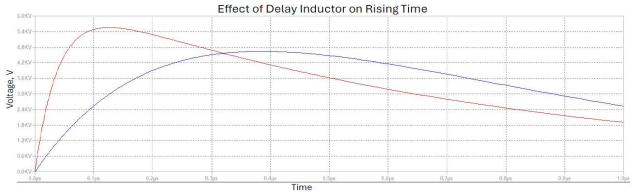

Fig.2. The effect of a 10uH delay inductor on pulse output (blue), compared to the circuit without an inductor (red).

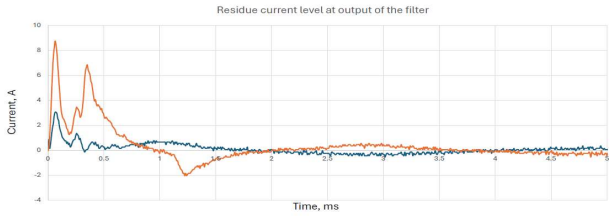

Fig.3. Residue current level of the EMP hardening circuit with (blue) and without (red) the surge arrester spark gap.

REFERENCES

[1] MIL-STD 188-125-1 HEMP Protection for Ground-Based C4i Facilities Performing Critical, Time-Urgent Missions Part 1 Fixed Facilities,1998

[2] Q. Fu, Y. Duan, L. Shi, H. Chen, J. Wang," Protection Performance Test of Power Line Filter by Pulsed Current Injection Method", Letters on Electromagnetic Compatibility Practice and Applications, Vol. 2, No. 4, pp. 115-118, 2020.

[3] J. Cameron Pouncey, Jane M. Lehr, "A spark gap model for LT Spice and similar circuit simulation software", IEEE Pulsed Power Conference, 2015

Semiconductor Switches for High Power Applications

Research Lines at the University of New Mexico

Nicolas Gonzalez, David Oh Smith, Jane Lehr
Electrical and Computer Engineering Department,
University of New Mexico
Albuquerque, NM, USA
negonzalezp2304@unm.edu, jmlehr@unm.edu

Abstract— This document presents a brief description of active research lines currently under study at UNM's Aperiodic labs on solid-state High-Power switches and latest experimental results.

Keywords- solid state, pulsed power, PCSS, DSRD, FID, SOS.

I. INTRODUCTION

With the evolution of semiconductor manufacturing techniques over the last few years, solid state devices capabilities have grown in terms of power handling, commutation speed and efficiency; not only new materials are implemented but new devices are proposed, broadening the applications where solid-state devices can be used. As well as many other technology areas, high power pulse generation is starting to migrate into solid state due to the growing availability of devices that can be used as high power, low-jitter, fast switches. At Aperiodic Labs at UNM, some of these new devices are currently under study. Device physics along with solid-state pulsed power generators are being explored in collaboration with multiple National Labs.

II. PHOTOCONDUCITVE SEMICONDUCTOR SWITCH (PCSS)

Originally developed at Sandia National Labs (SNL), the PCSS is an optical activated switch able to operate in two different modes. The first mode is called linear due to the linear dependence between the intensity of incident light that interacts with the switch and the amount of current that conducts through its terminals. On the other hand, the second mode is known as non-linear or "lock-on mode" for which the incident light pulse triggers an avalanche generation of carriers causing the PCSS to latch (Lock-on) until the current provided by an external circuit extinguishes. Unlike linear mode, lock-on was only reported in semi-insulating GaAs and InP based devices and it was considered elusive for wide-band gap semiconductors such as GaN [1].

Recent studies in collaboration between UNM and Sandia National Labs (SNL) collected evidence of Lock-on in lateral GaN based PCSS using different wavelength sources from 532nm to 1050nm near-IR.

III. FAST IONIZATION DYNISTOR (FID)

Since the first observations of shock ionization waves on semiconductors, multiple devices have been developed using this phenomenon as driving principle for closing switches. Contrary to avalanche transistors, FIDs are capable of handling currents of few kA while reaching sub-nanosecond switching times that makes them especially attractive candidates to replace high power gas switches such as thyratrons due to their remarkable features and long lifetime.

Long term projects between several American research institutions including UNM, are currently working on the study and design of FID-based sub-nanosecond High Power generators.

IV. SOLID-STATE OPENING SWITCHES

Even though traditional pulse power paradigms recur to capacitive energy storage to produce high power pulses, inductive energy storage has always been attractive due to its higher energy density capabilities; nonetheless, due to the nature of inductive circuits they generally require opening switches capable of interrupting high currents in order to generate high power pulses.

DSRDs are semiconductor devices initially introduced by the Ioffe Institute [2, 3] that can interrupt high current densities in a few nanoseconds. Their operation principle relies on the extraction of charge previously injected in a forward biased diode rather than mere carrier recombination. Due to their underlying physics some of these components operate faster with higher current densities, making them suitable for MW-GW pulse generation.

UNM's Aperiodic labs is currently working on SPICE modeling and characterization of these devices in collaboration with multiple National laboratories, these efforts are expected to result on a suitable design tool for multi-MW generators design.

REFERENCES

[1] F. J. Zutavern and A. Rosen, High-power optically activated solid-state switches, Boston: Artech House, 1994.

[2] I. Grekhov, V. Efanov, A. Kardo-Sysoev and S. Shenderey, "Power drift step recovery diodes (DSRD)," *Solid-State Electronics,* vol. 28, no. 6, pp. 597-599, 1985.

[3] S. Lyubutin, G. Mesyats, S. Rukin, B. Slovikovskii and A. Turov, "New solid state opening switches for repetitive pulsed power technology," in *XI Int. Conf. on High Power Particle Beams.*, Prague, 199

Topology Optimization of an X-Band Cavity-Based Slow Wave Structure for Enhanced Bandwidth, Gain, and Efficiency

Moza Mohamed[1,2], Jane M.Lehr[1], E.Neira[2], A. Elfrgani[1], F. Albarracín[2], F. Vega[2], C. Kasmi[2]

[(1)]Applied Pulsed Energy, Ionization and Discharge Center, The University of New Mexico, Albuquerque, NM, USA

[(2)] Directed Energy Research Center, Technology Innovation Institute, Abu Dhabi, United Arab Emirates.

moza95@unm.edu

Abstract**—**This study aims to investigate cavity slow-wave structure (SWS) topology optimization methods computationally. The focus is on increasing the structure's bandwidth, gain, and efficiency through design optimization while considering manufacturing constraints. A sinusoidal cavity design working in X-band is parameterized and subjected to two topology optimization techniques: the Level Set Method (LSM) and Adjoint Variable Method (AVM). An iterative simulation process compares both methods to identify the most feasible technique for improving the addressed figure of merits.

Keywords- adjoint variable method, level set method, slow wave structure, topology optimization

I. INTRODUCTION

Designing and optimizing cavity based slow wave structures are critical for the operation of backward wave oscillators (BWOs) and traveling wave tubes (TWTs). The design of the SWS influences key performances parameters in both the BWOs and TWTs, such as the frequency of operation, gain, output power, and efficiency[1]

For this study, an slow wave structure(SWS) working in X-band, similar to the one presented in [2] was chosen as the reference design (see Figure 1). The cavity is composed of 9 periods, with a total length of 14.14 cm. The periods are equally spaced, with a distance of 1.29 cm.

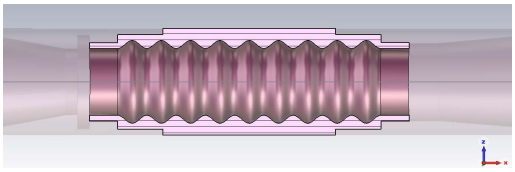

Figure 1 Sinusoidal cavity slow wave structure.

Due to the complex interaction of electromagnetic phenomena involved, present design methods can often fall short in meeting the increasing demands for broader bandwidth and efficiency.

This study aims to leverage topology optimization to enhance the performance of cavity based slow wave structure in the X-band frequency regime.

Topology optimization (TO) is a computational design technique that optimizes a structure's topology within a given design space with a goal to minimize or maximize specific performance parameters. TO is preferred than traditional methods because it allows greater design freedom. Various possibilities can be explored by TO. This design freedom can enable the discovery of novel SWSs that can outperform traditional SWSs.

II. PROCEDURE

This study focuses on refining a pre-existing cavity. The objective is increasing the structure's bandwidth, gain, and efficiency which are the figures of merits of the structure. The design is parameterized and subjected to two topology-optimization methods. Each optimization method is assessed for its feasibility to enhance the figures of merit while maintaining dimensional and manufacturing constraints.

Two methods are explored, the Level Set Method (LSM) and Adjoint Variable Method (AVM). The LSM was reported to be successful for optimizing the topology of waveguides in [3]. On the other hand, AVM offers computational efficiency by calculating the sensitivity of the objective function.

Through iterative simulation, both methods are compared to identify which yield to better outcomes in the specified figures of merit while considering manufacturability and size constraints. The comparative analysis aims to pinpoint the most feasible optimization techniques for slow wave structures. The preliminary results will be presented at the conference.

REFERENCES

[1] A. S. Gilmour, *Principles of traveling wave tubes*. in Artech House radar library. Boston: Artech House, 1994.

[2] Elfrgani, Ahmed. "Relativistic backward wave oscillator with a Gaussian radiation pattern and related technologies." (2016). available from digitalrepository.unm.edu.

[3] S. Yamasaki, T. Nomura, A. Kawamoto, K. Sato, and S. Nishiwaki, 'A level set-based topology optimization method targeting metallic waveguide design problems', *Numerical Meth Engineering*, vol. 87, no. 9, pp. 844–868, Sep. 2011, doi: 10.1002/nme.3135.

Revisiting the Design Ideas Behind the Mitigation of Conducted HEMP and IEMI PLENARY PAPER

Sergio N. Longoria
Technical Product Line Manager, RF Filters
ETS-Lindgren Inc., Cedar Park, Texas, USA
Sergio.longoria@ets-lindgren.com

Abstract—This paper discusses and reviews the reasons a combination Filter/ESA is recommended for the mitigation of conducted disturbances such as the E1 and E2 pulses from a HEMP and IEMI. We begin with a brief explanation of HEMP and IEMI for the newcomer to the subject and the reason for treating all electrical POEs. The paper will discuss the design concepts and standards for HEMP/IEMI protection filters, filter design topology and important considerations in selecting the appropriate components. The paper will also discuss the commercial and military grade standards used for verifying the suitability of a Filter/ESA combination for meeting the E1 and E2 mitigation requirements. Finally, the paper will address recent changes made to the military grade standard MIL-STD-188-125-1 and what challenges this presents to the Filter industry.

Advances in HPM technologies (keynote)

Gun-Sik Park, Sun-Hong Min, Matlabjon Sattorov[1], and Varun Dixit
Advanced Institute of Convergence Technology
Seoul National University
Seoul, South Korea

Hojun Jeong[2] and Sang Hoon Nam
Nawoo Pulse Tech, Co.
Seoul, South Korea

[1]Seoul-Teracom, Co.

Abstract
This presentation provides insights into recent advancements in high-power microwave (HPM) technology, showcasing innovative approaches to enhancing key characteristics. Furthermore, it explores both the current state and future prospects of HPM technology.
Keywords, High-power microwaves(HPM), HPM sources, EMP, DEW

I. INTRODUCTION

High-Power Microwave (HPM) technology has undergone significant advancements, notably in recent years, characterized by intense bursts of microwave radiation. Utilizing advanced devices like vircators and relativistic magnetrons, HPM systems efficiently convert energy into radiated electromagnetic energy, finding widespread use in disrupting electronic equipment, particularly in military applications. Recent breakthroughs in electromagnetic wave-generating devices, especially those utilizing electron beams, have broadened their applicability, driven by the demand for innovative direct-energy weapons amidst modern electronic complexities. In this context, HPM technologies play a crucial role, capable of creating artificial electromagnetic environments to harm electronic devices through the intentional generation of electromagnetic pulses (EMPs), exhibiting precise targeting, adaptability to diverse conditions, and versatility across various platforms.

II. KEY CHARACTERISTICS

In the realm of High-Power Microwave (HPM) technologies, crucial characteristics define the capabilities of HPM sources for RF-directed energy weapons (DEWs). Figure 1 illustrates the RF power versus frequency relationship for solid-state devices and HPM vacuum electronic devices (VED), with dashed blue and thick red lines representing the high-power and average-power frontiers. DEWs utilize radiated waves or beams of microscopic particles, drawing from various electromagnetic sources, including lasers, charged particle beams, radio frequency devices, and HPMs. Within HPM technologies, devices such as magnetically insulated line oscillators, relativistic magnetrons, and relativistic backward wave oscillators (RBWOs) play pivotal roles. Flexible frequency tuning ensures adaptability crucial for dynamic electronic warfare, while downsizing enables deployment across vehicles, drones, and aircraft, enhancing operational versatility. Phased-array antennas and digital beamforming optimize targeting accuracy, while advancements in radiation precision and control maximize target engagement capabilities. Safety protocols and fail-safe mechanisms mitigate risks, ensuring responsible use. The exploration of space-based applications unlocks strategic possibilities, including satellite defense and directed energy initiatives.

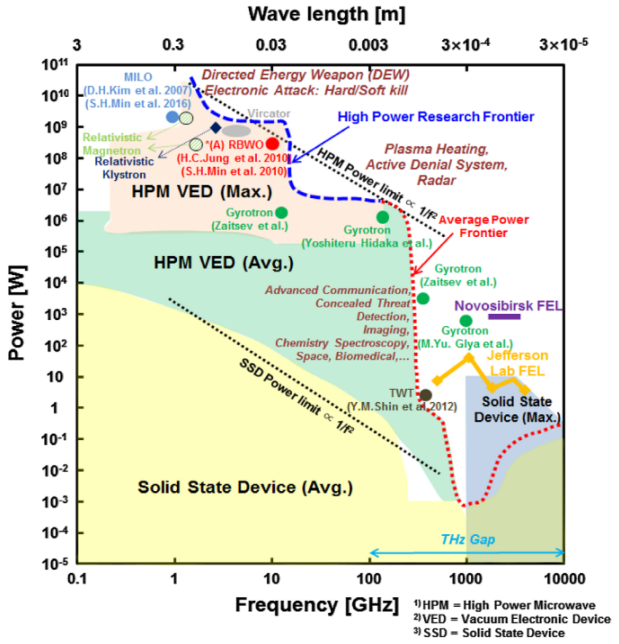

Figure 1. Domain of HPM
(Sun-Hong Min *et. al.,* Effects on electronics exposed to high-power microwaves on the basis of a relativistic backwardwave oscillator operating on the X-band, Journal of Electromagnetic Waves and Applications, 31:17, 1875-1901 (2017)

REFERENCES

[1] Weise THGG, Jung M, Langhans D, et al. Overview of directed energy weapon developments, 12th Symposium on Electromagnetic Launch Technology, 2004, Snowbird, UT, USA
[2] Schamiloglu E. High power microwave sources and applications. Preprint of paper presented at 2004 IEEE MTTS, Fort Worth, TX.
[3] Ni G, et al, J. Research on High Power Microwave Weapons. 2005 Asia-Pacific Microwave Conference Proceedings; China.
[5] Min S-H, *et. al.* Mode conversion of high-power electromagnetic microwave using coaxial-beam rotating antenna in relativistic backward-wave oscillator. IEEE Trans Plasma Sci. 2010;38:1391–1397.

Plenary Paper

CenterPoint Energy's RDSM Program: Strengthening Grid Resilience with Adaptable Deployment Strategies

Eric Easton, Ph.D., P. E., Ryan Marietta P.E.

CenterPoint Energy's Resilient Digital Substation Module (RDSM) program is a forward-thinking initiative spanning 12 years, featuring a dynamic 10-year deployment plan. This initiative is crafted to bolster grid resilience, offering agility in response to financial constraints or opportunities for acceleration. Through a meticulously structured phased approach, CenterPoint Energy's standardized design framework ensures seamless deployment, optimizing resource allocation and risk mitigation. Moreover, by harnessing the utility's extensive expertise and cutting-edge technology, the RDSM program fosters innovation in substation deployment practices. As a testament to its commitment to modernizing grid infrastructure, CenterPoint Energy's RDSM initiative not only enhances resilience but also champions adaptability and scalability in the face of evolving energy landscapes, thereby ensuring the sustainability of energy provision for communities served.

Evolution of CenterPoint Energy's Resilient Digital Substation Module (RDSM): Enhancing Reliability and Efficiency through Design Innovations

Author: Ryan Marietta, P.E. Eric Easton, PhD P.E.

CenterPoint Energy's Resilient Digital Substation Module (RDSM) has undergone significant evolution in design, aimed at improving reliability, efficiency, and maintenance. Initially employing multiple bolted connections, the RDSM has transitioned to a streamlined design featuring a minimized number of bolted and compression connections. This transition has reduced installation complexities and potential points of failure. Furthermore, notable improvements have been made in the main module's design, including the integration of a single-piece sub-enclosure. This innovation optimizes ingress protection and ensures seamless integration of components into the main module, enhancing overall system robustness and operational resilience.

Looking ahead, the focus shifts towards future design enhancements aimed at further bolstering reliability and reducing system wear. One such prospect involves the revision of the door latching system to mitigate wear and tear, thereby augmenting the enclosure's longevity and reliability. This abstract provides an overview of the evolutionary journey of CenterPoint Energy's RDSM, highlighting key design transitions from its inception to its current iteration. By embracing innovative design strategies and anticipating future advancements, CenterPoint Energy continues to demonstrate its commitment to delivering resilient and efficient substation solutions in the dynamic landscape of energy distribution.

A Compact Spiral Generator for High-Power Electromagnetic Systems

Aaesha AlAli, Gideon Nimo Appiah, Umar Hashmi, Hamad Deiban, Fernando Albarracin, Felix Vega and Chaouki Kasmi
Directed Energy Research Center, Technology Innovation Institute, Abu Dhabi, United Arab Emirates
aaesha.alali@tii.ae

Abstract—This work presents a practical implementation of a compact spiral generator for high-power electromagnetic systems (HPEM) applications. An analytical design is presented and validated via measurements. A prototype of a spiral generator with a 40 kV peak output amplitude and a 0.28 kV/ns rate-of-rise voltage is manufactured and tested in the laboratory.

Keywords: copper strip, HPEM applications, Kapton, insulator, spiral generator

I. INTRODUCTION

Compact pulsed power systems generating nanosecond multi-kV high-voltage output are increasingly utilized in HPEM applications due to their numerous advantages, such as their portability, reduced footprint, and energy efficiency[1]. Recently, compact spiral generators have been an attractive alternative to traditional pulsed generators, such as the Marx and pulsed transformers, due to their ease of construction and reduced number of input switches to generate a high-voltage output waveform [2] [3]. In this work, four different geometries of spiral generators are built with copper widths of 15 mm and 25 mm each, with thicknesses of 0.05 mm and 0.1 mm, respectively. The copper strips are wound on a molded nylon holder with inter-turn Kapton insulation for a 100 kV/mm dielectric breakdown strength. We study the effects of the copper widths on the efficiency, as well as the amplitude and shape of the output pulsed voltages of the generator. A spiral generator with a peak output amplitude of 40 kV and a 0.28 kV/ns rate-of-rise voltage is designed and modeled. The presented prototype has been experimentally tested to verify the analytical design.

II. DESIGN OF THE SPIRAL GENERATOR

The equivalent circuit model of the spiral generator is shown in Figure 1(a). It comprises the input switch, represented as inductance (L_s), and the load, which is a combination of inductance (L_L), resistance (R_L), and the capacitance (C_L). The total inter-turn capacitance and the spiral inductance are represented by C_0 and L_N, respectively, which are calculated as [1]

$$C_0 = \epsilon_r \epsilon_0 \frac{\pi D W}{2Nt} \quad (1)$$

$$L_N = k' \frac{\mu_r \mu_0 \pi D^2 N^2}{2w} \quad (2)$$

Where W is the width of the copper tape, t is the thickness of the single insulation layer, ϵ_0 and μ_0 are the permittivity and permeability of the free space, respectively. ϵ_r and . k' determines the geometric losses; in this paper, the k' is 0.195. The first design aimed to reach a 40 kV output voltage with a 20% multiplication efficiency [i.e. the ratio $V_{out}/(2 \cdot n \cdot V_{charge})$]. In this design a copper strip 12.7 mm width and 0.05 mm thick is used. The insulation layer is Kapton with a thickness of 0.15 mm. The number of turns has been calculated to be 20 with a winding diameter of 100 mm. The calculated output inductance and capacitance were 142 µH and 24 pF, respectively.

III. EXPERIMENTAL RESULTS

A cylindrical Nylon holder, fabricated using in-house 3D printing technology, has been utilized in the winding process, ensuring precise control over the turn diameter, and minimizing errors. A spark gap with a 5-kV hod-off voltage has been integrated across the input strips to trigger the generator, as depicted in Figure 1(b). Two voltage probes have been used to measure both the charging voltage and the output voltage. An open load output voltage of 39 kV, 60 ns rise time, and 93 ns pulse duration was measured when the spiral generator was charged to -5 kV, as shown in Figure 2. These results encourage the authors to extend the experiment to other types of loads, including resistive and capacitive.

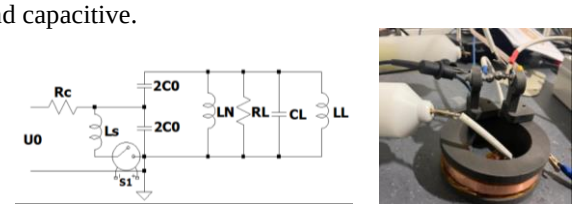

Figure 1. (a) Spiral generator circuit model. (b) Experimental setup of the spiral

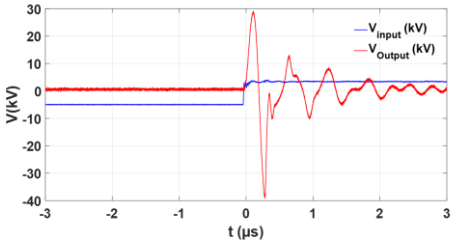

Figure 2. The experimental waveform of the input & output voltage

REFERENCES

[1] J. Yan, S. Parker, and S. Bland, 'An Investigation Into High-Voltage Spiral Generators Utilizing Thyristor Input Switches', IEEE Trans. Power Electron., vol. 36, no. 9, Sep. 2021.

[2] D. Harthan et al., 'Impedance Characterization of a Spiral Generator with a Frequency Response Analyzer', in 2023 IEEE Pulsed Power Conference (PPC), San Antonio, TX, USA: IEEE, Jun. 2023, pp. 1–4.

[3] I. J. Cohen et al., 'Demonstration of a High Repetition Rate Solid-State Switched Spiral Generator', in 2023 IEEE Pulsed Power Conference (PPC), San , TX, USA: IEEE, Jun. 2023.

Experimental Tests of a 300-kV PFN-Marx Generator for Low Impedance Loads

Umar Hashmi, Aaesha AlAli, Gideon Appiah, Hamad Deiban, Fernando Albarracin, Felix Vega, Chaouki Kasmi
Directed Energy Research Center, Technology Innovation Institute, Abu Dhabi, United Arab Emirates
umar.hashmi@tii.ae

Abstract— This work presents the design and preliminary experimental tests of a PFN-Marx generator for low impedance loads. A pulse forming network PFN approach is implemented at each stage of the Marx generator to widen the pulse length to 150 ns. The design and simulated results are presented along with experimental results on a 33.6 Ω load.

Keywords- MARX generator, pulse forming network, PFN.

I. INTRODUCTION

Pulsed high-voltage generators are the angular stone for a variety of scientific and industrial applications. The Marx generator, characterized by the parallel charge and subsequent series discharge of multi-staged capacitors, exhibits a nanosecond double-exponential output voltage waveform profile [1]. To drive high-power microwave (HPM) sources, the Marx's output pulse must be widened to values of dozens of nanoseconds. The implementation of pulse forming networks, PFN, at each stage is one method to widen the pulse from a Marx generator [2].

This work presents the preliminary experimental results of a 12-stage PFN-Marx generator optimized for a 33.6 Ω load. A prototype of the generator is presented and experimentally verified.

II. DESIGN AND SIMULATION

The voltage across the load is designed to be regulated from 100 kV to 600 kV. The full width at half maximum (FWHM) of the output pulse should exceed 100 ns with a risetime of around 25 ns. The initial estimation of FWHM and impedance of PFN-Marx can be done as follows.

$$T_{FWHM} = 2 \cdot S \cdot \sqrt{LC} \quad (1)$$

$$Z_{PFN} = N.\sqrt{L/C} \quad (2)$$

Where S is the number of capacitors in a single PFN and N is the number of PFN-stages. In this PFN-Marx design the four capacitors, each of 10 nF, are connected in series using two aluminum strips, and the inductance of these strips between two capacitors was estimated to be 35 nH. The total number of PFN stages is 12. From this data the expected value of $T_{FWHM} = 150$ ns and impedance of complete PFN-Marx will be $Z_{PFN-Marx} = 22.5\ \Omega$.

Prior to manufacturing, the 12-Stage PFN Marx generator was simulated in three stages. First, the circuit simulation using LT-spice, second, the electrostatic simulations of the 3D-structure for voltage breakdown analysis is done in Ansys-Maxwell, and third, the full wave simulation of the model is done using CST-Microwave studio.

III. EXPERIMENTAL RESULTS

The 12 PFN stages were assembled using the zig-zag design [2] to form a Marx generator as shown in Figure 1. The complete PFN-Marx was mounted on a trolley, so that it can be connected to a load easily. For diagnostics, a commercially available CVR and in-house developed Rogowski coils and V-dot sensors were used.

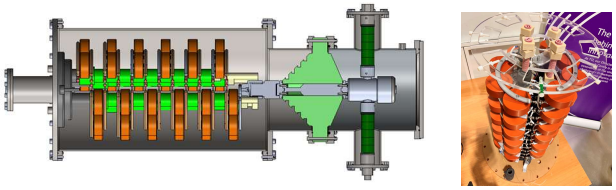

Figure 1. (a) CAD model of the PFN-MARX (b) Inner structure.

To characterize the PFN-Marx parameters, atmospheric pressure, each stage was able to hold-off 6.7 kV. From this analysis the equivalent inductance of the Marx is estimated to be 1.6 uH. A resistive load for higher pressure testing was chosen to 33.6 Ω, a more realistic value for a HPM source. The output voltage waveforms for different pressure values, ranging from 1 to 4 bar, are shown in Figure 2. A risetime of 23 ns, and a pulse width higher than 150 ns were observed. Further effort is being exerted to achieve a 300 kV voltage level across the load and will be presented at the conference.

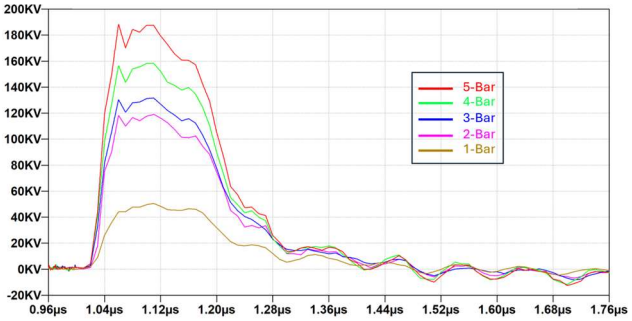

Figure 2. Measured voltage waveform.

REFERENCES

[1] Appelgren, Patrik & Akyuz, Mose & Hurtig, Tomas & Larsson, Anders & Nyholm, Sten. (2009) "Circuit simulation analysis of a vircator powered by different high-voltage pulse sources." in *PPC2009 - 17th IEEE International Pulsed Power Conference.*

[2] F. Lassalle et al., "Development and Test of a 400-kV PFN Marx With Compactness and Rise Time Optimization," *in IEEE Transactions on Plasma Science,* vol. 46, no. 10, pp. 3313-3319, Oct. 2018.

A 700W Amplifier System For L-Band Applications

B. Sugumaran(1), O. Silva(1), W. Khattak(1), A. Baba(1) , M. Almansoori(1), F. Vega(1), C. Kasmi (1)

(1) Directed Energy Research Center, Technology Innovation Institute, Abu Dhabi, United Arab Emirates
Bharathidasan.Sugumaran@tii.ae , Oliver.Silva@tii.ae , wajid.khattak@tii.ae , abdul.baba@tii.ae, Mae.Almansoori@tii.ae , felix.vega@tii.ae , chaouki.kasmi@tii.ae

Abstract—In this paper, an amplifier system operating in the 1.5 to 1. GHz frequency range is presented. The saturated output power reaches 700 Watts and the Power Added Efficiency (PAE) is 49%. To our knowledge, the energy efficiency and compactness ratio is higher than any commercially available solution in the market.

I. INTRODUCTION

High power RF amplifies are mainly used in mission critical RF applications where energy consumption and space requirements are of paramount importance. The Power Added Efficiency (PAE) is a key performance indicator of an amplifier which shows how efficiently a power amplifier converts a DC and RF input power to higher RF output power [1]. The energy efficiency of power amplifier system depends on the PAE of the high-power amplifier stage, PAE of the driver stage amplifier and the combining efficiency of the power combiner.
Based on these principles, we introduce an L-Band, 700 Watts RF amplifier, supported by a compact and efficient Gysel power combiner [2] and two 400 Watts power amplifiers [3]. The whole system is compact, fitting on a 3U rack system.

II. ARCHITECTURE

The general architecture is shown in Figure 1. It consists of a 27 Watts driver amplifier, a 2 to 1 30 Watts power divider, two 400 Watts power amplifiers and a 2 to 1 Gysel power combiner. In addition, three GaN DC sequencer circuits are integrated in the system to drive the drain sides with 55 V and 16 A capacity and -5 V and -2.7 V for the gate sides. The combiner, the 27 Watts driver amplifier and the 400 Watts power amplifiers are built on the RT6035HTC substrate, to take advantage of the high thermal conductivity and dissipation efficiency.

III. MEASUREMENT RESULTS

The RF performance of the power amplifier was measured using LA1000 attenuator, Rhode & Schwarz NRX power meter and NRP18S-10 power sensor. A Rhode & Schwarz SMB 100A signal generator and Keysight N8737A DC power supply were used to provide necessary RF input and DC power for the amplifier system. The results are shown in Figure 2.
The measured output power is 58.48 dBm and the Power Added Efficiency (PAE) is 49%.

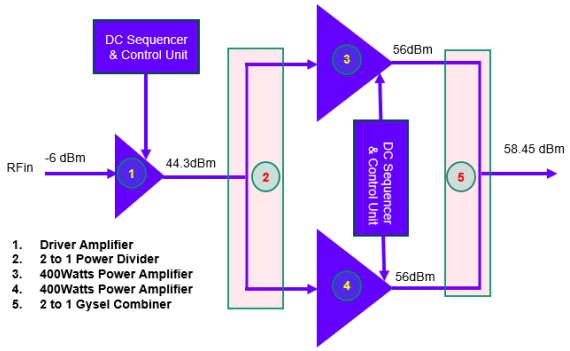

Figure 1: Architecture of 700 Watts Power Amplifier

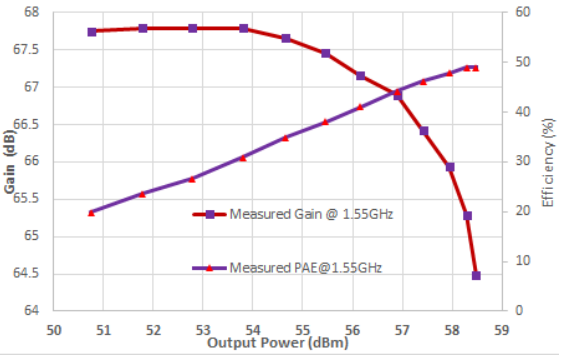

Figure 2 : Measured gain, efficiency vs output power of the 700 Watts Power Amplifier system

REFERENCES

[1] Steve Marsh “Practical MMIC Design” ISBN 1-59693-036-5
[2] B.Sugmaran, O.Silva, F.Vega, C.Kasmi,” Single Layer Microstrip Gysel Combiner for High-Power CW Applications”GlobalEM 2022.
[3] B.Sugmaran, O.Silva, F.Vega, C.Kasmi ,”A 400 W Continuous Wave Power Amplfier in L-Band with Single GaN Transistor” *URSI GASS 2023, Sapporo, Japan, 19 – 26 August 2023*

Enhanced landmine discrimination from GPR data using AI-based algorithms

A. Rangel, F. Ruiz, C. Pedraza.
Dept. of Electrical and Electronic Engineering
Universidad Nacional de Colombia
Bogotá, Colombia
jarangelr@unal.edu.co

F. Vega, L. Prado, M. Mansoori, S. Ghazal, A. Almesmari, O. Lapuz, C. Kasmi.
Directed Energy Research Center
Technology Innovation Institute
Abu Dhabi, United Arab Emirates

Abstract— This paper focuses on improving the discrimination ratio between target and clutter in Ground Penetration Radar (GPR) acquired data. The approach proposed involves using Artificial Neural Networks (ANNs) and Machine Learning (ML) techniques applied to GPR data to detect and classify the characteristic hyperbolic signature from specific buried objects, with a particular emphasis on Improvised Explosive Devices (IEDs), specifically improvised antipersonnel landmines.

Keywords-Ground Penetrating Radar (GPR), Machine Learning, Deep Learning, Improvised landmine.

I. INTRODUCTION

An IED is a device assembled in an improvised manner, incorporating explosive material or chemicals, intended to destroy, disfigure, distract, or harass. While it may include military stores, an IED is typically devised from nonmilitary components [1]. At its core, an IED includes essential components: a switch, a power source, an initiator, a container, and explosives [2]. Due to their nonstandard nature, IEDs exhibit diverse characteristics; for instance, their casings can vary from plastic pipes to wooden cases, glass bottles, or plastic cans. Furthermore, these explosive devices may contain substantial amounts of dielectric material like plastic beads, stones, bamboo, glass, and other nonmetallic components, often used as shrapnel.

IEDs operate on the same principle as industrially manufactured landmines, yet they differ from improvised devices in their use of military-grade materials and adherence to standard geometries.

II. GPR APPLIED TO LANDMINE DETECTION

In humanitarian demining operations involving Ground Penetration Radar (GPR), a comprehensive multi-stage process is undertaken. Initially, data acquisition occurs with an affordable and practical GPR system, aiming to determine the backscattered signal from the targets of interest. Subsequently, signal processing techniques are applied to mitigate unwanted return signals, commonly known as clutter, which may encompass reflections between the soil and the antenna, antenna effects, and other sources of interference. Following this, radar imaging generates an image to identify areas of interest or irregularities indicative of landmines or clutter presence.

Finally, the humanitarian demining process culminates in decision-making, a pivotal step crucial for discriminating between targets, effectively distinguishing landmines from other objects within the soil.

This study is focused into the humanitarian demining domain, incorporating an investigation that extends to the detection of IEDs through the use ANNs and ML techniques.

The use of ANNs enables the categorization of areas that potentially display characteristic reflection events from buried objects, such as IEDs. The multilayer structure of ANNs offers notable advantages, requiring minimal pre-processing of the data to attain optimal results in classifying areas with characteristic reflections. This capability enhances the overall effectiveness of the GPR system.

ML, a robust pattern recognition technique, is instrumental in identifying hyperbolic anomalies associated with buried targets. This application of Machine Learning substantially contributes to generating valuable information necessary for informed decision-making actions. The effectiveness of classifiers within this framework is closely linked to the ratio of IEDs to non-IEDs present in the training dataset.

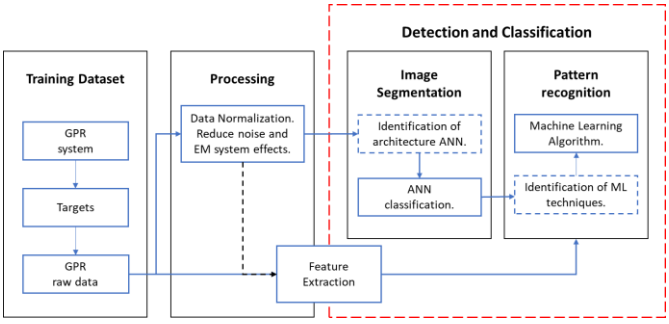

Figure 1. Multi-stage process of GPR humanitarian demining.

REFERENCES

[1] United Nations Mine Action Service, 'International Mine Action Standards 04.10. Glossary of mine action terms, definitions and abbreviations'. United Nations Mine Action Service, New York, p. 44, 2019.

[2] Monitoring and Research Committee, ICBL-CMC Governance Board "Landmine Monitor 2022 – Colombia impact", International Campaign to Ban Landmines – Cluster Munition Coalition (ICBL-CMC) Nov. 2022.

SUMMA
FOUNDATION

ETS·LINDGREN®
An **ESCO Technologies** Company

ets-lindgren.com